



UNIVERSITAT POLITÈCNICA DE CATALUNYA
BARCELONATECH
Escola d'Enginyeria de Barcelona Est

Final Thesis Degree

Materials Engineering Degree

**MICROSTRUCTURAL DESIGN THROUGH 3D DIRECT INK
WRITTING OF CAO FROM VARIOUS ORIGINS TO ENHANCE
THE CARBON CAPTURE PROCESS.**



Memòria i Annexos

Author: Dan Noah Vivas Glaser

Director: Joan Josep Roa Rovira

Co-Director: Jordi Llorca Piqué

Call for proposal: June 2021

Resum

La fabricació additiva ha progressat de forma notable en els últims anys. En especial, la impressió 3D ha permès la utilització de ceràmics en una gran varietat d'aplicacions gràcies a l'habilitat d'aquesta tècnica per poder fabricar capa a capa geometries complexes. Entre aquestes aplicacions, l'ús de ceràmiques en l'energia, com per exemple en la fabricació de catalitzadors ha tingut resultats alentidors. Al mateix temps, la família dels ceràmics és cada cop més el centre de les investigacions en la captura de carboni (CC).

Aquest treball de final de grau (TFG) ha estudiat l'òxid de calci (CaO) i la seva optimització per ser processat de forma correcta per impressió 3D. Això s'ha fet per crear estructures de geometria complexa mitjançant la tècnica de Direct Ink Writing (DIW, en anglès). El CaO s'ha obtingut a partir de closca d'ous. Durant el TFG s'ha pogut optimitzar el mètode de neteja d'aquest residu fins a arribar a pureses per sobre del 98% de CaO. Per fomentar l'estabilitat química i mecànica dels productes s'han sinteritzat materials amb fases inerts d'alúmina (Al_2O_3) i zircònia (3Y-ZrO₂). La 3Y-ZrO₂ utilitzada en aquest TFG també ha servit per donar una segona vida a un residu, en aquest cas, industrial. A més, s'ha trobat que la temperatura de sinterització dels materials basats en el CaO era de 800 °C. A aquesta temperatura es van sinteritzar diverses pastilles i es va analitzar la seva estabilitat química a temperatura ambient. Finalment, també es van realitzar diversos post-tractaments una vegada sinteritzada les mostres per evitar reaccions paràsites amb l'humitat ambiental.

Com conclusió d'aquest TFG es va poder destacar que la sinterització de CaO amb una carburació posterior incompleta és el tractament que permet obtenir el material desitjat amb una major estabilitat tant química com mecànica, podent imprimir peces per la metodologia DIW i posteriorment sinteritzar-les.

Paraules clau: Captura de carboni, Òxid de Calci, Carbonat Càlcic, Closca d'Ou, Impressió 3D, Zirconia, Alúmina

Resumen

La fabricación aditiva ha evolucionado en los últimos años de forma más que notable. Entre esta, destaca la impresión 3D, que ha abierto un nuevo abanico de aplicaciones para la familia de los cerámicos debido a la posibilidad de fabricar geometrías complejas. Un claro ejemplo ha sido el uso de cerámicos en catalizadores con resultados muy favorables. Al mismo tiempo, los cerámicos centran cada vez más las investigaciones en torno a la captura de carbono (CC).

Este trabajo de final de grado (TFG) ha estudiado la optimización del óxido de calcio (CaO) para ser procesado de forma correcta por impresión 3D. El objetivo de dicho estudio es poder crear estructuras de geometría compleja mediante la técnica de *Direct Ink Writing* (DIW, en inglés). El CaO se ha obtenido a partir de cáscara de huevo, la cual se ha podido optimizar su limpieza, llegando a purezas por encima del 98% de CaO. Para fomentar la estabilidad química y mecánica de este compuesto, se ha estudiado la adición de fases inertes de alúmina (Al_2O_3) y zirconia (3Y-ZrO₂). La 3Y-ZrO₂ utilizada provenía también de un residuo, en este caso industrial. Además, se ha encontrado que la temperatura de sinterización de los materiales basados en CaO es de 800 °C. A esta temperatura se sinterizaron varias pastillas y se analizó su estabilidad química a temperatura ambiente. También, para lograr mayor estabilidad química, se realizaron varios tratamientos tras el sinterizado, para evitar reacciones secundarias con la humedad ambiental.

Como conclusión de este TFG se puede destacar que la sinterización de CaO seguida de una carburación incompleta es el tratamiento que permite obtener el material deseado con una mayor estabilidad tanto química como mecánica, y permitiendo imprimir y sinterizar piezas por la metodología DIW para la CC.

Palabras clave: Captura de Carbono, Óxido de Calcio, Carbonato Cálcico, Cáscara de Huevo, Impresión 3D, Zirconia, Alúmina.

Abstract

Additive manufacturing has progressed notably in recent years. Notably, 3D printing of ceramics has unlocked a wide variety of applications due to the ability of this methodology to form complex geometries. Among these, the use of ceramics in catalysis has had promising results in research. At the same time, ceramics such as Calcium Oxide (CaO) have been every time more in the centre of research related to the carbon capture (CC) process.

This degree thesis has studied the optimal CaO-based feedstock and processing for the correct 3D printing of scaffoldings by means of the *Direct Ink Writing (DIW)* technique for the CC process. Parting from eggshell waste, distinct feedstocks were synthesized to achieve the maximum carbonation-calcination efficiencies while maintaining adequate chemical and mechanical stability. To reduce impurities which could negatively affect carbon capture results, an optimal cleaning method for eggshell waste was found that achieved over 98% CaO purity. To increase stability, feedstocks with inert zirconia (3Y-ZrO₂) and Alumina (Al₂O₃) phases were made. While commercial α -Al₂O₃ was bought, 3Y-ZrO₂ from industrial waste was used. Next, the sintering temperature of CaO-based feedstocks was determined to be 800 °C. At this temperature, several pellets of each material were synthesized were sintered and their chemical stability analysed. Finally, to maintain mechanical stability, various post-sintering treatments were carried out to try to avoid secondary reactions with atmospheric humidity at room temperature. Ultimately, CaO synthesis with a posterior incomplete carbonation had the highest chemical and mechanical stability, from which a 3D printed scaffolding was successfully manufactured.

Key words: Carbon Capture, Calcium Oxide, Calcium Carbonate, Eggshells, Zirconia, Alumina, 3D printing, Direct Ink Writing

Agraïments

Agradecer en primer lugar a mi familia y amigos por apoyarme en estos últimos meses sin los cuales no me hubiese sido posible finalizar este trabajo. Thank you for your patience, I know I have not been easy.

Al Dr. Joan Josep Roa Rovira agradecerle el apoyo y la confianza que me brindó desde el principio, sin el cual ni siquiera hubiese surgido la idea que finalmente se vio realizada en este proyecto. Dar las gracias también a los y las compañeras de TFG, TFM y doctorado que me enseñaron gran parte de lo que conozco ahora, y que me ayudaron a continuar esforzándome en los momentos más difíciles.

Glossary

CO_2	<i>Calcium Dioxide</i>	<i>LD</i>	<i>Laser Diffraction</i>
<i>CC</i>	<i>Carbon Capture</i>	<i>Y-TZP</i>	<i>Yttria Stabilized Zirconia</i>
<i>CaO</i>	<i>Calcium Oxide</i>	<i>SE</i>	<i>Secondary Electrons</i>
<i>3D</i>	<i>Three-dimensional</i>	<i>BSE</i>	<i>Back-Scattered Electrons</i>
Al_2O_3	<i>Alumina</i>	<i>EDS</i>	<i>Energy Dispersive X-Ray</i>
<i>DIW</i>	<i>Direct Ink Writing</i>	<i>CIP</i>	<i>Cold Isostatic Pressing</i>
TiO_2	<i>Titanium Oxide</i>	<i>HV</i>	<i>Vickers Hardness</i>
$-NH_3$	<i>Amine based</i>	$Ca_{12}Al_{14}O_{33}$	<i>Mayenite</i>
K_2CO_3	<i>Potassium Carbonates</i>	$Ca(OH)_2$	<i>Calcoum Hydroxide</i>
CH_4	<i>Methane</i>	<i>CaL</i>	<i>Calcium Looping</i>
O_2	<i>Oxygen</i>	<i>ES</i>	<i>Eggshell</i>
<i>UV</i>	<i>Ultraviolet</i>	<i>AM</i>	<i>Additive Manufacturing</i>
<i>MOF</i>	<i>Metal Organic Framework</i>	<i>CAD</i>	<i>Computer-Aided Design</i>
MgO	<i>Magnesium Oxide</i>	<i>XRD</i>	<i>X-Ray Diffractometry</i>
$CaCO_3$	<i>Calcium Carbonate</i>	<i>SEM</i>	<i>Scanning Electron Microscope</i>
H_2O	<i>Water</i>	<i>TT</i>	<i>Thermal Treatment</i>
<i>Ca</i>	<i>Calcium</i>	<i>CaO-b</i>	<i>Commercial Calcium</i>
ZrO_2	<i>Zirconia</i>	<i>RA</i>	<i>Yttria Stabilized Zirconia (without binder)</i>
$CaZrO_3$	<i>Calcium Zirconate</i>		

Figure Index

<i>Figure 1 – Key greenhouse gasses in 2010 compared by CO₂ equivalent emissions [5].</i>	5
Figure 2 – Global greenhouse emissions by sectors in 2016 measured through CO ₂ eq., and emphasizing in the energy sector [6].	6
Figure 3 - Graph showing evolution of articles published in the ISI Web of Science database during the last 15 years with the titles "Carbon Capture". [8]	7
Figure 4 - Illustration of the second stage of the carbonatation reaction of CaO.	11
Figure 5 – (a) Carbonation/calcination microstructural process for particles above 500 nm and (b) incomplete carbonation process after each cycle [17].	11
Figure 6 – Carbonation – calcination reaction equilibrium temperature at various CO ₂ pressures [21].	12
Figure 7 – Variation of the CO ₂ absorption of CaO for various calcination temperatures [22].	13
Figure 8 - CaO/Ca(OH) ₂ equilibrium pressure at different temperatures [27].	15
Figure 9 – Schematics representation of the post-combustion CC system placed at La Pereda 1.7 MW _{th} Carbon power plant [28].	17
Figure 10 – SEM micrographs of (a) fresh calcined eggshell and (b) of eggshell after 20 carbonation-calcination cycles [31].	18
Figure 11 – Schematic diagram of the DIW or robocasting method [39].	20

3D Printing of CaO for Carbon Capture

Figure 12 – Calcination conversion with number of cycles for calcined eggshel (CES) and commercially available CaCO ₃ (CCA) [20].	25
Figure 13 – Pictures of the process followed to obtain a high purity CaO. (a) Initial ES, (b) bleach treatment, (c) drying of ES, (d) initial hand milling and (e) feedstock after calcination.	29
Figure 14 – (a) Nabatherm and (b) Energon ovens used in this Bachelor’s project.	30
Figure 15 – Turbula® ball mill used in this Bachelor’s project.	31
Figure 16 – Rotary evaporator set-up used to dry the powders after ball milling.	31
Figure 17 – SEM equipment used in this Bachelor’s project.	33
Figure 18 – Carbon Coating equipment for SEM analysis.	34
Figure 19 – Optical arrangement followed in XRD measurements [45].	35
Figure 20 - D8 Advance D83 EDX equipment used in this Bachelor’s project.	35
Figure 21 – Masersizer 3000 Hydro EV laser diffraction equipment used in this Bachelor’s project.	36
Figure 22 – Sintered CIP samples breaking (left) and enlarging after reacting with water vapor in the air in comparison with unreacted sample (centre tablet).	36
Figure 23 – CIP machine used in this Bachelor’s project.	37
Figure 24 – Manual vacuum sealer used to reduce interaction between samples and air.	38

Figure 25 – Picture taken of CaO sample that reacted with water, inducing the induced fracture of the Bakelite where it was held. _____	39
Figure 26 – Mettler Toledo XS3035 Archimedes balance used in this bachelor’s project.	40
Figure 27 – DuraScan 65 Vickers microhardness equipment used in this Bachelor’s project. _____	41
Figure 28 – (a) Shape of a Vickers indentation tip and (b) theoretical mark done by the indenter [44]. _____	42
Figure 29 – Cracks at an indentation that allow for the measurement of K_{Ic} [12]. _____	42
Figure 30 – SpeedMixer™ used in this Bachelor’s project _____	44
Figure 31 – (a) DIW printer used for this Bachelor’s project and (b) Printing syringe. _	44
Figure 32 – XRD spectrum for treated ES. _____	46
Figure 33 – LD results for $CaCO_3$ (calcite) synthesized from ES waste. _____	47
Figure 34 – SEM micrograph of ES waste before calcination. _____	47
Figure 35 – EDX analysis intensity spectrum of ES waste. _____	48
Figure 36 – XRD spectra for F1, F2, F3 and F4. _____	49
Figure 37 – SEM micrographs of calcined ES (a) F1 (b) F2 (c) F3 and (d) F4. _____	49
Figure 38 – Comparison of SEM micrographs for (a) CaO-b and (b) F3 CaO. _____	51

3D Printing of CaO for Carbon Capture

- Figure 39 – CaO-b XRD spectrum showing CC (calcite), CO (CaO), CA ($\text{Ca}_3\text{Al}_2\text{O}_6$) and MO (MgO) compounds. _____ 52
- Figure 40 – XRD spectra for Al 1/10, Al 2/10, Al 3/10 and Al 4/10 showing M (Mayonite), CO (CaO), A (Al_2O_3), CA ($\text{Ca}_2\text{Al}_3\text{O}_6$) and CH ($\text{Ca}(\text{OH})_2$) compounds. _____ 53
- Figure 41 – LD particle size distribution of Al 1/10, Al 2/10, Al 3/10 and Al 4/10. ____ 54
- Figure 42 – Weight loss during sintering process for the various Al-CaO feedstocks in comparison with F3 CaO weight loss during calcination. _____ 55
- Figure 43 – SEM micrographs of (a) Al 1/10, (b) Al 2/10, (c) Al 3/10, and (d) Al 4/10. _ 55
- Figure 44 - XRD spectra for feedstocks R60, RA and R60C. _____ 57
- Figure 45 – SEM images of (a) R60 (b) RA and (c) R60C. _____ 58
- Figure 46 – LD size distribution for R60, RA and R60C both (a) without applying US and (b) applying US. _____ 59
- Figure 47– XRD spectra for Zr 1/10, Zr 2/10 and Zr 3/10 showing CO (CaO), Z_t (tetragonal ZrO_2), Z_m (monoclinic ZrO_2) and CZ (CaZrO_3) phases. _____ 60
- Figure 48 – Particle size distribution of Zr 1/10, Zr 2/10 and Zr 3/10 measured by LD. 61
- Figure 49 – Weight loss during sintering for Zr – CaO feedstocks in comparison with F3 CaO. _____ 62
- Figure 50 – SEM micrographs of (a) Zr 1/10, (b) Zr 2/10 and (c) Zr 3/10. _____ 63

- Figure 51 – Ca(OH)₂ XRD diffraction pattern showing CH (Ca(OH)₂ and possible CaO (CO).
_____ 64
- Figure 52 – Particle size distribution of Ca(OH)₂ both with and without US measured by LD.
_____ 64
- Figure 53 – Ca(OH)₂ SEM micrograph. _____ 65
- Figure 54 – Weight loss during sintering for temperatures ranging from 500 to 800 °C,
showing theoretical weight loss as a dotted line at 44.0%. _____ 66
- Figure 55 – XRD spectra for CaCO₃ calcination at temperatures ranging from 500 to 800 °C,
showing CC (Calcite CaCO₃), CO (CaO) and a third unknown compound (*). _____ 67
- Figure 56 – Particle morphology of calcined CaCO₃ at (a) 500 °C, (b) 550 °C, (c) 600 °C, (d)
650 °C, (e) 700 °C, (f) 750 °C and (g) 800 °C. _____ 68
- Figure 57 – Samples after being kept 2 days in ethanol. _____ 69
- Figure 58 – Sinter samples that had been dipped in oil after (a) 4 days and (b) 7 days. 70
- Figure 59 – Samples that had been applied Lacquer after 2 days. _____ 70
- Figure 60 – Mass gain for the different feedstocks sintered after 3 and 7 days. _____ 71
- Figure 61 – Images of (a) Zr 1/10, (b) Zr 2/10, (c) Zr 3/10, (d) Al 1/10, (e) Al 2/10, (f) Al 3/10,
(g) Al 4/10 and (h) CaO pellets sintered after (.1) 3 days and (.2) 7 days left in contact
with air. _____ 72
- Figure 62 – Incomplete carbonation pellets after (a) 3 days and (b) 7 days. _____ 73

3D Printing of CaO for Carbon Capture

Figure 63 – Ca(OH)₂ sintered pellets once taken out of the oven. _____ 73

Figure 64 – SEM micrograph of pellet that underwent incomplete carbonation and sintering. _____ 74

Figure 65 – Honeycomb monolith with 50% infill after synthesis and incomplete carburation treatment. _____ 74

Figure 66 – EDX intensity patterns for F1. _____ 103

Figure 67 – EDX intensity patterns for F2. _____ 104

Figure 68 – EDX intensity patterns for F3. _____ 104

Figure 69 – EDX intensity patterns for F4. _____ 105

Figure 70 - EDX intensity patterns for R60. _____ 106

Figure 71 - EDX intensity patterns for R60C. _____ 107

Figure 72 - EDX intensity patterns for RA. _____ 107

Index of Tables

Table 1 - List of solid sorbents synthesized and their performance in CO ₂ capture [3].	_9
Table 2 – AM techniques for ceramic materials, organized by feedstock form [33,39].	21
Table 3 – ZrO ₂ Industrial residues used, and the initialism chosen to represent it throughout this Bachelor’s project.	_____ 32
Table 4 – EDX composition analysis by weight of F1, F2, F3 and F4.	_____ 50
Table 5 – Composition of comparison of CaO-b and F3 CaO from ES origin measured through EDX.	_____ 52
Table 6 – EDX composition analysis for Al 1/10, Al 2/10, Al 3/10 and Al 4/10.	_____ 56
Table 7 – Weight concentration of the various elements as a function of intensity found in EDX analysis.	_____ 57
Table 8 – Crystallite size (nm) of CaO feedstocks F1, F2, F3 and F4 based on XRD diffraction pattern.	_____ 58
Table 9 – Crystallite size calculated from the XRD diffraction pattern for CaO and ZrO ₂ peaks	_____ 61
Table 10 – EDX Composition analysis for Zr 1/10, Zr 2/10 and Zr 3/10.	_____ 62
Table 11 – Crystallite sizes calculated from the XRD patterns of the various sintering temperatures.	_____ 68
Table 12 – Sustainability Matrix elaborated by Climent et al. [49]	_____ 75

3D Printing of CaO for Carbon Capture

Table 13 – Questions parting from the sustainability matrix elaborated by Climent et al. [49]	76
Table 14 – Ecological Footprint calculations for this Bachelor’s project.	77
Table 15 – Ecological footprint of 1 scaffold if it were to be mass produced.	78
Table 16 – Cost of the equipment used during this Bachelor’s project	80
Table 17 – Cost of the materials used for this Bachelor’s project.	80
Table 18 – Cost and time spent by the engineers and technicians in this Bachelor’s project.	80
Table 19 – Total cost of this Bachelor’s project as a sum of the three scopes explained in Tables 16 - 18.	81
Table 20 – Costs associated to the manufacture of one incompletely calcined scaffolding.	81
Table 21 – Table showing XRD 2θ values for CaO, CaCO ₃ , α -Al ₂ O ₃ , Ca ₃ Al ₂ O ₆ , MgO, CaZrO ₃ , Ca(OH) ₂ , Ca _x Al _x O _x , ZrO ₂ and Y ₂ O ₃ .	108
Table 21 – Table showing XRD 2θ values for CaO, CaCO ₃ , α -Al ₂ O ₃ , Ca ₃ Al ₂ O ₆ , MgO, CaZrO ₃ , Ca(OH) ₂ , Ca _x Al _x O _x , ZrO ₂ and Y ₂ O ₃ (continuation).	109

Index

RESUM	I
RESUMEN	II
ABSTRACT	III
AGRAÏMENTS	IV
GLOSSARY	V
FIGURE INDEX	VI
INDEX OF TABLES	XII
1. PROLOGUE	1
1.1. Thesis origin.....	1
1.2. Motivation	1
2. INTRODUCTION	3
3. THEORETICAL BACKGROUND	5
3.1. Carbon dioxide and climate change.....	5
3.2. Current carbon capture technologies.....	6
3.3. CaO and its application as a carbon capture sorbent	9
3.4. Current use of CaO in carbon capture	16
3.5. CaO from waste sources.....	17
3.6. Additive manufacturing of ceramic materials	18
4. STATE OF THE ART	23
5. GOAL	27
6. EXPERIMENTAL PROCEDURE	28
6.1. Elaboration of CaO and CaCO ₃ from eggshell waste.....	28
6.2. Commercial CaO	30

3D Printing of CaO for Carbon Capture

6.3.	Ca ₁₂ Al ₁₄ O ₃₃ synthesis.....	30
6.4.	CaZrO ₃ synthesis	31
6.5.	Ca(OH) ₂ synthesis.....	32
6.6.	Feedstock and microstructural characterization	32
6.6.1.	Scanning Electron Microscope	33
6.6.2.	X-Ray Diffractometry.....	34
6.6.3.	Laser Diffraction	35
6.7.	Uniaxial pressing and Cold Isostatic Pressing.....	36
6.8.	Sintering Process.....	37
6.9.	Post-Sintering Treatment.....	38
6.10.	Sample characterization	39
6.10.1.	Polishing	39
6.10.2.	Microstructural characterization.....	40
6.10.3.	Mechanical properties	41
6.11.	Ceramic Inks and 3D printing procedure	43
6.11.1.	Ceramic inks fabrication	43
6.12.	3D Printing Process – DIW	44
7.	RESULTS AND DISCUSSIONS	46
7.1.	Synthesis of feedstocks.....	46
7.1.1.	CaCO ₃ synthesis.....	46
7.1.2.	CaO synthesis from ES.....	48
7.1.3.	Commercial CaO.....	50
7.1.4.	Ca ₁₂ Al ₁₄ O ₃₃ synthesis	52
7.1.5.	ZrO characterization and election	56
7.1.6.	CaZrO ₃ synthesis.....	59
7.1.7.	Ca(OH) ₂ synthesis	63
7.2.	CaO sintering temperature	65
7.3.	Post-sintering treatments	69
7.3.1.	Ethanol Bath	69



3D Printing of CaO for Carbon Capture	Memoria
7.3.2. Oil Bath	69
7.3.3. Lacquer treatment	70
7.4. Pellet synthesis and reaction in air	70
7.5. DIW printing.....	74
8. SUSTAINABILITY REPORT	75
8.1. Ecological scope.....	76
8.2. Economic scope	79
8.3. Social scope	83
9. CONCLUSIONS	85
BIBLIOGRAPHY	87
ANNEX A	95
A1. CaO feedstock data sheet.....	95
A2. α -Al ₂ O ₃ feedstock data sheet.....	99
A3. Datasheet for powders from which R60 and R60C originate.....	101
A4. Datasheet of the powders from which residue RA originates.	102
ANNEX B	103
B.1 EDX Results for <i>F1</i> , <i>F2</i> , <i>F3</i> , and <i>F4</i>	103
B.2 EDX results for R60, R60C and RA	106
ANNEX C	108
C1 XRD bibliography values for the various elements found in the diffraction patterns	108
ANNEX D	109
D.1 Ecological footprint EduPack calculations	110
ANNEX E	117
E.1 Cost of CC following the procedure defended in the present thesis	117

1. Prologue

1.1. Thesis origin

The background from which this thesis originates is that of catalytic research using three-dimensional (3D) printed scaffoldings to produce ethanol. Moreover, as commented later on, carbon capture (CC) technologies have been receiving every time more attention due to the necessity to reduce CO₂ emissions. Reviews of solid CC have also showed optimum results for CC using feedstocks originating from residues. Therefore, this Bachelor's project intends to put together the knowledge attained from these different sectors to obtain higher efficiencies in the CC process.

1.2. Motivation

We find ourselves amidst some of the greatest crisis humanity has ever faced. The climate crisis, with all its effects, has yet to show its worst face. Acting preventively, ambitiously, and fairly can save millions of lives. Materials engineering must, in my opinion, serve to help surpass these challenges successfully. Hence, I believe that research must be put to serve long-term sustainability goals in parallel to climate action in institutions. Carbon capture, even if still at a research stage, may help to reach negative emissions in those countries that have contaminated the most, allowing for a just arrival to neutral emissions by 2050. Moreover, creating durable products along with putting recycling and upcycling at the centre of all new technologies is not an if but a must. We must act now; we must act decisively. It is like this that I am determined to find a feasible way to enhance carbon capture using new and developing technologies such as three-dimensional printing. Another important aspect of this Thesis for me, was the col-laboration with the University of Birmingham and with the Saint Gobain company with the objective of upcycling wastes.

Finally, investigating and learning topics that have not been fully researched in the past motivated me the most for this Bachelor's project.

2. Introduction

For the first time in over 800.000 years, the concentration of carbon dioxide (CO₂) in the atmosphere has surpassed 410 ppm [1]. Provoked by anthropogenic emissions, this increase has and will provoke an increment in temperatures associated with a greater number of natural disasters [2]. Simultaneously, scarcity of several resources has also been an important limiting factor when finding long term sustainable solutions to the climate crisis [2]. To solve these problems, solid material carbon capture (CC) working in parallel with emission reductions has been seen as a plausible solution, limited though by low levels of efficiency, problems in scale-up manufacturing, and the difficulty to withstand large number of absorption/desorption cycles of present CC technologies [3].

Using ceramic materials may solve some of these issues due to their good chemical and structural properties. In the past, though, low surface areas, poor fluid travel design and highly technical manufacturing techniques have limited ceramic products in energy and catalysis processes. Recent advancements in ceramic three-dimensional (3D) printing may solve these problems and therefore present a better alternative for efficient CC. Ceramic 3D printed scaffolds have the ability of creating a tortuous path for the air fluid, increasing therefore the time of remanence of the gas in the material, and reaching a higher specific surface area. Also, 3D printing allows for good mechanical properties. This Bachelor's project will work from previous investigations that used alumina (Al₂O₃) based-ceramic materials for catalysis processes, and CC with Calcium Oxide (CaO) obtained from waste materials [3][4]. Within the aforementioned information, *this Bachelor's project aims to increase the efficiency of the CC process with the lowest ecological footprint.*

To do so, along this Bachelor's project will study the printability of 3D scaffolds through Direct Ink Writing (DIW) technique using CaO-based feedstocks, intending for most of them to originate from waste sources. By varying initial feedstocks and sintering parameters, this

Bachelor's project strives to find an effective way to synthesize physically and chemically stable 3D printed scaffolds for CC.

3. Theoretical Background

3.1. Carbon dioxide and climate change

Currently, as of April of 2021, the concentration of CO₂ in the atmosphere is at 416 ppm at the Mauna Loa observatory in Hawaii [1]. The importance of this magnitude does not rely on the toxicity of the gas, yet on the greenhouse effect it provokes, which has led to the increase of extreme natural disasters as well as the acidification of oceans and seas. As seen in **Figure 1**, CO₂ from industrial sources is the anthropogenic gas most responsible for the increase of temperature in the planet [5]. In the natural systems, the absorption and retention of CO₂ is done through photosynthesis in plants and adsorption in oceans and large wetlands as carbon sinks. The rate of natural absorption however is very much below current anthropogenic emissions [3].

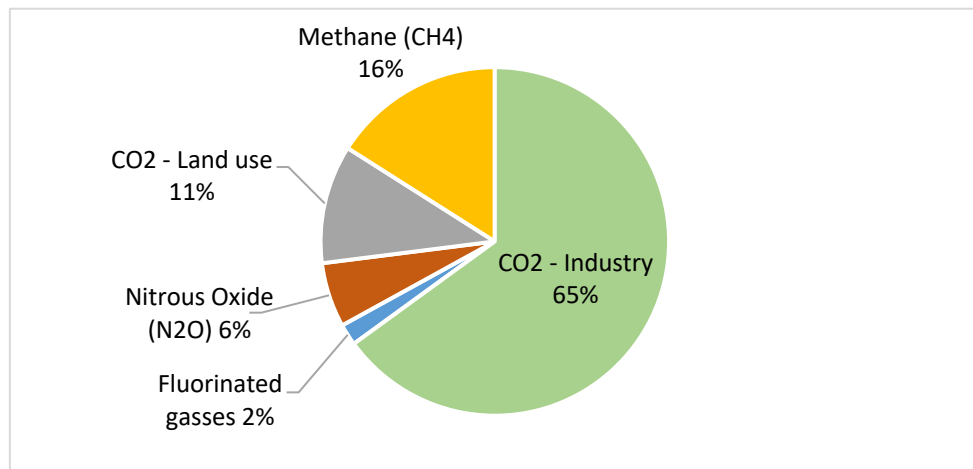


Figure 1 – Key greenhouse gasses in 2010 compared by CO₂ equivalent emissions [5].

As seen in **Figure 2**, these emissions are largely caused by the current energy, industrial and transport systems, accounting for up to 76% of CO₂ equivalent emissions. These sectors are heavily based on hydrocarbon fuels, being unlikely therefore that the strong reductions needed to mitigate climate change effects will come from these industrial sectors. The drastic and urgent need of reducing CO₂ concentrations in the atmosphere to stop the

increase of global change has pushed part of the scientific community to advocate for CC and storage, in parallel to other technologies and politics to reduce emissions [6].

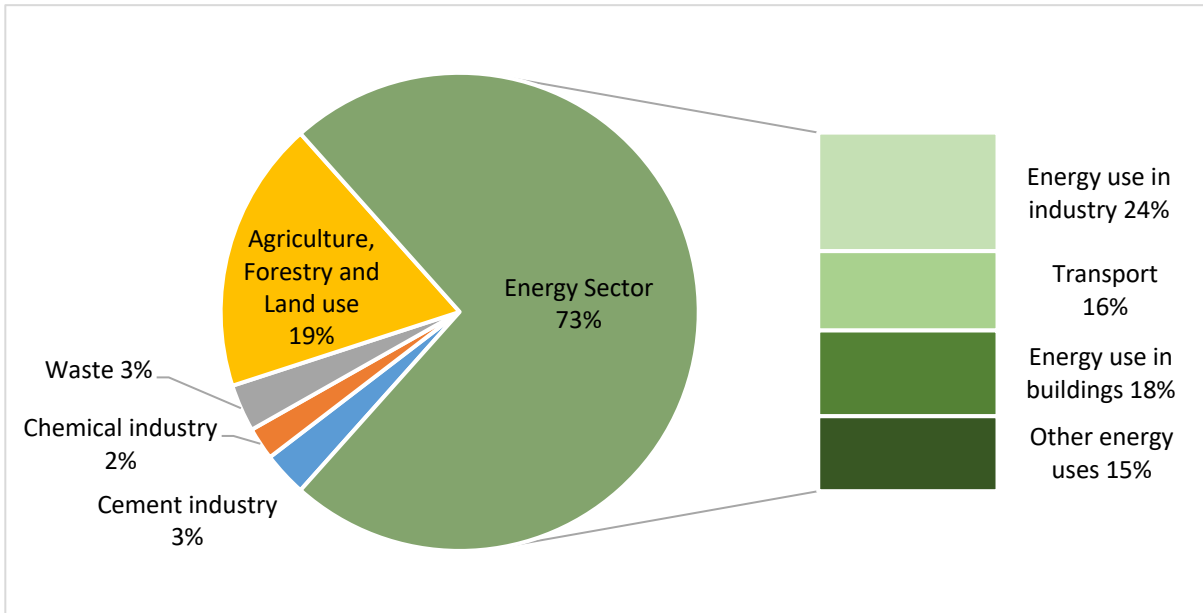


Figure 2 – Global greenhouse emissions by sectors in 2016 measured through CO₂ eq., and emphasizing in the energy sector [6].

3.2. Current carbon capture technologies

CC technologies are an area that is every time more in the focus point of the scientific community and companies worldwide. There are alternative methods to CC to be able to store CO₂. These methods consist basically in the combustion under pure oxygen atmosphere to generate CO₂ and water. These methods, though, entail high costs and have very limited applications in the industry. For this reason, sequestration of CO₂ has centered on post-combustion CC, both by solid and liquid route.

Liquid CC route is based on passing a gas, with predominant CO₂ concentrations through a fluidized bed containing amines that react with the gas, at temperatures between 40 and 60 °C. The liquid CC technique has been in use since the 1950s to enrich and purify natural gas. This approach, even if more advanced in investigation, requires high amounts of

3D Printing of CaO for Carbon Capture

energy to regenerate the amines, as well as elevated pressures and corrosion resistant equipment, all of which increase the final price of adsorption. Liquid CC alternatives use solid adsorbents in the form of powder in solutions. Hence, research in *solid CC* will aid *liquid CC* and vice versa [7].

As seen **Figure 3**, CO₂ sequestration investigation has seen a steady increase in the past 15 years [8]. A big part of this research has been centered in *solid CC methods*. These bases themselves in chemical or physical entrapment of CO₂ molecules in a solid solution. By changing the thermal properties of the medium, the solid can release such molecules for either storage or conversion for energy applications. These cycles are known as absorption and desorption cycles. Depending on the desorption/absorption temperature solid CC methods can be split into low (< 200 °C), intermediate (200-400 °C) or high temperature (> 400 °C [3].

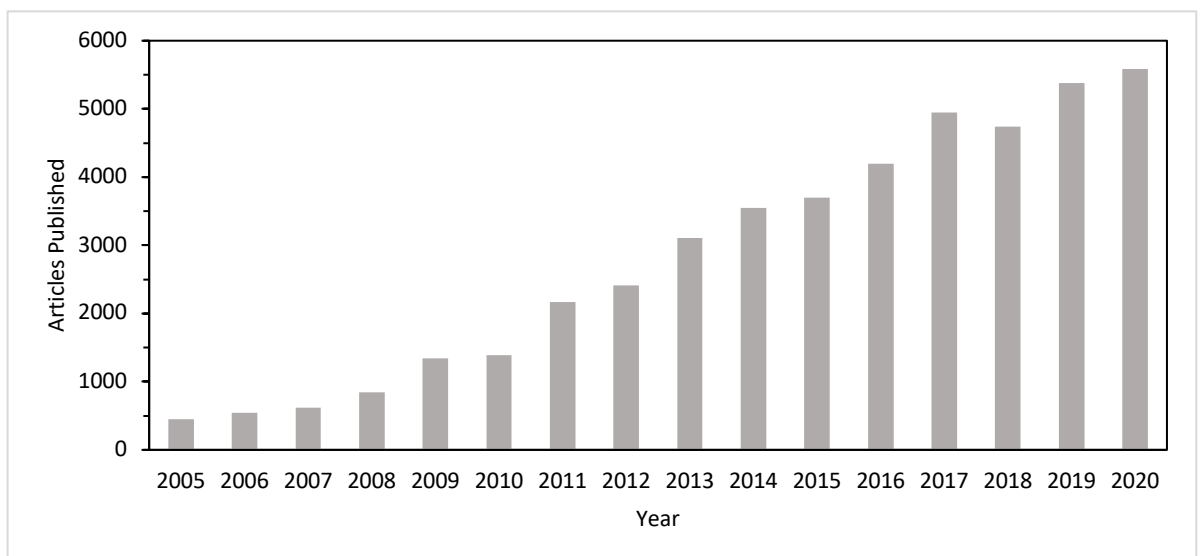


Figure 3 - Graph showing evolution of articles published in the ISI Web of Science database during the last 15 years with the titles "Carbon Capture". [8]

Among low temperature sorbents, titanium oxide (TiO₂), amine based (-NH₃) sorbents, and potassium carbonates (K₂CO₃) have centered most of the attention. TiO₂ has a photocatalytic effect, promoting the reaction of CO₂ with water to produce methane (CH₄) and oxygen (O₂) under ultraviolet (UV) light. Since the whole surface must be visible to UV

light, and a high CO₂ concentration of the flue gas is needed, its applications are limited. K₂CO₃ and NH₃ based sorbents, on the other hand, are used as coatings on sturdy structures, being able to expel the CO₂ at temperatures lower than 200 °C. K₂CO₃ reacts with CO₂ and water to produce 2KHCO₃ at an absorption/desorption temperature of around 90 °C. The low temperature, impeding many industrial applications, and the resulting brittle material limit it as a low temperature sorbent [9]. Amines consist of the functional -NH₃ group attached to an organic chain. The polar NH₃ group can be loaded upon a variety of materials, yet faces difficulty maintaining high efficiencies in the long run due to leaching of NH₃ molecules as well as its elevated costs associated to manufacture [3]. Other materials in this category which have not shown as good of a result in comparison to their cost include carbon, silica or some Metal Organic Framework (MOF) based adsorbents [10].

In intermediate temperature solid adsorbents magnesium oxides (MgO) and MOF have been upon the most studied options. The first, MgO, reacts with CO₂ in a slow reaction giving a mechanically unstable product. Moreover, MgO has a high irritation and environmental damaging potential [11]. On the other hand, MOF are synthesized using complex methods, elevating the cost for possible CC applications [3].

Finally, high temperature adsorbents, although facing a greater energy use, have shown high efficiencies and good mechanical properties. Among this category, CaO stands out. CaO greatest limitation is the number of cycles of adsorption/desorption that can be carried out before the efficiency is too low. Current research in this field have pointed towards the need of new designs of the CaO products as well as using non pure materials to achieve better results. Another field of investigation is CaO derived from waste products such as lime mud or eggshells. This can be seen in **Table 1**, where a variety of solid sorbents are exposed. Eggshell waste stands out as having reached one of the highest CO₂ uptakes. Note that materials were tested under different conditions.

Table 1 - List of solid sorbents synthesized and their performance in CO₂ capture [3].

<i>Sorbent Family</i>	<i>Material</i>	<i>CO₂ uptake [mmol g⁻¹]</i>	<i>Sorbent Family</i>	<i>Material</i>	<i>CO₂ uptake [mmol g⁻¹]</i>
<i>Carbon</i>	Olive stones waste	2.43	MgO	MgO on mesoporous Carbon	5.5
	Birch wood waste	15.91	CaO	Eggshell waste	14.29
	Coffee grounds waste	4.8		Lime mud waste	7.14
	Carbon Nanofibers	16.36		Scallop waste	6.36
	N-doped porous carbon	6.2		CaO by coprecipitation	15.9
	Graphene Nanoplates	56.36		CaO by sol-gel	13.4
<i>MOF</i>	Zn doped Ni-ZIF-8	4.3	Alkali Silicate	Rice Husk Ash waste	7.36
	Alkaline doping in MOF	19.85		Li ₄ SiO ₄	6.3
<i>Silica</i>	Conventional Silica	3.8	Polymer Based	Hyper-crosslinked Polymers (HCPs)	13.4
	Silica hollow spheres	6.0		Porous Aromatic Framework	60

3.3. CaO and its application as a carbon capture sorbent

Calcium (Ca) is the fifth most abundant compound on the earth's crust, normally in the form of calcium carbonate (CaCO₃), with either calcite or aragonite crystalline structure. Ca as a functional material is most used though as CaO, also known as lime. Pure CaO, with a high melting point of 2898 °C, and a density of 3.34 g/cm³, is a highly reactive compound. Reactions with compounds such as Al₂O₃, water (H₂O), or CO₂, and their simple decompositions, make lime a prime candidate for chemical bounding of CO₂ molecules. Another important aspect to lower energy consumption is heat capacity. CaO has a

moderate heat capacity of around $55 \text{ J/mol}\cdot^\circ\text{C}$, thus this not being inconvenient. Nowadays, the main use of CaO is in the cement industry, being the main ingredient of portland cement,. Other uses include the glass or paper industry [12]. Ca-based materials were not used in abundance though in the energy and chemical sector up to recent years, when it received increasing attention in research for CC. This is mainly due to the solid-gas reaction seen in **equation 1**. This reversible reaction through cycles of carbonation and calcination allows for the chemisorption of a large quantity of CO_2 at a comparatively low energetic demand [13]. Yet, it has been hindered by sharp decrease in efficiencies over large amount of absorption/desorption cycles [3,14] . Understanding the carbonation reaction as well as microstructural and chemical parameters is crucial to be resist the reduction in its performance.



The carbonation reaction can be divided in two stages. The first stage is a rapid conversion to CaCO_3 at the surface with a calcite structure, creating a layer of CaCO_3 that stops the reaction. A second stage then diffuses O^{2-} anions towards the surface. These anions react with CO_2 molecules to form CO_3^{2-} anions that penetrate the surface and diffuse inwards, increasing the width of the calcite layer and balancing the charge [15]. **Figure 4** illustrates the ionic diffusion occurring in the mentioned second stage. The calcite layer formed, and the ionic diffusion velocity make this second stage produce a noticeable decrease in the reaction speed. If such layer is not broken during the calcination process, this will lead to a reduction in efficiency in the next cycle [16]. Finally, if the cycle leads to incomplete carburation and calcination processes, an *inert* CaO skeleton as seen in **Figure 5** will be made, reducing therefore the CC capacity.

3D Printing of CaO for Carbon Capture

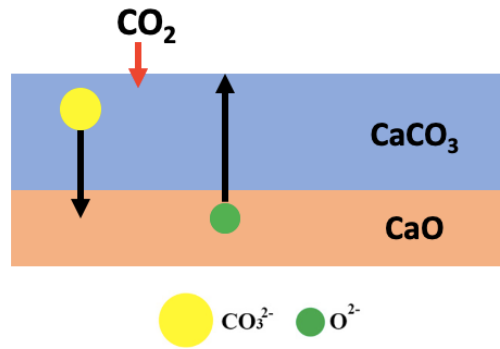


Figure 4 - Illustration of the second stage of the carbonation reaction of CaO.

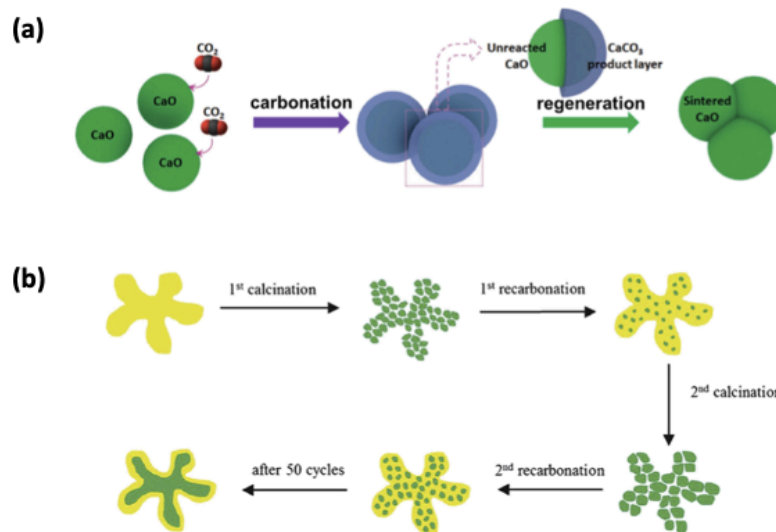


Figure 5 – (a) Carbonation/calcination microstructural process for particles above 500 nm and (b) incomplete carbonation process after each cycle [17].

CaO -CC is strongly depended on the *absorption/desorption temperature* used and on the CO₂ partial pressure at which it is submitted during the adsorption-desorption cycles. The carbonation reaction above 537 °C (810 K) starts to destabilize at atmospheric CO₂ pressure. Albeit, carrying out the reaction at this temperature occurs at extremely low rates due to the second stage of the reaction that was mentioned. Hence, for CaO to be a realistic candidate for CC, it must be carried out at temperatures between 600 and 750 °C with high CO₂ partial pressures [3,18]. The temperature and the pressure determine the final equilibrium concentration of CO₂ in the gas as seen in **Figure 6** which will determine a theoretical maximum of efficiency. As studied by *Ströhle et al.* [19], at 650 °C and a pressure of 1 bar, equilibrium will be reached at 1.2% volume of CO₂ in the gas. The initial CO₂

concentrations must be therefore higher than this equilibrium CO₂ volume percentage for carbonation to occur. Thus, applications of CaO - CC are limited to carbon intensive industries or processes. These industries however account for most of the CO₂ gasses emitted in our planet, being therefore the most useful sector, both from an economic as scientific point of view. Because the forward reaction in **Equation 1** is exothermic, less energy is needed to maintain the carbonation reaction. Exothermicity however may increase the temperature leading to particle sintering. Sintering occurs as the Tammann temperature of CaCO₃, the temperature from which the particles start to sinter, is of 533 °C [20]. Sintering reduces specific surface area and therefore reduces CC efficiency. Finally, the calcination reaction is usually set between 700 and 900 °C, resulting in the cycle having a change of temperature of around 200 °C [17]. Due to the low cost of the feedstock material, energy use is the most important cost in this CC technology [21].

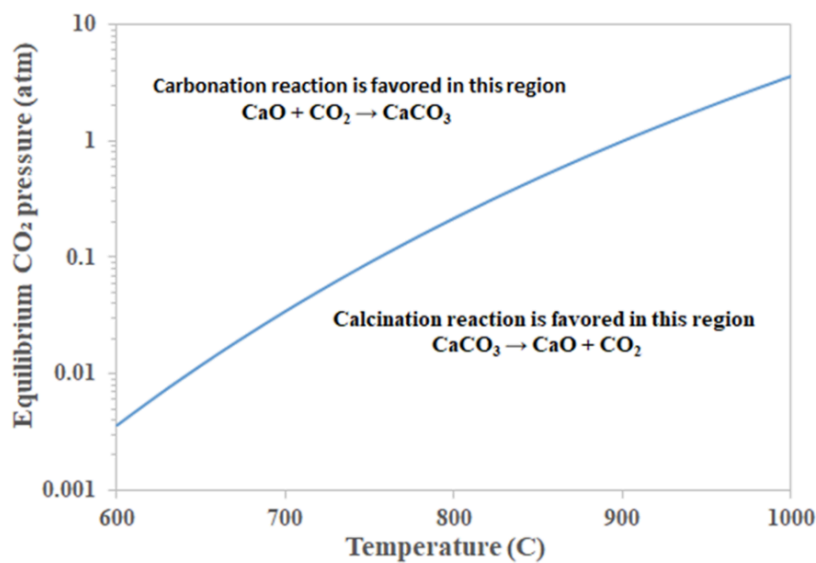


Figure 6 – Carbonation – calcination reaction equilibrium temperature at various CO₂ pressures [21].

The chemisorption of CO₂ molecules implies an increase in volume and weight that when calcinated leave a porous structure behind. The CaCO₃ layer has a higher molar volume than CaO (36.9 cm³/g vs. 16.7 cm³/g) and lower theoretical density, causing microstructural changes in the form of pores when calcinating, and closing these during carbonation [15].

3D Printing of CaO for Carbon Capture

Porosity has a great influence in the first stage of the reaction, as it increases the surface area of the material, and therefore increases the rate of the reaction. Calcination leads to a dense CaCO_3 inner part, surrounded by a porous CaO layer. The sintering of grains previously mentioned, lead to the closing and blocking of the pores after numerous cycles. Hence, preventing the formation of a stable thick calcite layer, improving the ionic diffusion, and diminishing the sintering effects are the paths followed by CC research to increase efficiencies [17,20]. In **Figure 7**, the loss of efficiency across absorption-desorption cycles can be observed.

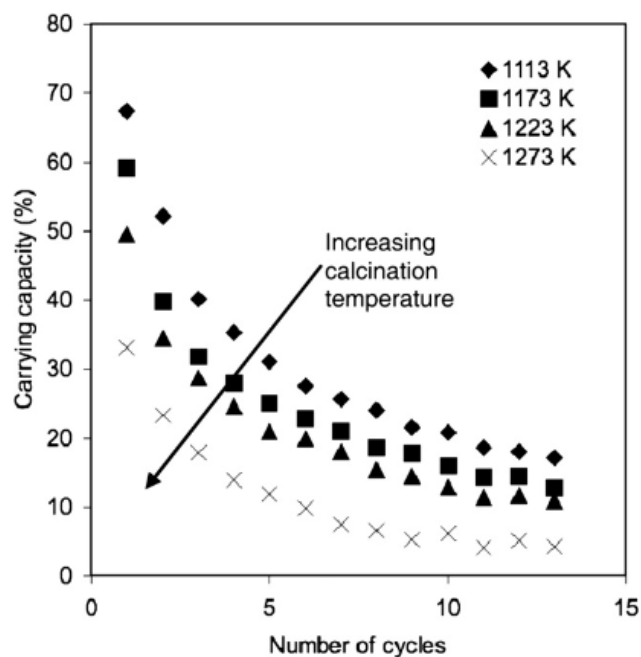


Figure 7 – Variation of the CO_2 absorption of CaO for various calcination temperatures [22].

To reduce the loss of efficiency research has focused in reducing crystallite size, changing pore structure, using inert phases and the use of hydration treatments [13]. Studies have shown that the crystallite or grain size of the CaO is inversely proportional to the CO_2 absorbed. Starting with a lower crystallite size or a grain morphology with higher specific surface area will therefore help to delay the sintering effect of particles. Grain growth reduces the specific surface area of the material and prevents the transfer of CO_2 molecules

into the material by creating a stable calcite layer [20]. At the same time, lowering the grain size is known to improve the toughness of materials [12].

Some of the most promising results in CaO for CC have been obtained through the addition of inert phases. These phases, obtained by mixing with Al_2O_3 , Yttria stabilized Zirconia (3Y-ZrO₂), Alkali Metals or TiO₂ among others, have shown the ability to improve the cyclic stability of CaO. Depending on the synthesis temperature, reaction of CaO with Al_2O_3 may form various phases including Mayenite ($\text{Ca}_{12}\text{Al}_{14}\text{O}_{33}$) and Aluminate ($\text{Ca}_3\text{Al}_2\text{O}_6$) [23]. Among these, Mayenite is the most present in literature due to an easier formation occurring at temperatures between 800 and 1000 °C [24]. The formation of this phase is possible due to the lower ionic radius of aluminum (Al) which may enter the CaO lattice structure [23]. This phase does not react with CO₂ yet it acts as a framework which binds CaO particles, preventing grain growth, and therefore maintaining the initial surface area. For instance, *Koirala et al.* [25] synthesized sorbents with Ca to Al molar ratios of 10:3 which showed stability after 100 cycles under normal conditions. The same authors also successfully prepared Calcium Zirconate (CaZrO_3) with a Ca to Zr molar ratio of 10:3 that resulted in a highly stable product yet having worse absorption properties. Further research showed that this is due to Zr ions occupying more space in the CaO lattice due to their larger ionic radius, preventing the entrance of CO₃²⁻ ions. Still, CaZrO_3 creates a perovskite structure that, as in Mayenite, prevents the grain growth of the CaO, stabilizing adsorption. In addition, inert phases also increase the Tammann temperature of the material, further decreasing the sintering of the CaO particles [23].

Recent investigations have also discussed improving CaO grain morphology to prevent efficiency loss across cycles. The most promising results have been observed when obtaining CaO from waste sources, calcium hydroxide ($\text{Ca}(\text{OH})_2$) or through acidic treatments. The first, CaO from waste resources,, will be analyzed later in **section 3.5**, due to its relevance. $\text{Ca}(\text{OH})_2$ is obtained from the hydration of CaO. After a dehydration treatment, grain morphology has shown to significantly increase the specific surface area. These hydration – dehydration treatments may be applied either before or during the CC

3D Printing of CaO for Carbon Capture

process. *Yoosuk et al.* [26] showed that the hydration – dehydration treatment reduces the crystallite size and modify the morphology of the grains effectively, by increasing the specific surface area and the material's reactivity with CO₂. Hydration of CaO is a spontaneous reaction used in the energy sector since it is exothermic and simple to reverse. This is due to the low enthalpy of the **equation 2** of -104 kJ·mol⁻¹. Ca(OH)₂ decomposes in between 500 and 550 °C at atmospheric pressures, as seen in **Figure 8**, meaning it is reversed at lower temperatures than that of the carbonation reaction [27]. Hydration treatments therefore require lowering the temperature under 500 °C or alternatively increasing vapor pressure for the CaO to react. Due to the reaction, if CaO comes in contact with water during its processing below 550 °C it will transform into Ca(OH)₂ [26].

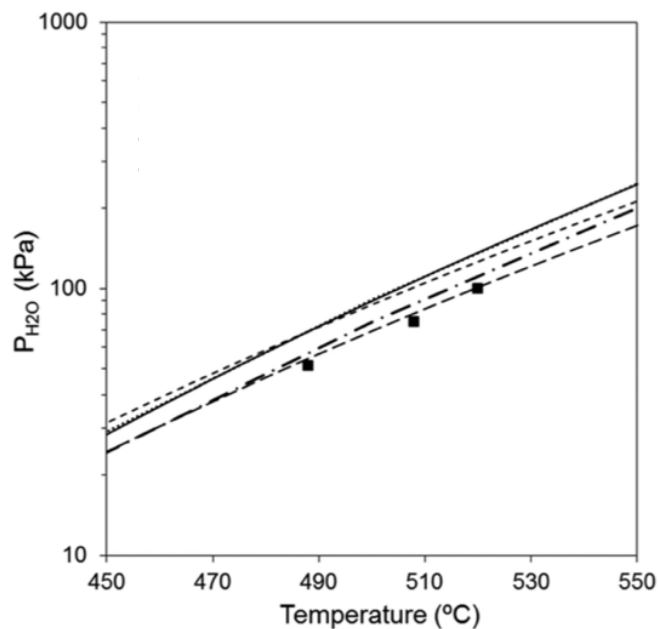
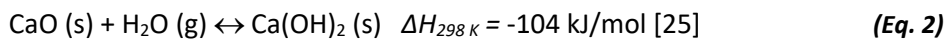


Figure 8 - CaO/Ca(OH)₂ equilibrium pressure at different temperatures [27].



CaO is also highly reactive with Sulphur dioxide (SO₂), forming Gypsum (CaSO₄). This product cannot be regenerated at the carbonation-calcination cycle temperatures, hence effectively deactivating the CaO. Regeneration of the CaO from Gypsum is not advised due

to sintering effect on particles. The use of CaO in CC is preferable therefore in atmospheres with low to no SO₂ [17].

3.4. Current use of CaO in carbon capture

The CC technologies most available for commercial use are based on amine scrubbing processes. These require a high energy input (4 GJ per ton of CO₂), and therefore have an elevated cost of around \$60/ton CO₂. To reduce these costs and therefore facilitate the introduction of CC technologies in the industry, several pilot projects have embarked in the use of CaO solid sorbent CC [19]. One of the most advanced projects is placed in the 1.7 MW_{th} coal plant of *La Pereda*, Spain [28]. This plant uses a Calcium Looping (CaL) process in a fluidized bed as seen in **Figure 9**. Even though it has shown good results, fluidized beds increase the price of installation and limit the use to large industrial complexes. Due to the loss of CaO caused by attrition and the loss of efficiency after each cycle, this set up also requires the periodic input of CaO from limestone. Even though the overall avoided CO₂ percentage is not stated for the case of *La Pereda*. *Nevertheless* similar cases have shown up to 90% reduction in the emitted CO₂, including the emissions generated by energy usage of CaL and liquification and storage of the CO₂ rich gas. Currently, real case scenarios carried out have accomplished much lower prices than ammine scrubbing processes, achieving prices under \$24/ton CO₂ [19]. Moreover, CaL has been proven to be less energy intensive than Ammine scrubbing processes. When translated to net efficiency losses of an industrial complex, ammine scrubbing has shown up to 14% net losses in power plants in comparison with the 7% net losses of CaL [29]. CaO use as a CC technology has shown therefore a promising start when put in place. However, a need to optimize the overall efficiency and reduce the loss per cycle, as well as being able to find economic ways to implement the technology is necessary to generalize CaO based CC.

3D Printing of CaO for Carbon Capture

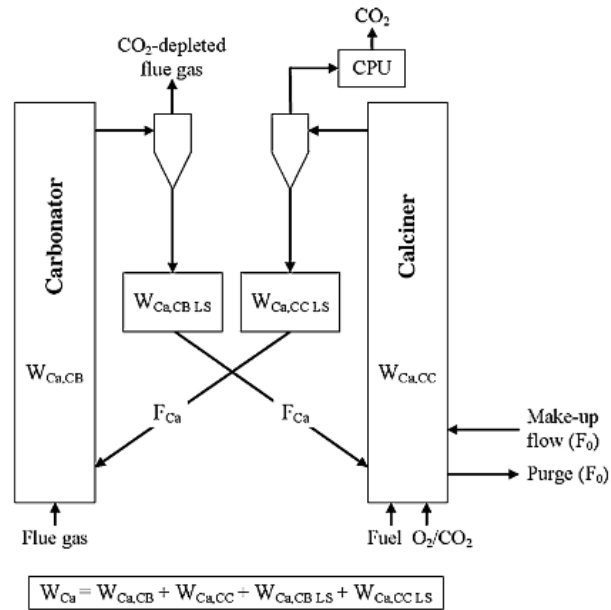


Figure 9 – Schematics representation of the post-combustion CC system placed at La Pereda 1.7 MW_{th} Carbon power plant [28].

3.5. CaO from waste sources

As commented in **section 3.2**, CaO from waste products have shown promising results as feedstock for CC technologies. CaCO₃ and Ca(OH)₂ can be found in multiple waste products such as lime-mud, mollusks or eggshells. From these, eggshells (ES) have attracted the most attention in CC as they are abundant worldwide, can be processed easily to give highly pure CaO, and show an optimum particle morphology for CC. ES waste has also become a concern due health issues derived from attracting rats and other vermin to landfills, as well as implying an extra cost for the companies [20].

Only in the United States of America (USA), more than 150,000 tones of ES waste are generated each year from industrial sources, 26% of which are discarded in municipal dumps [20]. ES waste has proved however to be an optimal source of CaCO₃. This is so as 94% of the eggshell is composed by CaCO₃, the rest being organic material. By maintaining the feedstock at 300 °C, together with lengthy treatments under low bleach concentration,

previous research has shown that a feedstock of over 99% purity can be achieved at low prices [20,30]. Moreover, an elevated surface area of around $4 \text{ m}^2/\text{g}$, and porous structure as seen in **Figure 10 (a)** results from these treatments [30]. Due to the higher surface area, more energy is needed to sinter the particles, which in term reduces the efficiency loss [16]. The interconnected pore structure enhances the diffusion of CO_2 as well as complicates the closing of the pores [32]. Still, as seen in **Figure 10 (b)**, the material is affected by sintering effects. Finally, CaO originating from ES have shown a better regeneration when hydration or acidic treatments are applied [31].

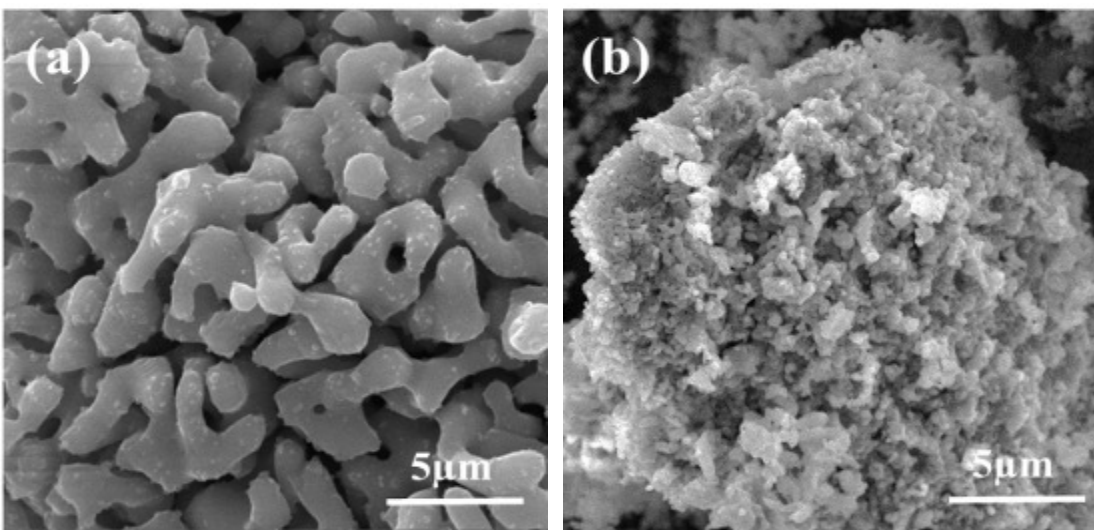


Figure 10 – SEM micrographs of (a) fresh calcined eggshell and (b) of eggshell after 20 carbonation-calcination cycles [31].

3.6. Additive manufacturing of ceramic materials

Ceramic materials used in catalysts applications range from biofuel to purification of water, showing high efficiencies. Still, due to limitation in the final product designs, their implementation in industries has been limited up to now. Recently, *additive manufacturing* (AM) has proven to be a solution to this problem. AM, also known as *Solid Freeform Fabrication* or *Three-Dimensional (3D) Printing*, is defined as the point by point, line by line, or layer by layer deposition of ceramic material according to a *Computer-Aided Design*

3D Printing of CaO for Carbon Capture

(CAD) [33]. Consequently, a great flexibility in the design of the product is achieved, maximizing heat and mass transfer, while obtaining a higher surface area. However, AM is a slower process that requires more technical equipment. Because of the advantages and limitations of the technique, the energy sector is optimum for the AM of ceramics [34].

AM of ceramics can be categorized depending on the form of the feedstock between: slurry-based, powder-based, and bulk solid-based. The first category involves the use of ceramic particles in a liquid or semi-liquid suspension, to later be solidified through photopolymerization, inkjet printing or extrusion [33]. Powder-based 3Dprinting, on the other hand, uses powder beds containing loose ceramic particles which are bonded together either through liquid binders or by means of fusion and sintering of the particles. Finally, bulk solid-based technologies can be subcategorized into laminated object manufacturing, where a laser cuts the material according to the design, or fused deposition modelling, where a filament with a high charge of ceramics in a polymer is extruded above the melting temperature of the polymer. The three families of AM first produce a green body followed by a sintering stage to obtain dense products. The techniques in AM and their processing are summarized in **Table 2** [33].

Out of these techniques, Direct Ink Writing (DIW) has shown the best results for ceramic AM in the manufacturing of complex shapes with good mechanical properties. DIW was originally patented by *Cesarano* under the name of “*Robocasting*”, consisting in the layer-by-layer deposition of a ceramic loading through a micrometrical nozzle. Concentrations of the ceramic charge can range from lower 2 up to higher than 70% of the ceramic ink, depending on the ceramic feedstock used. The rest of the paste consists of a solution containing an organic or inorganic binder. Among binders, Pluronic hydrogels are one of the most abundant suspensions for DIW. When looking at Pluronic hydrogels, the triblock copolymer polyethylene oxide-polypropylene oxide-polyethylene oxide (PEO-PPO-PEO) with a PEO:PPO ratio of 2:1, rather known as *Pluronic F127*[®], is the most widely used Pluronic [34]. In concentrations above 20% in an aqueous solution, *Pluronic F127*[®] shows a critical gel formation temperature, which marks the difference between a viscous gel and

a liquid at lower temperature. This viscous gel is able to retain a large concentration of ceramic charge, allowing for the manufacturing of complex shapes, which after sintering can reach densities up to 98% [35, 36, 37].

A key parameter in the DIW technology is the nozzle diameter. This depends on the particle size of the ceramic ink, as the nozzle must be at least three times bigger than the largest particle diameter, to avoid nozzle blocking. Smaller nozzle diameter leads to a higher specific surface area which in term leads to better chemical properties. In **Figure 11** a schematic diagram of the DIW process can be observed. DIW in catalysis has shown that rectilinear geometry with 50% infill is able to retain the gas up to 460% longer than commercial monolithic catalysts as found in Ref. [4]. Even though DIW has been studied abundantly in other ceramic materials, being researched in the field of catalysts prior to 2004, in the case of applications for CC, no information has been found [4, 38].

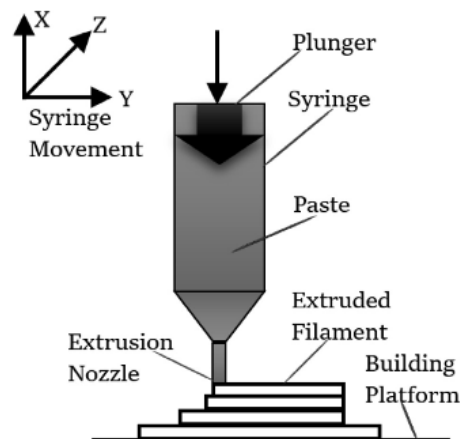


Figure 11 – Schematic diagram of the DIW or robocasting method [39].

3D Printing of CaO for Carbon Capture

Table 2 – AM techniques for ceramic materials, organized by feedstock form [33, 39].

Feedstock form	Technique	Summary of the process
Slurry-based		
	<i>Stereolithography</i>	Selectively cures a liquid surface containing photopolymerizable monomers. High ceramic loadings lead to possible segregation problems.
	<i>Two-photon polymerization</i>	Polymerization through the absorption of two photons used in nanotechnology.
	<i>Inkjet printing</i>	Method for creating two-dimensional figures.
	<i>Direct Ink Writing</i>	Extrudes a viscous paste at room temperature or similar through nozzles. The viscous paste allows for shape retention allowing for complex shapes. The higher the ceramic volume of the paste, the lower the shrinkage, allowing for sintered densities up to 90% of the theoretical.
Powder-based		
	<i>3D printing</i>	Technique not far from inkjet printing, using powder beds. Has shown difficulties obtaining dense structures.
	<i>Selective laser sintering</i>	Technique using a high-powered laser which sinters the particles it hits. It must be done under inert atmospheres and usually results in a high porosity.
Solid-based		
	<i>Laminated Object Manufacturing</i>	Generally, involves computer-controlled laser cutting and adhesion of multiple layers through heat and compression.
	<i>Fused Deposition Modelling</i>	A part polymer part ceramic composite filament is supplied to a nozzle where it is heated and extruded. Binder removal and sintering is needed for higher densities.

Equally important in DIW is the rheology behaviour of the ceramic paste. Higher ceramic charges lead to a higher viscosity, hindering the extrusion capacity of the printer, yet reducing shrinkage and improving mechanical properties. Hence, rheological properties can help to determine the optimal ceramic charge for DIW. To measure this charge, viscosity (η) is the most common parameter used. Apparent η relates shear stress (τ) with shear strain rate ($\dot{\gamma}$), as seen in **equation 3.1**. If the η is independent of the $\dot{\gamma}$, the material is said to be Newtonian. On the contrary, if η is not independent of $\dot{\gamma}$ the material is said to be non-Newtonian, following **equation 3.2**. If the η increases with increasing $\dot{\gamma}$, the behaviour is called *shear thickening*. The opposite behaviour is known as *shear thinning*. At

low or high strain rates, most liquids approximate Newtonian behaviour. Furthermore, most concentrated solutions show a combination of viscous response and elastic behaviour, known as viscoelastic behaviour. The shear modulus of such materials is often explained by **equation 4.1**, where G' is the storage modulus and G'' is the loss modulus. Then again, these parameters are dependent on the frequency and amplitude of the applied shear rate. Because of this, rheological measurements are usually done as a function of the shear stress, following **equations 3.5** and **3.6**. Here, G_p represents the pressure on the plate, ω the frequency and λ the relaxation time [36][4].

$$\tau = \eta * \dot{\gamma} \quad (\text{eq. 3.1})$$

$$\eta(\dot{\gamma}) = \frac{d\tau}{d\dot{\gamma}} \quad (\text{eq. 3.2})$$

$$G^* = G' + iG'' \quad (\text{eq. 3.3})$$

$$G'(\omega) = G_p * \frac{\omega^2 \lambda^2}{(1 + \omega^2 \lambda^2)} \quad (\text{eq. 3.4})$$

$$G''(\omega) = G_p * \frac{\omega \lambda}{(1 + \omega^2 \lambda^2)} \quad (\text{eq. 3.5})$$

4. State of the art

As previously pointed out, research in CaL has increased greatly derived from the need to find a sustainable, economic, and efficient CC technology, as expressed by Wang *et al.* [3] in “*Recent advances in solid sorbents for CO₂ capture and new developments*”. CaO has shown high uptake capacities, yet as previously explained, CaO suffers from sintering in the calcination step after extensive cycling. Summarized below are, a series of articles covering CaO in CC, CaCO₃ synthesis from eggshell waste, incorporation of inert phases in CaO - CC, and hydration of CaO for CC. This is done to contextualize and present the point from which this Bachelor’s project departs.

Wang, J. et al. Recent advances in solid sorbents for CO₂ capture and new development trends. At: *Energy and Environmental Science*. Royal Society of Chemistry, 2014, Vol. 7, núm. 11, p. 3478-3518. ISSN 17545706. DOI 10.1039/c4ee01647e.

This article is able to describe and compare the great majority of solid sorbent technologies for CC researched up to 2014. Wang *et al.* [3] assesses the technical viability, sorption capacity, durability and cost of more than 185 different materials. The authors also review which techno-economic conditions are necessary to make CC a widespread technology, from which they center in the cost of the materials, the selectivity of the material towards CO₂, and their durability. Finally, the work emphasizes the waste and benefits potentials derived from CC technologies in real industrial applications such as in the energy or cement industries.

Sun, H. et al. Progress in the development and application of CaO-based adsorbents for CO₂ capture—a review. At: *Materials Today Sustainability*. 2018, Vol. 1-2, p. 1-27. ISSN 25892347. DOI 10.1016/j.mtsust.2018.08.001.

The authors of this article centered their review on the challenges facing CaO - CC technologies and the solutions being proposed up to 2018. Among the challenges, the article focuses on the problems derived from the formation of a stable calcite layer, and

those derived from the sintering of particles. In this section, a comparison on the models explaining each problem is done, as well as how different carbonation and calcination parameters seem to affect the process. The article also talks extensively about current research to reduce these problems, explaining how grain size reduction, increasing surface area or addition of inert phases have shown promising results. From these results, the use of Al_2O_3 mixed with CaO in different compositions seems to have shown the highest resistance to elevated number of cycles without reducing the CC efficiency drastically. *Sun et al.* [16] also deliberates on possible treatments to restore spent CaO efficiencies such as hydration or acidic treatments. Finally, the article discusses the techno-economic aspects of CaO - CC and its possible applications, concluding that this technology is able to reduce prices greatly, yet further investigation is needed to evaluate the proposed solutions to the sintering effect.

Witton, T. Characterization of calcium oxide derived from waste eggshell and its application as CO₂ sorbent. At: *Ceramics International*. 2011, Vol. 37, núm. 8, p. 3291-3298. ISSN 02728842. DOI 10.1016/j.ceramint.2011.05.125.

Witton explains in said article the potential of CaO derived from eggshells to replace amine-based CC technologies [20]. The article analyzes a series of parameters including specific surface area, crystallite size and weight change in calcination – carbonation cycles. In all the stated parameters, eggshell waste derived CaO showed better properties for reaction purposes in comparison with commercially available CaCO_3 feedstock. Because of the lower crystallite size and higher surface area, ES derived CaO showed a greater adsorption capacity and greater stability at larger number of cycles, as seen in **Figure 12**. Finally, the article concludes that the adequate carbonation and calcination temperatures are 700 and 900 °C respectively.

3D Printing of CaO for Carbon Capture

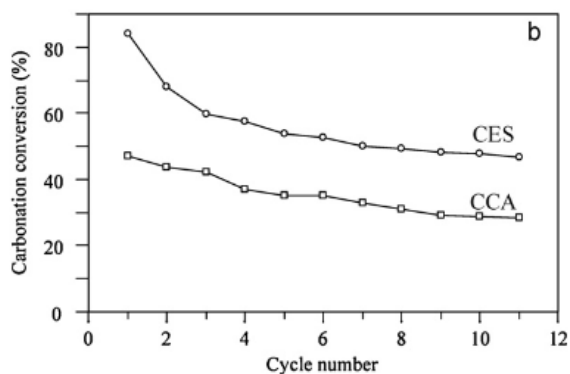


Figure 12 – Calcination conversion with number of cycles for calcined eggshell (CES) and commercially available CaCO_3 (CCA) [20].

Cree, D. i Rutter, A. Sustainable Bio-Inspired Limestone Eggshell Powder for Potential Industrialized Applications. At: *ACS Sustainable Chemistry and Engineering*. 2015, Vol. 3, núm. 5, p. 941-949. ISSN 21680485. DOI 10.1021/acssuschemeng.5b00035.

Eggshell use for CC requires for a low-cost, sustainable, and a feasible way to scale up its conversion to either CaO or CaCO_3 . The research carried out by *Cree et al.* [30] in this article is centered exactly on this topic. The article compares the synthesis of CaCO_3 through either temperature or acid treatments, to obtain the highest purity possible by analysis using X-Ray Diffractometry (XRD) and Scanning Electron Microscope (SEM). It concludes that the optimum heat treatment for the removal of all organic parts is of 300 °C during 2 hours, obtaining similar results to the treatment under a 10% bleach solution for 48h. Bleach treatment was deemed unsustainable though. CaCO_3 with purity of above 98% was obtained in this article.

Hu, Y. et al. Incorporation of CaO into inert supports for enhanced CO_2 capture: A review. At: *Chemical Engineering Journal* [online]. Elsevier, 2020, Vol. 396, núm. April, p. 125253. ISSN 13858947. DOI 10.1016/j.cej.2020.125253.

Hu et al. [23] focus in this article in the different approaches that have been taken to enhance CO_2 capture using inert phases in CaO up to 2020. The article first describes the various methods that have been used to ensure the dispersion of the inert supports in CaO

sorbents. Among these, it outlines the Sol-Gel, Flame-Spray Pyrolysis, and physical mixing techniques as both the most popular and effective. The authors continue by describing various inert materials that have been studied to enhance CC. The researchers conclude that Al and Magnesium (Mg) solid solutions in CaO are the most cost-effective techniques while being abundant in the earth.

5. Goal

CC technologies face a great challenge in having to be able to be implemented in the industry in a fast manor, at low cost and with high efficiencies. DIW has shown to have the potential to obtain the above goals. Therefore, the long-term goal of this Bachelor's degree project is to **obtain a feasible process to manufacture porous CaO scaffolds through DIW technique to enhance efficiencies in the sequestration of CO₂.**

Furthermore, the project wishes to minimize its environmental impact by using eggshell waste and zirconia from industrial waste as a raw materials.

To achieve such goal, the project is divided among 3 secondary goals:

- i. Determine the optimum way to convert eggshell waste to CaCO₃ and CaO.
- ii. Determine the **optimum CaO based feedstock** for DIW among CaZrO₃, Ca₁₂Al₁₄O₃₃, Ca(OH)₂, CaO and CaCO₃, and their corresponding **optimal synthesizing method** as well as characterization of all the powders.
- iii. Determine the **optimum DIW parameters** for those feedstocks adequate for 3D printing.

6. Experimental procedure

The experimental procedure of this Bachelor's project has been subjected to constant changes due to the little prior information about conformation of CaO both through conventional as well as AM conforming techniques. In this section, the procedure followed is explained, including those processes that were discontinued. This is done to clarify the path taken to reach the project's results.

6.1. Elaboration of CaO and CaCO₃ from eggshell waste

Initially, ES waste from the researchers participating and other members of the UPC community was collected (see **Figure 13 (a)**) and treated initially under a 5% bleach treatment for 48h, as seen in **Figure 13 (b)** [30]. After this, the ES was washed under deionized water for 60, 120, 240, 480 s. Hereinafter, these treatments will be alluded as *F1*, *F2*, *F3*, and *F4* respectively. Next, the ES were dried at 70 °C for 3 hours to eliminate all humidity (**Figure 13 (c)**). The ES was crushed by hand until submillimeter size in an Agate mortar, and subsequently, the thermal treatment (TT) was applied (**Figures 13 (d)** and **(e)**). Such treatment consisted in increasing the temperature to 300 °C for 2 hours to eliminate all resting organic matter, then increasing up to 900 °C and held constant for 3 hours. The heating rate was kept constant at 5 °C·min⁻¹, while cooling was done in the oven, following the TT presented in Refs [40, 41].

When withdrawn from the oven, the powder was hand-milled again in the Agate mortar. Due to the porosity of the powder, and as explained in the results **Section 7.1.2** obtained from scanning electron microscopy (SEM) micrographs and Laser Diffraction (LD), the resulting powder's size was small enough so that no further mechanical milling was needed. Subsequently, the characterization of the ES feedstock was done by means of SEM, laser diffraction and X-Ray Diffraction (XRD) to find the optimum cleaning method of the ES.

3D Printing of CaO for Carbon Capture

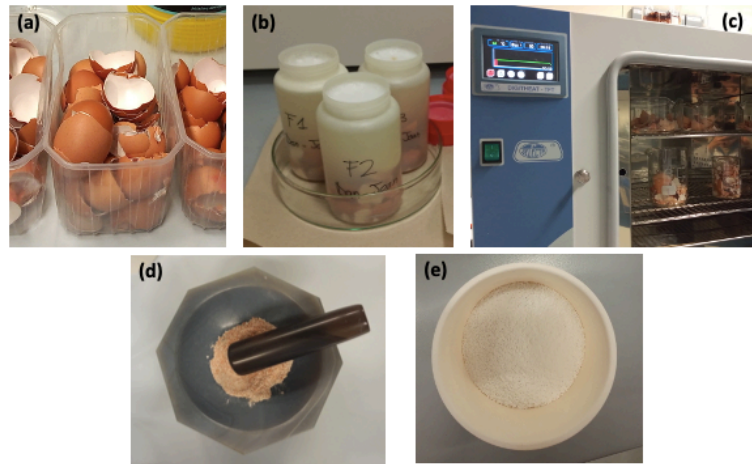


Figure 13 – Pictures of the process followed to obtain a high purity CaO. (a) Initial ES, (b) bleach treatment, (c) drying of ES, (d) initial hand milling and (e) feedstock after calcination.

As it will be explained in **Section 6.6**, when elaborating samples made of CaO, problems derived from the reaction with H₂O molecules in the air lead to disintegrate the material. To solve this problem, the initial feedstock was changed to calcite, inert at ambient conditions. Furthermore, ES waste was also brought from the University of Birmingham, after undergoing a centrifuge treatment to separate the ES from the organic membrane. Finally, the feedstock was previously sieved, being given a powder with particle sizes under 80 μm. To ensure pure CaCO₃, the powder was processed at 300 °C during 2 hours with a heating and cooling speed of 10 °C·min⁻¹. Finally, characterization of this feedstock was done following the protocol presented in [30]. The ovens used for this Bachelor degree consisted in a *Nabatherm* oven which withstood temperatures of up to 3000 °C (see **Figure 14 (a)**), and a *Energon MEC-14* oven that withstood temperatures up to 1400 °C (see **Figure 14 (b)**).

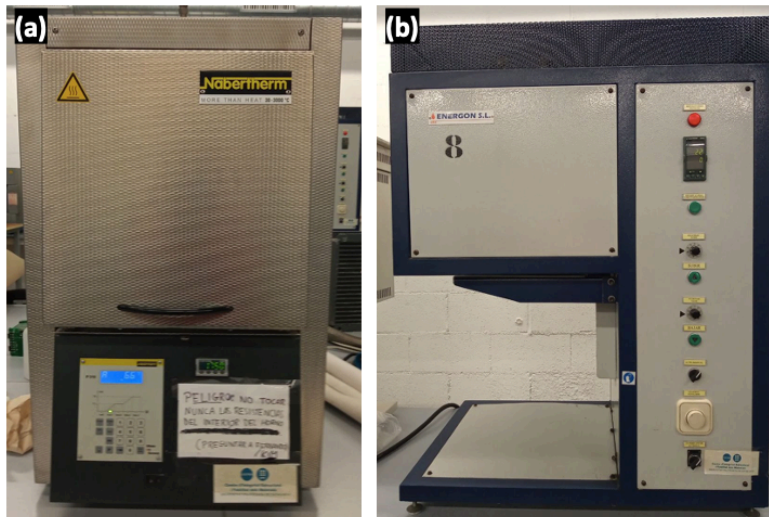


Figure 14 – (a) Nabatherm and (b) Energon ovens used in this Bachelor's project.

6.2. Commercial CaO

The calcined CaO from ES waste was then compared with commercial CaO (CaO-b). The data sheet for the bought CaO can be seen in **Annex A1**. The analysis was done using SEM, XRD, and LD analysis.

6.3. $\text{Ca}_{12}\text{Al}_{14}\text{O}_{33}$ synthesis

To synthesize Mayenite, $\alpha\text{-Al}_2\text{O}_3$ was wet-milled with the CaO from ES sources. A *Turbula*[®] mixer (see **Figure 15**) was used for this. Furthermore, Ytria Stabilized Zirconia (Y-TZP) balls were used, with a diameter of 5 mm, in an ethanol solution for 12 hours at 100 rpm. A ball to powder mass ratio of 5:1 was prepared following examples in literature [42]. Finally, different Al to Ca molar ratios of 1:10, 2:10, 3:10 and 4:10 were prepared to ensure the right amount of Mayenite phase in the CaO. Henceforth, such ratios will be referred to as *Al 1/10*, *Al 2/10*, *Al 3/10* and *Al 4/10* respectively.

The powder was dried using the rotary evaporator setup seen in **Figure 16**, followed by drying in an oven at 100 °C for 24 hours. Subsequently, the powders were sintered at 800

3D Printing of CaO for Carbon Capture

°C for 2 hours with a heating and cooling rate of 3 °C·min⁻¹ [23,35]. Characterization of all the powders was done using XRD, LD and measuring the weight loss during sintering.

The α -Al₂O₃ was bought from *Almatis* with over 99.8% purity, specific surface area of 7.8 m² g⁻¹ and particle size distribution with 90% under 2.0 μm, as specified in the data sheet of the product in **Annex A2**.

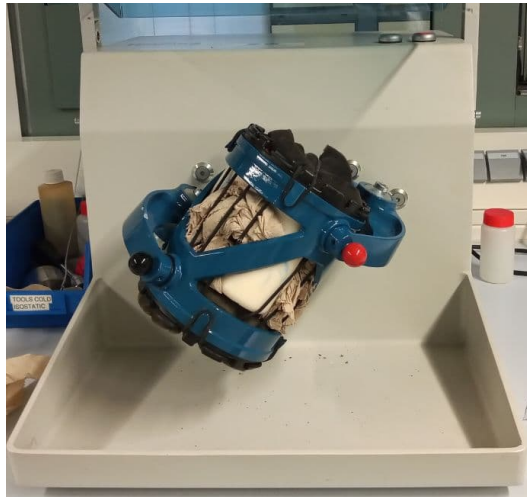


Figure 15 – Turbula® ball mill used in this Bachelor's project.

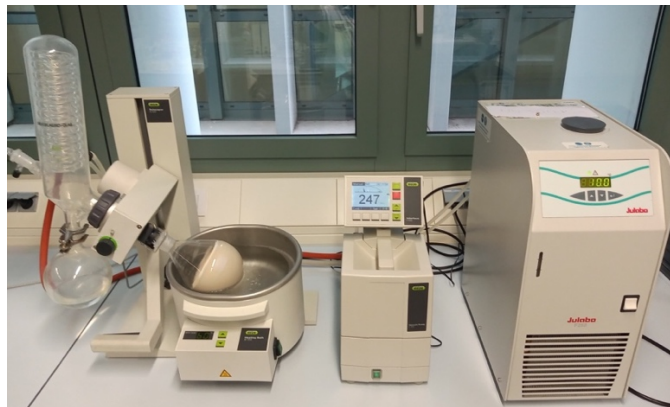


Figure 16 – Rotary evaporator set-up used to dry the powders after ball milling.

6.4. CaZrO₃ synthesis

CaZrO₃ was also obtained through wet milling. ZrO₂ from waste sources were mixed with the CaO from the ES. Three different types of Zirconia powder coming from different industrial wastes were supplied by *Sant Gobain - Research Provence (Cavaillon, France)* (see

Table 3). Data sheet for the powders from which the three wastes originate is found in **Annexes A3** and **A4**. First, these were analysed using SEM, XRD and LD. Once the optimum waste source was chosen, the same parameters and procedure as for the synthesis of $\text{Ca}_{12}\text{Al}_{14}\text{O}_{33}$ was used to make $\text{CaZrO}_3 - \text{CaO}$ powders. Finally, Zr to Ca molar ratios of 1:10, 2:10 and 3:10 were used to ensure the right amount of CaZrO_3 phase in the CaO without negatively affecting the CC process [43]. Henceforth, such ratios will be referred to as *Zr 1/10*, *Zr 2/10*, and *Zr 3/10* respectively.

Table 3 – ZrO_2 Industrial residues used, and the initialism chosen to represent it throughout this Bachelor's project.

Industrial Source	Initialism
GY3Z R60 Granules	R60
Dry Powder CY3Z RA	RA
GY3Z – R60	R60C

6.5. $\text{Ca}(\text{OH})_2$ synthesis

$\text{Ca}(\text{OH})_2$ feedstock was prepared by mixing at 60°C for 6 hours CaO with distilled water, after which the same distillation process followed for the synthesis of Mayenite was followed to obtain pure dry powders [26].

6.6. Feedstock and microstructural characterization

As part of feedstocks came from natural waste, powder characterization was essential to ensure purity and to know its properties. This was done by dividing the analysis among microstructural observation and by checking the initial composition analysis through SEM. Next composition, phase, and crystallite size was seen through XRD. And finally, particle size distribution through LD.

3D Printing of CaO for Carbon Capture

6.6.1. Scanning Electron Microscope

Scanning Electron Microscope (SEM) was used in the process of feedstock characterization as well as analysis of thermal treatments effects and DIW products. The SEM consists of an electron beam that scans a surface. These electrons hit the surface at high energies, causing part of the electrons within 20 nm of the surface to be expelled from their orbit. These can either be secondary electrons (SE) or back-scattered electrons (BSE). SE are created when the beam hits electrons close to the nucleus. As these have low energy, only those coming from within 2 nm of the surface are detected. BSE occur when the beam hits the atoms nucleus in a straightforward manner, causing the electrons to be repelled in the opposite direction. These can be measured from atoms up to 300 nm below the surface [44]. The shot electrons also provoke X-Ray scattering, called Energy-Dispersive X-Ray (EDS). EDS analysis can show qualitative and semiquantitative results with an accuracy of around $\pm 5\%$, by knowing the characteristic wavelength or wavelengths that each element emits [36]. From here, the computer analyzes relative X-Ray counts for each wavelength and can give the compositions for each sample. For this Bachelor's project a *Phenom XL Desktop* SEM equipment was used, as can be seen in **Figure 17**.



Figure 17 – SEM equipment used in this Bachelor's project.

As a beam of electrons is used, the surface of the material analyzed must be conductive or semiconductive to avoid accumulation of charge. For CaO and CaCO₃ it is necessary to cover the sample with a conductive coating. In this Bachelor's project a carbon coating was

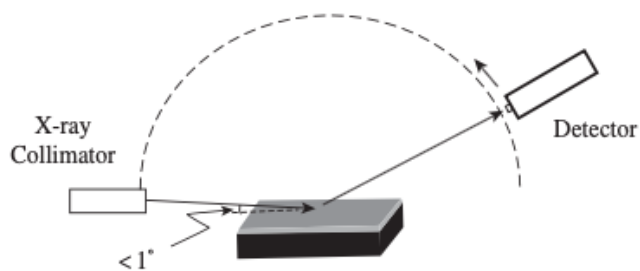
applied over the samples by using an *Emitech K950X* carbon coating equipment (see **Figure 18**).



Figure 18 – Carbon Coating equipment for SEM analysis.

6.6.2. X-Ray Diffractometry

X-Ray Diffractometry (XRD) is one of the most used techniques in materials characterization. Its main purpose is to analyze crystal structure of both powder and manufactured samples. In this technique, an X-Ray beam of a single wavelength is directed at the sample changing the incident angle continuously and analyzing the diffracted intensity, as can be seen in **Figure 19**. By doing so, XRD allows us to determine the crystal structure, crystallite size and the purity of the sample. XRD can only detect phases though with compositions higher than 1-5%, depending on the equipment used. The equipment used in this Bachelor's project was a *D8 Advance D83* using a *Linx Eye* detector (see **Figure 20**). The measurements were taken from 20 to 100 ° (2θ) with step-size of 0.01 °.



3D Printing of CaO for Carbon Capture

Figure 19 – Optical arrangement followed in XRD measurements [45].

To analyse the crystallite size, the Scherrer equation (**equation 5**) was used for the most intense peak, where d is the mean crystallite diameter, λ is the X-ray wave length (1.5405 Å for this Bachelor's project) and B is the full width at half of the maximum [20]:

$$d = \frac{0,89 \cdot \lambda}{B \cdot \cos\theta} \cdot \frac{180^\circ}{\pi} \quad (\text{eq. 5})$$



Figure 20 - D8 Advance D83 EDX equipment used in this Bachelor's project.

6.6.3. Laser Diffraction

CaO in CC and, more importantly, DIW, require knowing the particle size distribution of our feedstock. This can be figured out using LD. This technique is based on a laser of known wavelength impacting a solution with particles of the feedstock. Knowing the index of refraction of the liquid and of the phase of the particles in the feedstock, the machine calculates the particle size distribution from the diffraction of the laser. The equipment used for this Bachelor's project consisted of a *Mastersizer 3000 Hydro EV* (see **Figure 21**), which uses a He-Ne laser with $\lambda = 632.8$ nm (red light) and 470 nm (blue light). The equipment measures with both wavelengths separately to get more accurate

measurements. For the measurements, feedstock was inserted so obscuration would be found between 5 and 10% for red light. The measurements were done in water when the feedstock was CaCO_3 and in ethanol solution when CaO was analysed. This was done setting the mixing pace at 3000 rpm, measuring both with and without ultrasounds.



Figure 21 – Mastersizer 3000 Hydro EV laser diffraction equipment used in this Bachelor's project.

6.7. Uniaxial pressing and Cold Isostatic Pressing

As can be observed in **Figure 22**, CaO samples reacted with water molecules in the air, leading to desintegration of sintered pellets fabricated by uniaxial pressing and cold isostatic pressing (CIP). With this knowledge, this Bachelor's project set itself the goal of obtaining a feedstock that once sintered would not loose mechanical stability in air. Hence, pellets from the various feedstocks were fabricated by Uniaxial pressing followed by CIP using a CIP-30MA YLJ-20TA Machine from MTI Corporation, as seen in **Figure 23**.



Figure 22 – Sintered CIP samples breaking (left) and enlarging after reacting with water vapor in the air in comparison with unreacted sample (centre tablet).

3D Printing of CaO for Carbon Capture

Pellets were manufactured initially using a 42 MPa force for Uniaxial pressing for 30 seconds. If pellets broke when withdrawn, lower forces and longer periods of time were used. This happened for $\text{Ca}(\text{OH})_2$ and CaO-Al based feedstocks, where 17 and 25 MPa had to be applied respectively during 60 seconds to prevent premature fracture. Next, CIP was applied using a 120 MPa force during 60 seconds. Pictures were taken throughout the process to justify whether each feedstock would be deemed adequate or not for the CC and DIW process.



Figure 23 – CIP machine used in this Bachelor's project.

6.8. Sintering Process

The temperature and time at which calcite converted completely to CaO was deemed to be the synthesis temperature for all samples. This was figured out by heating calcite at $3\text{ }^{\circ}\text{C}\cdot\text{min}^{-1}$ up to the desired temperature, maintained for 2 hours, and then cooled down inside the oven. Sintering of the feedstocks was done starting at $500\text{ }^{\circ}\text{C}$, after which the sample was analyzed under XRD, SEM and LD. If the feedstock was determined to not be completely calcined, the treatment was repeated at $50\text{ }^{\circ}\text{C}$ above the previous temperature.

Once the temperature was known, samples prepared through uniaxial and CIP were sintered and stored for 1 week in air. After this period, if the samples proved to be mechanically stable, i.e. did not disintegrate, they were deemed adequate for 3D printing.

Once the adequate feedstock for AM was found, sintered samples were kept at low vacuum by means of the manual vacuum sealer of **Figure 24**.

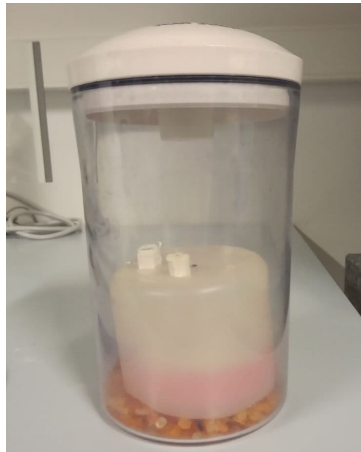


Figure 24 – Manual vacuum sealer used to reduce interaction between samples and air.

6.9. Post-Sintering Treatment

To maintain structural integrity of the printed samples, the following post-sintering treatments were done on the CaCO_3 feedstock printed samples:

- Standard:** Sample that after sintering had no treatment done.
- Oil bath:** Samples were dipped in oil for 5 minutes after sintering.
- Ethanol bath:** Samples were stored in high purity ethanol obtained through distillation from ball-milling.
- Lacquer:** Lacquer was thoroughly applied over the samples on all sides after sintering.
- Carbonation:** Incomplete carbonation of the sintered samples was done to obtain an outer inert calcite layer. This was done by passing a 100% CO_2 gas flow of 50

3D Printing of CaO for Carbon Capture

$\text{mL}\cdot\text{min}^{-1}$, from 700 °C down to 550 °C in the cooling of the sintering process. The rest of the cooling was done in this CO_2 atmosphere.

6.10. Sample characterization

Characterization of sintered pellets deemed mechanically and chemically stable was to be done in terms of density, Vickers hardness, indentation fracture toughness and *SEM* analysis. Unfortunately, as finding the adequate feedstock that would not react in air took longer than expected, no measurements were taken for this section. Nevertheless, they are explained as for future investigations should carry them out.

6.10.1. Polishing

Prior to microstructurally and mechanically characterize, the surface should be polished until reaching a mirror-like surface. Due to the reaction between CaO and water, fine polishing using diamond and Al_2O_3 aqueous solutions could not be done. Rough polishing using sandpaper together with ethanol was tested, yet finally discarded as surface tensions seemed to enhance the reaction with water in the air, as can be seen in **Figure 25**, where the CaO broke the Bakelite where it was held two days after rough polishing. For this reason, even though mechanical properties measured were to be less reliable, polishing was disregarded to reduce possible contamination of samples.

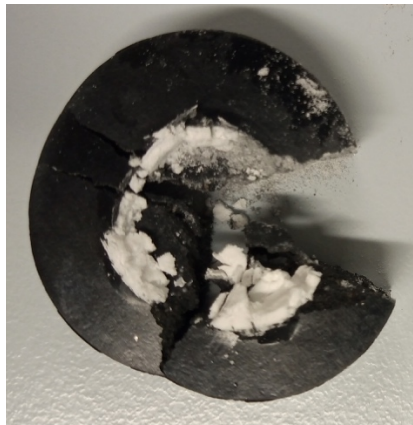


Figure 25 – Picture taken of CaO sample that reacted with water, inducing the induced fracture of the Bakelite where it was held.

6.10.2. Microstructural characterization

Using the *SEM* microscope (see **section 6.6.1**), a qualitative analysis was be done to compare the morphology of different sintered printed cubes, to observe the different printing defects and be able to quantify them. This comparison was to be carried out at the same magnification to ensure maximum objectivity. Next, density was to be measured to understand the porosity of the samples.

6.10.2.1. Density

Density is an important parameter in AM as a minimum of 20% of the sample will initially be hydrogel and therefore it is expected to have low densities. This is significant as mechanical properties depend largely on the final density of the product.

As CaO reacts with water, density had to be measured in ethanol. To do so, equipment such as the Mettler Toledo XS3035 Archimedes balance can be used, as seen in **Figure 26**. This equipment bases its operation on measuring the mass of the sample both outside and inside the liquid, and by knowing the temperature it is working at, give a precise density measurement, using **Equation 3.9**. As ethanol is used, it is essential to measure with the glass enclosure shut to prevent evaporation of the liquid.

$$\rho = \frac{m_A}{m_A - m_W} * (\rho_L - \rho_0) + \rho_0 \quad (\text{Eq.6})$$

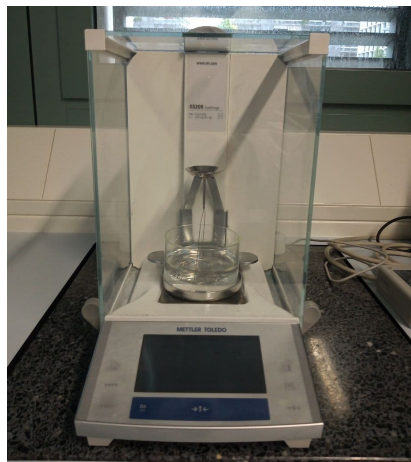


Figure 26 – Mettler Toledo XS3035 Archimedes balance used in this bachelor's project.

6.10.3. Mechanical properties

Mechanical properties of the sintered samples were to be measured through a Vickers hardness (HV) test. To do so, a *DuraScan 65* from *emcoTest* equipment would be used, as seen in **Figure 27**, which measures at the micrometric scale. *HV* is measured using a Diamond-pyramid indenter as the one seen in **Figure 28 (a)**, and weight as the variable for the applied load (P). Measuring the size of the diagonals (d_1 in **Figure 28 (b)**), and using **equation 6**, the machine gives the results in *HV*. *HV* should be measured for those sample that did not disintegrate after being stored for 1 week. For one of the samples sintered at the desired temperature and ceramic feedstock, the process was to be done using loads from 0.01 up to 5 Kgf. As a result, it would be expected to see that the *HV* would stabilize above a certain weight. The rest of the samples should be measured using this weight.



Figure 27 – *DuraScan 65* Vickers microhardness equipment used in this Bachelor's project.

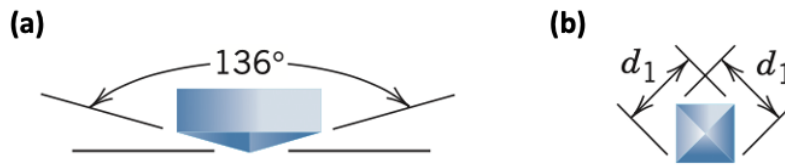


Figure 28 – (a) Shape of a Vickers indentation tip and (b) theoretical mark done by the indenter [44].

$$HV = \frac{1,854 \cdot P}{d_1^2} \quad (\text{eq. 7})$$

In brittle materials such as CaO, the indentation fracture toughness (K_{Ic}) can be estimated with a high certainty through indentation tests. This is based on the principle that the applied stress caused by the indenter is equal to the critical stress intensity for crack propagation. By knowing the hardness value for the indentation (H), the total width of the cracks caused by the indentation from the center (c), and the applied load (P), the K_{Ic} value can be obtained. In **Figure 29**, the parameters c and α can be visualized. Even though there have been numerous derivations for semi-empirical formulas, the **equation 8** derived by Anstis *et al.* [46]

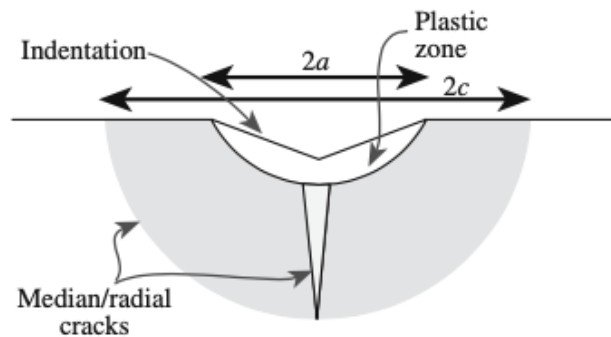


Figure 29 – Cracks at an indentation that allow for the measurement of K_{Ic} [12].

$$K_{Ic} = \frac{\alpha \cdot (E/H)^{0.5} \cdot P}{c^{3/2}} \quad (\text{eq. 8})$$

6.11. Ceramic Inks and 3D printing procedure

As there was no previous information about Ca based inks for DIW processing, an initial stage of finding the adequate hydrogel (for CaO feedstock) and ceramic charge was needed.

6.11.1. Ceramic inks fabrication

Ceramic inks used for DIW, as explained previously in **section 3.6**, require the mixture of the feedstock with an hydrogel to produce a viscous paste that can both be printed and hold its shape once manufactured.

Initially, as the intention was to print using CaO powder, a non-aqueous hydrogel was investigated. Following on the research done by *Chaibundit et al.* [47] and *Pandit et al.* [37], a series of experiments with hydrogels based on ethanol and propylene glycol were done, including using different Pluronic F-127® concentrations and varying its temperature from 100 °C to below 10 °C. The most promising results observed were for 3 parts propylene glycol, 2 parts Pluronic mixture, which formed a highly viscous gel above 65 °C, below which it liquified and then solidified below room temperature. This would have required changing the printing parameters, which also due to the difficulties explained previously brought using CaO, was disregarded [37, 47].

The hydrogel used for the CaCO₃ and CaO with inert phases feedstock paste was made from an aqueous solution of Pluronic F-127®, in a 1:4 water to Pluronic ratio. After mixing for 10 minutes at 3500 rpm, the gel was stored in the fridge at temperatures around 4 °C for 24 h so it would liquify due to its inverse rheology [4]. The ceramic paste meant for printing was done by mixing the feedstock with the prepared hydrogel. As the optimal concentration was unknown, ceramic percentages of 60, 65, 70, 75 and 80 % of ceramic charge were made, by means of the *SpeedMixer* (see **Figure 30**) during 1 minute at 3500 rpm to obtain an homogeneous mixture [4].



Figure 30 – SpeedMixer™ used in this Bachelor's project

6.12. 3D Printing Process – DIW

The DIW technique was done using a 3D printer prototype made by the *CIM-UPC* foundation, as can be seen in **Figure 31 (a)**.

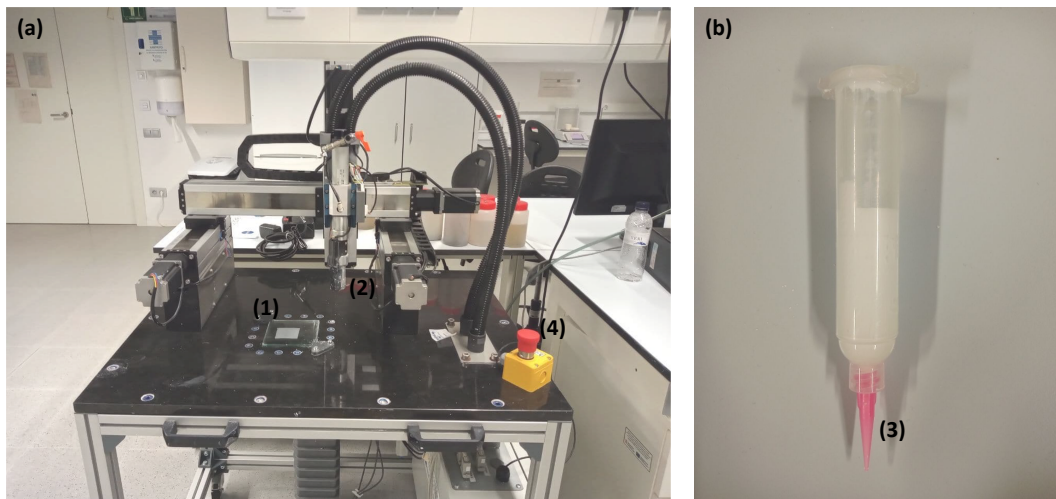


Figure 31 – (a) DIW printer used for this Bachelor's project and (b) Printing syringe.

The most important parts of the printer are briefly explained:

3D Printing of CaO for Carbon Capture

- a) **The printing bed**, labelled as (1) in *Figure 31 (a)*, is where the printer extrudes. To minimize adhesion of the printed pieces to the bed, a paraffin film was layed onto the bed for each piece.
- b) **Printing head**, labelled as (2) in *Figure 31 (a)*, has the syringe that holds the paste, as well as exerts the force to extrude it. In *Figure 31 (b)*, the syringe with the paste can be visualized before being placed into the printing head.
- c) **Nozzle**, labelled as (3) in *Figure 31 (b)*. The chosen diameter of the nozzle for this Bachelor's project was of 420 μm .
- d) **Emergency stop button**, labelled as (4) in *Figure 31 (a)*, to be used when any error that could damage the machine.

The DIW procedure is affected by environmental conditions, mainly humidity and temperature. As for temperature, all printed samples were done at room temperature. Note that ideally ceramic ink was to be done not long before printing to avoid drying. The samples were then stored in a chamber with a controlled humidity of above 70 %. These were stored here for a minimum of 72 h, measuring their mass frequently. This was done to know the time needed for the samples to dry, seen in a stabilization of the mass.

7. Results and discussions

The results obtained are discussed below, paying special attention to the properties that benefit a possible CC technology; simple and scalable procedures, high surface area, and structural and chemical stability.

7.1. Synthesis of feedstocks

7.1.1. CaCO₃ synthesis

XRD and LD analysis of the received ES waste, as well as weight loss due to burning of organic matter led to the conclusion that the received waste was up to 97.8% calcite by weight. Treatment at 300 °C caused a weight loss of 2.2 ± 3.0 %. This percentage can be attributed to both organic residue in the waste and resting humidity. When the treated ES was analyzed in XRD (see **Figure 32**), all peaks coincided with CaCO₃ calcite peaks found in literature (see **Annex B**) with a maximum discrepancy of 0.7 ° for the smallest peaks at higher ranges. Since XRD can omit up to 5% of existing elements, as explained in **section 6.5.2**, the optimal cleaning procedure of ES was determined with the additional help of SEM analysis in the next sub-section. LD results show at least two peaks coinciding at particle sizes under 100 μm with crests at approximately 4 and 33 μm (see **Figure 33**), which would be optimal for the correct printing due to the small diameter of the nozzle.

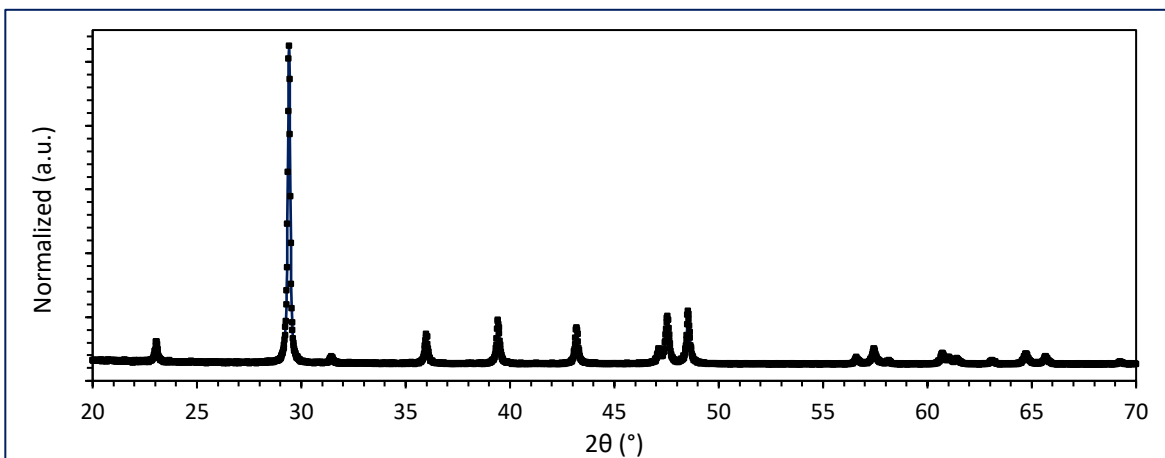


Figure 32 – XRD spectrum for treated ES.

3D Printing of CaO for Carbon Capture

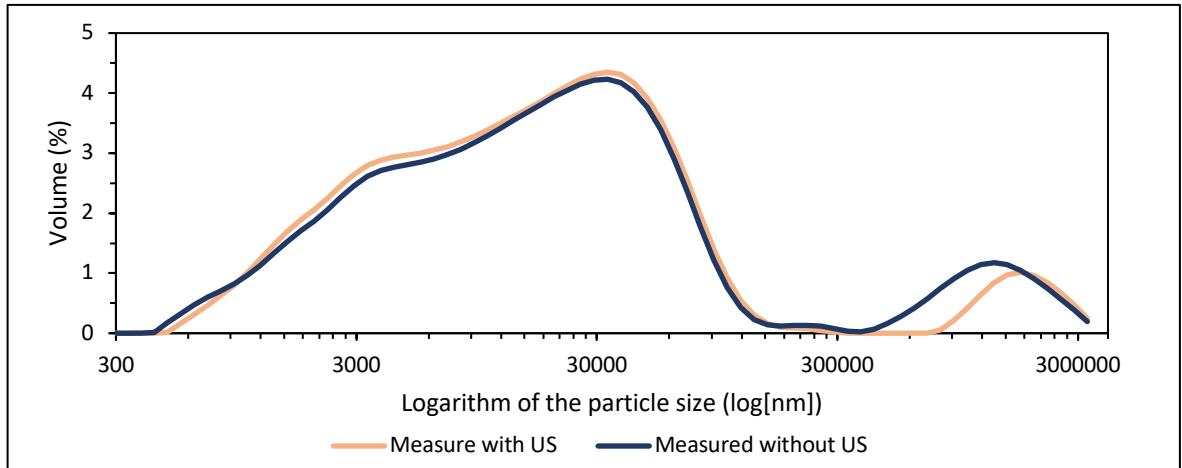


Figure 33 – LD results for CaCO_3 (calcite) synthesized from ES waste.

Further analysis of the brought feedstock was done using the SEM. First, the particle morphology was observed (see **Figure 34**), where particles of up to 20 μm were observed together with sub-micrometrical particles. Furthermore, an EDX analysis of the composition was done, which confirmed a high purity feedstock with only MgO as possible impurity (see **Figure 35**), optimal for CC as MgO also serves as a phase to aid CC [23]. Still, further purity was attempted (see **section 7.1.2**).

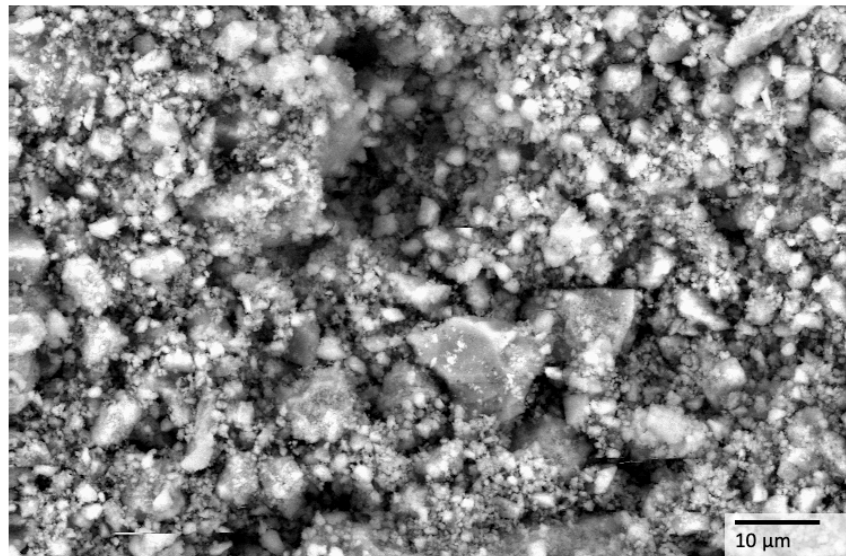


Figure 34 – SEM micrograph of ES waste before calcination.

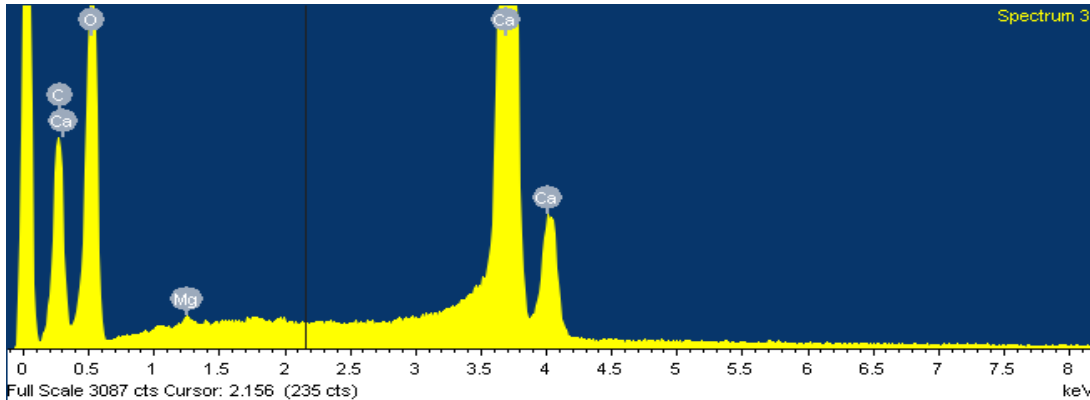


Figure 35 – EDX analysis intensity spectrum of ES waste.

7.1.2. CaO synthesis from ES

Following the protocol presented in **section 4.1**, CaO was obtained from ES origin. These steps were taken prior to observing the high reactivity of CaO with water molecules in the air, which is why synthesis of CaO instead of CaCO₃ was targeted. The XRD results for the different cleaning times can be seen in **Figure 36**. When compared to results in the bibliography (see **Annex B**), all peaks coincided with those of CaO, with little to no discrepancy. Furthermore, *F3* and *F4* show slightly higher degrees of purity as the peaks are slimmer.

In **Figures 37 (a)** and **(b)**, SEM micrographs of *F1* and *F2* reinforced this conclusion, as bright points were observed which could correspond to impurities. From **Figure 37**, it is important to remark the high porosity of the particles and a finger-like structure with diameter around 4 μm for all feedstocks. Such morphology, with high surface area, can lead to higher efficiencies as studied by Nawar *et al.* [31].

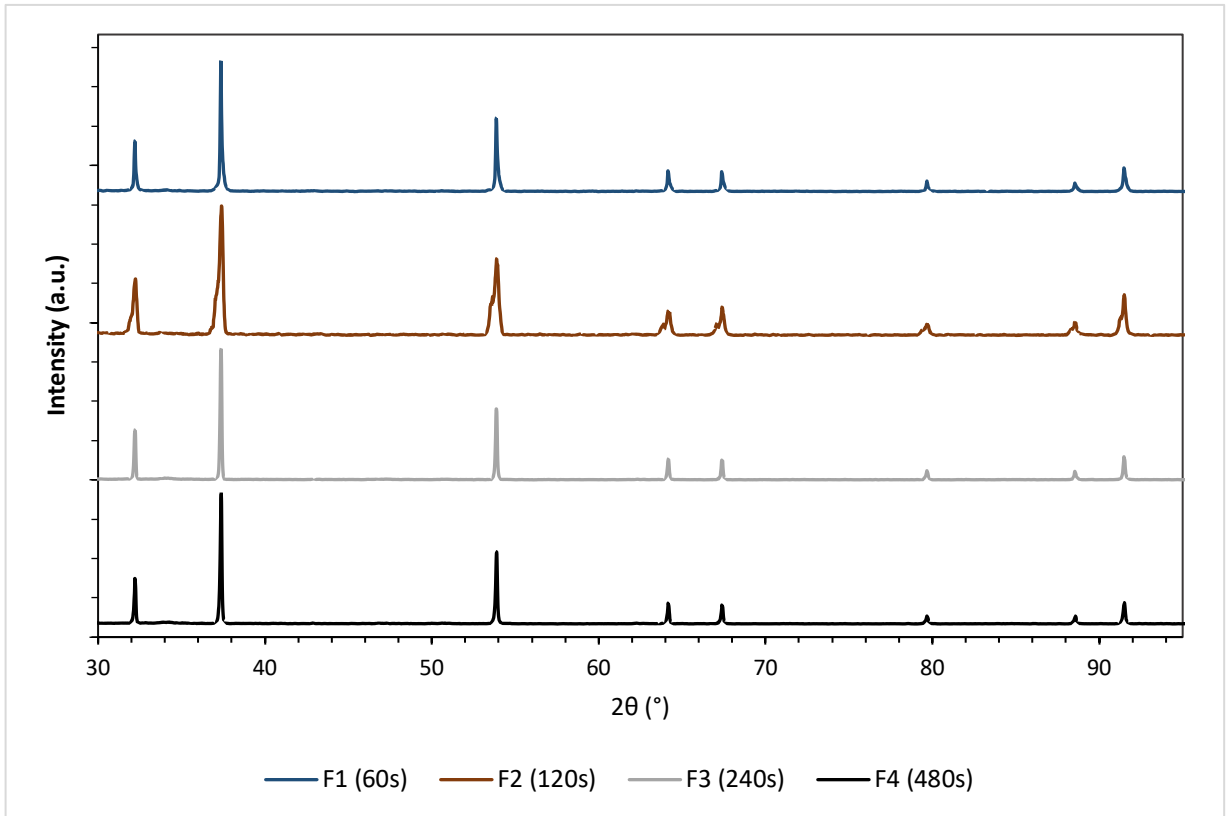


Figure 36 – XRD spectra for F1, F2, F3 and F4.

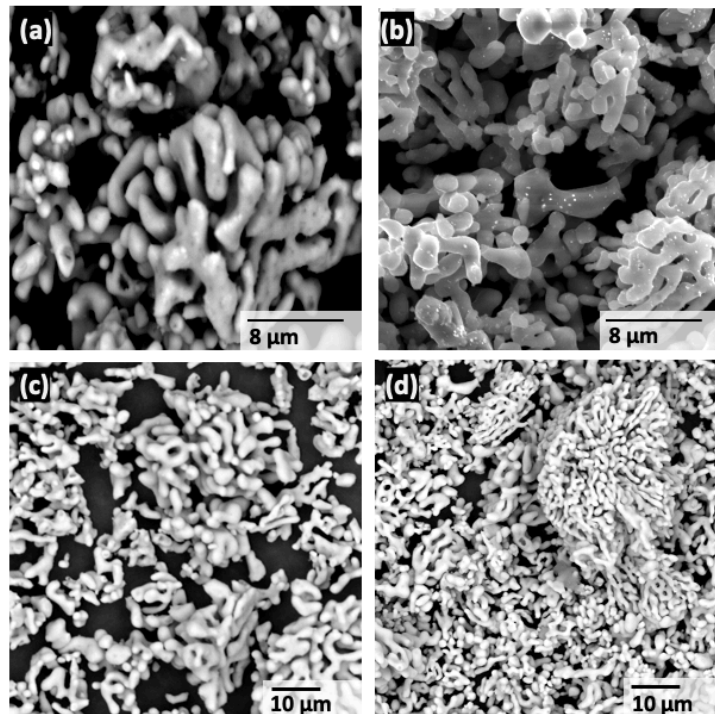


Figure 37 – SEM micrographs of calcined ES (a) F1 (b) F2 (c) F3 and (d) F4.

The composition analysis with EDX confirmed complete calcination, with CaO purity of above 98,2%, as well as traces of Magnesium (MgO) and Yttria (Y₂O₃) oxides in 0.2 and 1.4 % respectively (see **Table 4**). Even though EDX results are semiquantitative, together with the results from XRD analysis it can be concluded that CaO was obtained with purity above 98% with high certainty for all feedstocks, impurities being Y₂O₃ and MgO which in literature have not shown to be detrimental for the CC purpose [31]. These results provided enough qualitative information to deduce that *F3* and *F4* provided the least concentration of impurities. In **Annex B.1**, EDX intensity graphic results can be observed reaffirming this conclusion. Since no notable difference between *F3* and *F4* was found, *F3* was chosen as the optimal cleaning procedure due to slightly lower cost and environmental impact (reduced cleaning time).

Table 4 – EDX composition analysis by weight of *F1*, *F2*, *F3* and *F4*.

Compound	F1		F2		F3		F4	
	Weight (%)	St. dev. (%)	Weight (%)	St. dev. (%)	Weight (%)	St. dev. (%)	Weight (%)	St. dev. (%)
CaO	98	± 1.3	98	± 2	98.2	± 0.3	98	± 1
MgO	2	± 1.6	0.7	± 0.6	0.2	± 0.3	1	± 0.8
Y ₂ O ₃	-	-	-	-	1.4	± 0.1	0.4	± 0.9

For *F3* feedstock, the weight loss resulting from the chemical attack with bleach was of **4 ± 1%**, while calcination reduced **45.3 ± 0.4%** of the weight. As theoretical calcination of pure calcite results in a 44.0% reduction, by molar weight, it can be deduced that the bleach treatment eliminated almost aof the organic element as calcination only eliminated a 1.3% weight over the expected weight. This surplus of loss weight can be attributed both to resting organic elements as well as present humidity in the sample.

7.1.3. Commercial CaO

The results in the previous section were compared with commercial CaO (CaO-b), comparing purity, particle morphology and particle size. As can be seen in **Figure 38 (a)**,

3D Printing of CaO for Carbon Capture

the morphology of CaO-b is cubic formed, similar to the ES before calcinating (see **Figure 34**), which could mean high levels of CaCO₃ along with other impurities. Furthermore, the particles seem to have larger size and be more compact in comparison to *F3* CaO in **Figure 38 (b)**. When analysed through XRD, CaO-b had a greater number of peaks which, as seen in **Figure 39**, corresponded to various impurities, where observed. Among these MgO did not appear in the EDX analysis (see in **Table 5**), although Y₂O₃ and Calcite oxides did. Background noise is much more present in the XRD analysis of CaO-b respect to *F3* CaO, which might be linked to a more amorphous structure, contrary to what could be deduced from the SEM micrographs. Even though the presence of MgO and solid solutions with Al₂O₃ would not interfere negatively in the CC process, as explained in **section 6.1**, as the objective is to obtain pure CaO to eliminate possible interferences caused by impurities, it was seen that *F3* CaO from ES origin was a better candidate for this bachelor's project. Henceforth, CaO-b was disregarded.

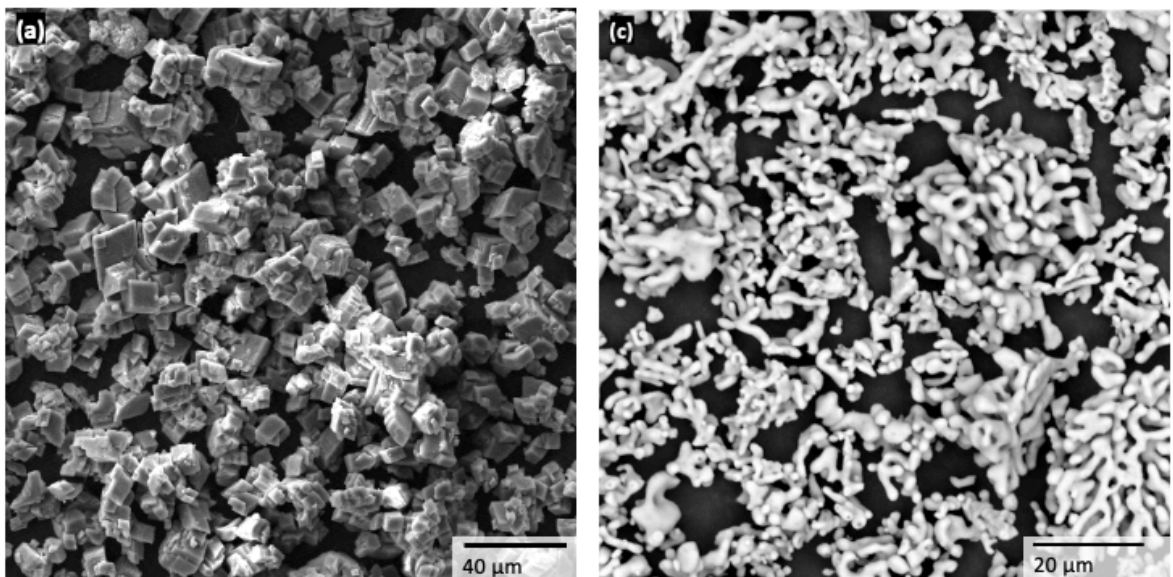


Figure 38 – Comparison of SEM micrographs for **(a)** CaO-b and **(b)** *F3* CaO.

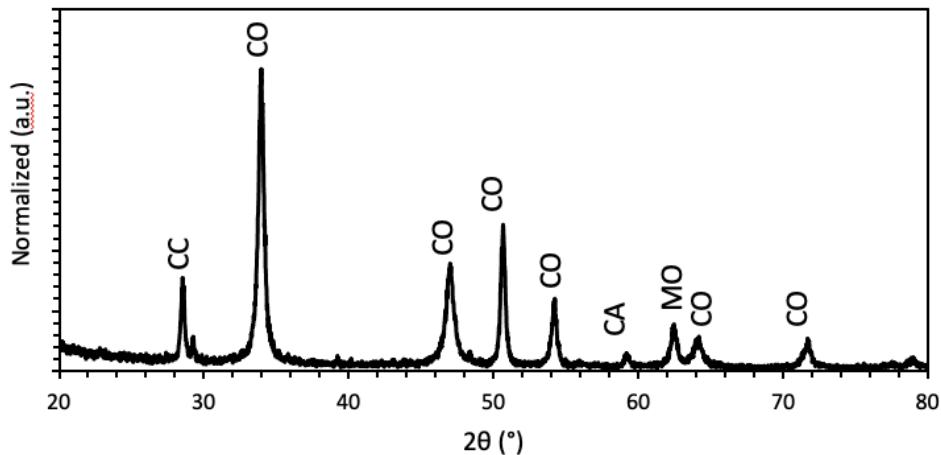


Figure 39 – CaO-b XRD spectrum showing CC (calcite), CO (CaO), CA ($\text{Ca}_3\text{Al}_2\text{O}_6$) and MO (MgO) compounds.

Table 5 – Composition of comparison of CaO-b and F3 CaO from ES origin measured through EDX.

Compound	CaO-b		F3	
	Weight (%)	St. dev. (%)	Weight (%)	St. dev. (%)
CaO	93	± 27	98	± 2
MgO	-	-	0.7	± 0.6
Y ₂ O ₃	1.2	± 0.9	1.4	± 0.1
CaCO ₃	6	± 5	-	-

7.1.4. $\text{Ca}_{12}\text{Al}_{14}\text{O}_{33}$ synthesis

From CaCO_3 elaborated in **section 7.1.1** and bought $\alpha\text{-Al}_2\text{O}_3$, $\text{Ca}_{12}\text{Al}_{14}\text{O}_{33}$ – CaO feedstock was prepared with the various proportions explained in **section 6.2**. From the XRD analysis, the background noise and lack of peaks that stood out, led to the deduction that the samples were highly amorphous, as can be seen in **Figure 40**. Furthermore, when analyzing the data received, it was seen that the highest peak for the 4 feedstocks was of 353 PSD, in comparison to the 4881 PSD of F3 CaO. Less intensity in XRD is linked to amorphous materials. Moreover, when identifying the peaks, up to five different compounds were found. From these, Al_2O_3 had the highest and sharpest peaks, which led to the conclusion that ball-milling and subsequent synthesis was insufficient. Nonetheless, it can be observed in **Figure 40** that Al_2O_3 peaks were higher at higher Al to Ca ratios. Therefore, it could be concluded that longer synthesis and milling times would be beneficial for higher ratios of Al_2O_3 . When compared to the bibliography, the conclusions from Zaki *et al.* [48], showed

3D Printing of CaO for Carbon Capture

that Mayenite synthesized under 1000 °C is amorphous and therefore does not appear in the XRD analysis. Hence, assuming the XRD diffraction pattern shows those compounds except Mayenite, it cannot be concluded quantitatively if such compound was or not synthesized, yet there are elements that direct towards such conclusion.

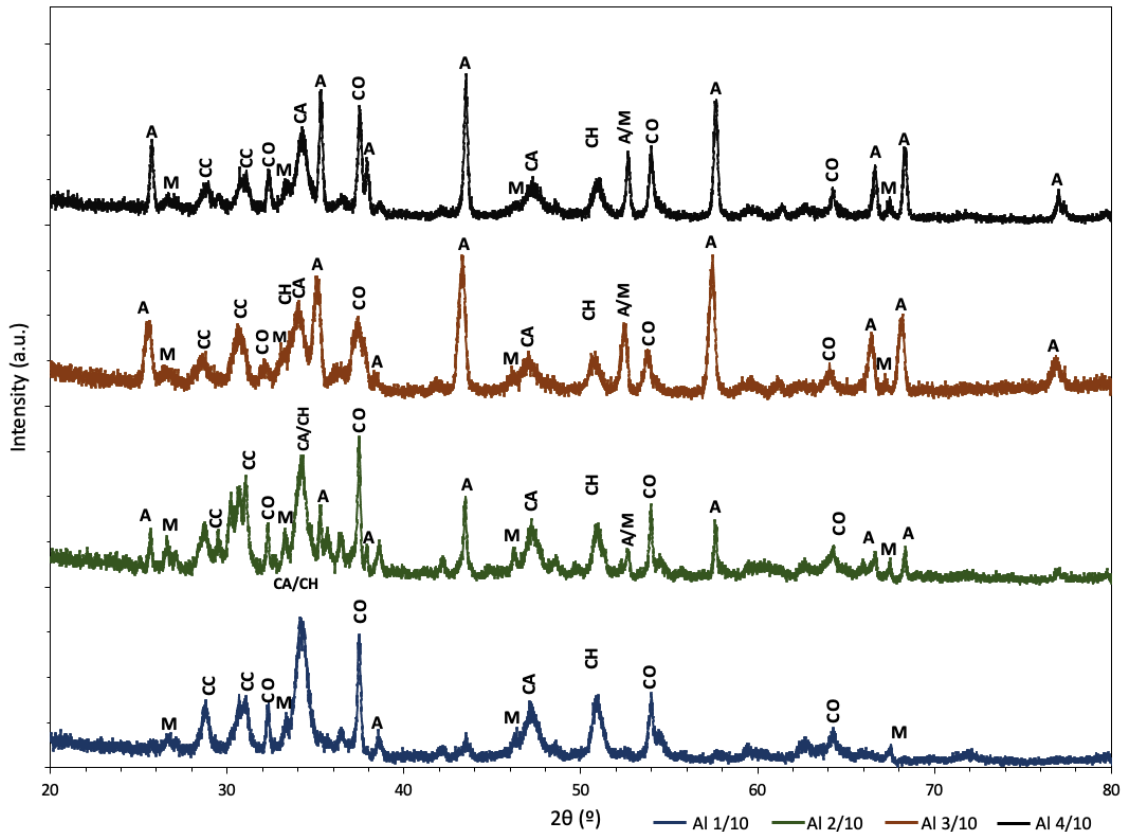


Figure 40 – XRD spectra for Al 1/10, Al 2/10, Al 3/10 and Al 4/10 showing M (Mayenite), CO (CaO), A (Al_2O_3), CA ($Ca_2Al_3O_6$) and CH ($Ca(OH)_2$) compounds.

The particle size distribution was analyzed through LD, given the particle distribution of **Figure 41**. Since the equipment used in this Bachelor's project did not allow for multiphase parameters, CaO optical parameters were used. Therefore, results from this analysis might be slightly skewed. Taking this into account, the particle size distribution showed to a bimodal distribution with wide peaks at 5 and 140 μm , except for Al 1/10 which has slightly larger sizes. When applying US to disintegrate conglomerates, results were irrational showing particle sizes up to the millimeter thick when no particles were observed in the solution. Hence, it was assumed that US changed optical properties of the feedstock and

therefore results for LD measured under US are not shown. Ultimately, it can be concluded that the feedstock has a small particle size adequate for DIW printing.

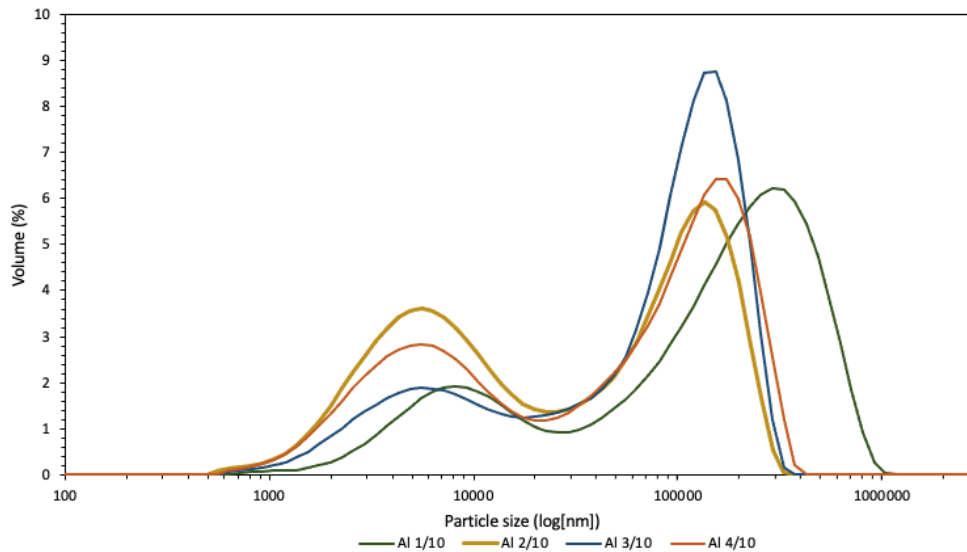


Figure 41 – LD particle size distribution of Al 1/10, Al 2/10, Al 3/10 and Al 4/10.

As seen in **section 7.1.2**, weight loss when calcinating CaCO_3 is an easy and trustworthy way to compare the compounds in a feedstock. Hence, weight loss was also measured for the distinct Mayenite feedstocks, as seen in **Figure 42**, compared to the weight loss during calcination for $F3$ CaO. From here we can visualize that weight loss diminished up to a ratio of Al to Ca of 3:10, from which weight loss increases partially. This could be due to in part to standard error, yet unfortunately further measurements could not be done due to lack of time in this bachelor's degree project and remains to be further observed. Nonetheless, it should be considered that this could also be due to a secondary phase of Al_2O_3 forming which does not deter the hydration reaction.

When analyzing the particle morphology, all four feedstocks seem to share similar traits. As seen in **Figure 43**, mostly small particles can be observed, yet no large conglomerates. This would indicate good properties for CC purposes as good mechanical properties can be obtained from small particle size. Due to problems associated with the only available SEM equipment, larger magnifications were not possible and therefore it was not possible to determine if particle morphology would aid chemical stability.

3D Printing of CaO for Carbon Capture

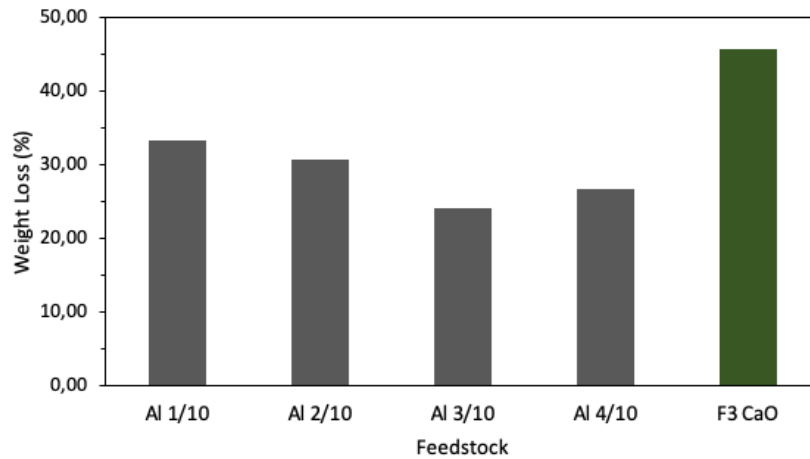


Figure 42 – Weight loss during sintering process for the various Al-CaO feedstocks in comparison with F3 CaO weight loss during calcination.

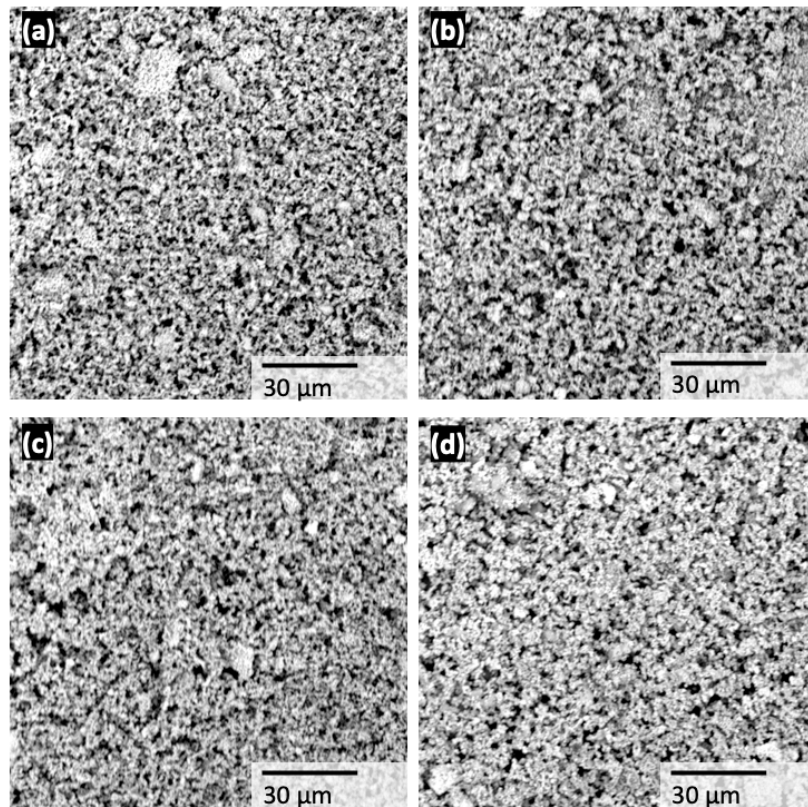


Figure 43 – SEM micrographs of (a) Al 1/10, (b) Al 2/10, (c) Al 3/10, and (d) Al 4/10.

In **Table 6**, the composition analysis through EDX can be observed. The results confirm the elements presents that could be expected yet do not allow for more conclusive remarks as the compositions vary greatly between feedstocks with unexpected ratios like in the case

of *Al 2/10* (for CaO is too high) or *Al 3/10* (for CaO is too low). Furthermore, Mayenite was not detected as the SEM equipment measured common oxides, so it is highly possible that part of the CaO and Al₂O₃ phase was actually Ca₁₂Al₁₄O₃₃. Finally, EDX results for MgO had a high associated error and therefore results are not conclusive for this element.

Table 6 – EDX composition analysis for *Al 1/10*, *Al 2/10*, *Al 3/10* and *Al 4/10*.

Oxide	Composition			
	<i>Al 1/10</i>	<i>Al 2/10</i>	<i>Al 3/10</i>	<i>Al 4/10</i>
CaO	86 ± 3	95 ± 5	36 ± 5	87 ± 11
Al ₂ O ₃	12 ± 4	5 ± 4	64 ± 5	10 ± 8
MgO	2.1 ± 0.3	0.5 ± 5	-	3 ± 3

7.1.5. ZrO characterization and election

As explained in **section 6.3**, ZrO₂ feedstock was chosen among three different industrial wastes. To ensure purity, a first analysis with both XRD and EDX using the SEM was carried out. As can be seen in **Figure 44**, even though the three feedstocks showed high purity, with all peaks coinciding with either monoclinic or tetragonal phase of 3Y-ZrO₂. Nevertheless, *R60* showed somewhat a thinner peak with less background noise, which could be explained by lower levels of impurities. When analysed through EDX, *R60* and *R60C* showed slightly higher concentrations of Zr (see **Table 7**).

3D Printing of CaO for Carbon Capture

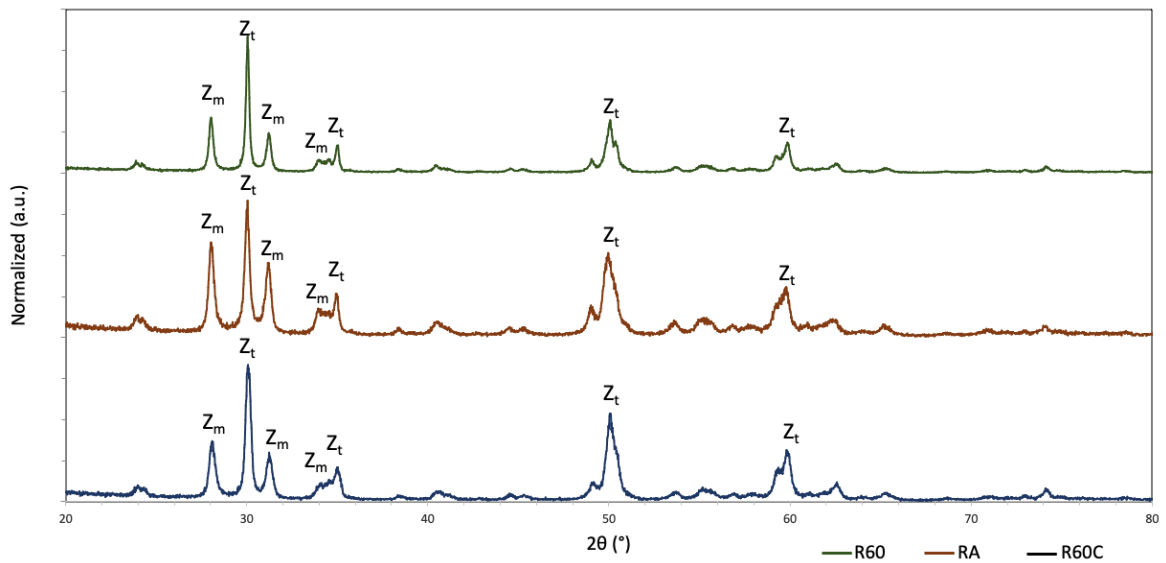


Figure 44 - XRD spectra for feedstocks R60, RA and R60C.

Table 7 – Weight concentration of the various elements as a function of intensity found in EDX analysis.

Element	Weight Concentration (%)		
	RA	R60	R60C
Zirconium (Zr)	62 ± 4	67 ± 4	65 ± 4
Oxygen (O)	27 ± 6	20 ± 4	23 ± 5
Yttrium (Y)	10 ± 1	10.5 ± 0.3	10.4 ± 0.5
Hafnium (Hf)	1.7 ± 0.4	1.9 ± 0.4	1.7 ± 0.2

When analyzing the micrographs taken with the use of the SEM, greater differences were observed. While *R60* and *RA* showed circular conglomerate particles with a large variety of diameters (see **Figure 45 (a)** and **(b)**), *R60C* showed smaller yet more porous agglomerate particles (see **Figure 45 (c)**). It can be observed, however, that the particles that make up these conglomerates are of the nanometric size. Since the objective of the addition of ZrO_2 to CaO was to obtain a more mechanically and chemically stable product, particle morphology from *RA* and *R60* was deemed as more optimal. This is so as a feedstock with denser particles of various diameters can guarantee a higher final density after sintering, which in term would benefit mechanical properties.

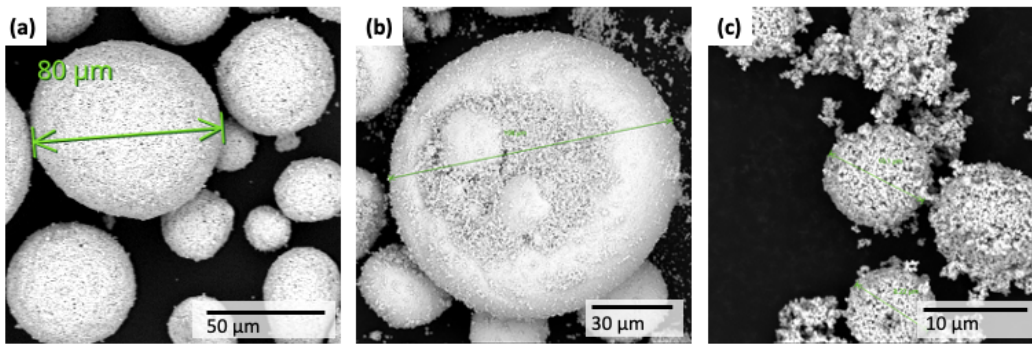


Figure 45 – SEM images of (a) R60 (b) RA and (c) R60C.

Finally, while studying particle size distribution through LD without US (see **Figure 46 (a)**), all feedstocks seemed to have a predominant mode at around 60 μm . This changed however when applying US, as seen in **Figure 46 (b)**, where R60C showed up to four modes, with a high peak at around 20 μm , reinforcing the conclusion that the large particles are conglomerates made out of smaller particle sizes. Furthermore, R60 included a wide variety of sizes from around 300nm up to 150 μm and RA showed a sharp peak at around 300 μm . Since the nozzle chosen for printing was of 520 μm , which limits the particle size to one third or 174 μm , the three feedstocks with preference for RA were seen as optimal for printing. Again, since mechanical and chemical stability were preferred, R60 was deemed slightly better since it would ensure lower porosity due to the combination of large and small particles. Next, crystallite size was calculated from XRD pattern (see **Table 8**), which showed high inconsistencies, thus unfortunately no firm conclusion could be extracted from this analysis.

Table 8 – Crystallite size (nm) of CaO feedstocks F1, F2, F3 and F4 based on XRD diffraction pattern.

Feedstock	F1	F2	F3	F4
Crystallite Size (nm)	150.8	58.0	125.6	125.6

3D Printing of CaO for Carbon Capture

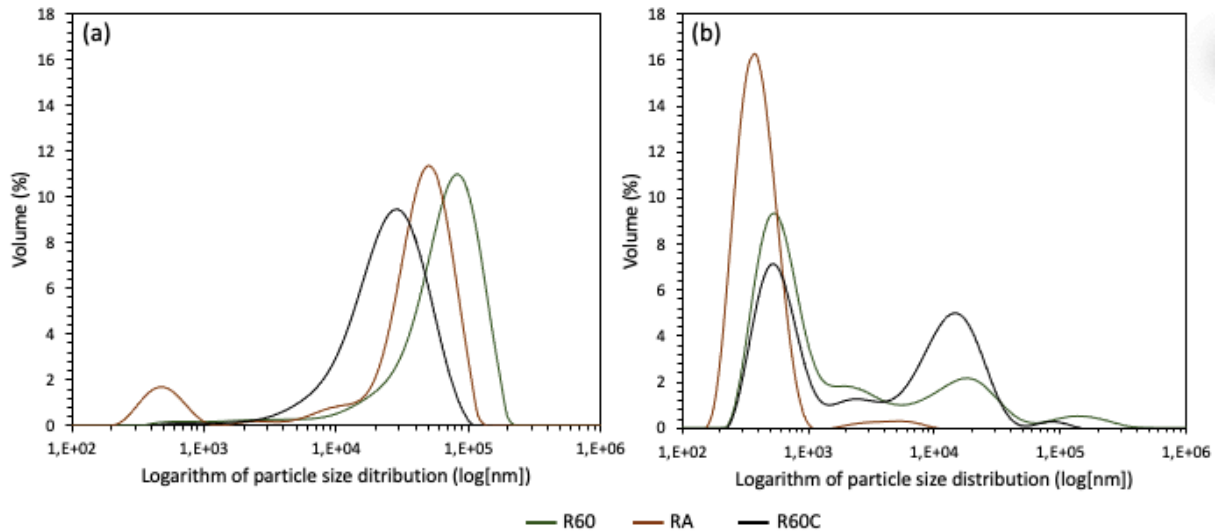


Figure 46 – LD size distribution for R60, RA and R60C both (a) without applying US and (b) applying US.

All in all, even though the three feedstocks showed high purity, adequate particle size for printing and a good particle morphology, *R60* was chosen as the feedstock from which to work on as its measured properties ensured higher mechanical and chemical stability. Therefore, *R60* and *R60C* were disregarded henceforth.

7.1.6. CaZrO₃ synthesis

Using *R60* 3Y-ZrO₂ and *F3* CaO, CaZrO₂ was synthesized and analysed under XRD, SEM, weight loss and LD. XRD diffraction patterns for the three Zr to Ca ratios can be seen in **Figure 47**. From these, CaZrO₃ is present in all cases, yet especially in the ratio 1:10. Moreover, peaks demonstrating pure Zirconia are more present at higher Zr ratios, similarly to the synthesis of Mayenite, yet CaO peaks are constant throughout the three feedstocks. Contrary to the case of Mayenite though, no proof of amorphous phases was found in literature or in the data analysis. The analysis of crystallite size showed that *Zr 1/10* had a slightly larger diameter than the other feedstocks, yet in all cases the crystallite size was below the μm . This contrasts with results from LD (see **Figure 48**) where *Zr 1/10* has the largest particle distribution with a bimodal pattern and peaks at 18 and 118 μm . Furthermore, *Zr 2/10* showed the lowest particle size distribution, preferable for both 3D printing and mechanical properties. Yet again, crystallite size calculations showed

irregularities not explained by the rest of the data (see **Table 9**). It is also important to comment that the three feedstocks showed a curious behaviour where small particles would shoot out when picked with a spoon as if high tensions had been accumulated. This can be explained by the inert phases not allowing for either reaction of CaO or for sintering of the particles, as has been hypothesized in literature [14]. Both explanations would benefit the chemical stability of final products.

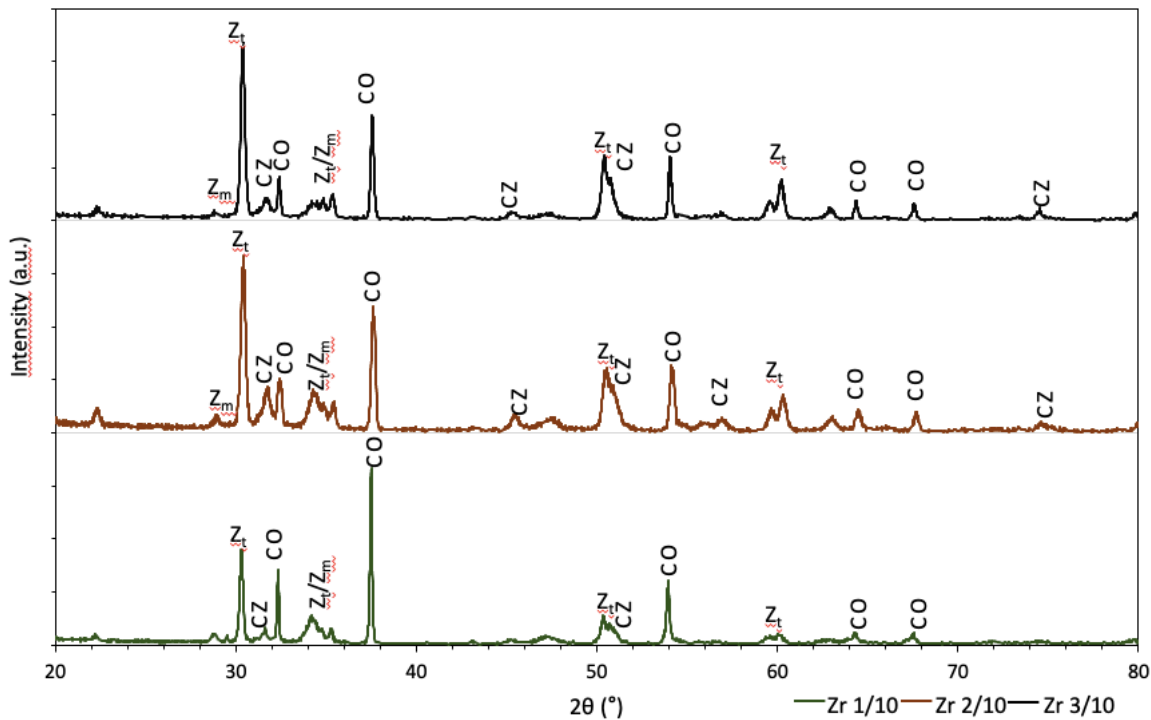


Figure 47– XRD spectra for Zr 1/10, Zr 2/10 and Zr 3/10 showing CO (CaO), Z_t (tetragonal ZrO₂), Z_m (monoclinic ZrO₂) and CZ (CaZrO₃) phases.

3D Printing of CaO for Carbon Capture

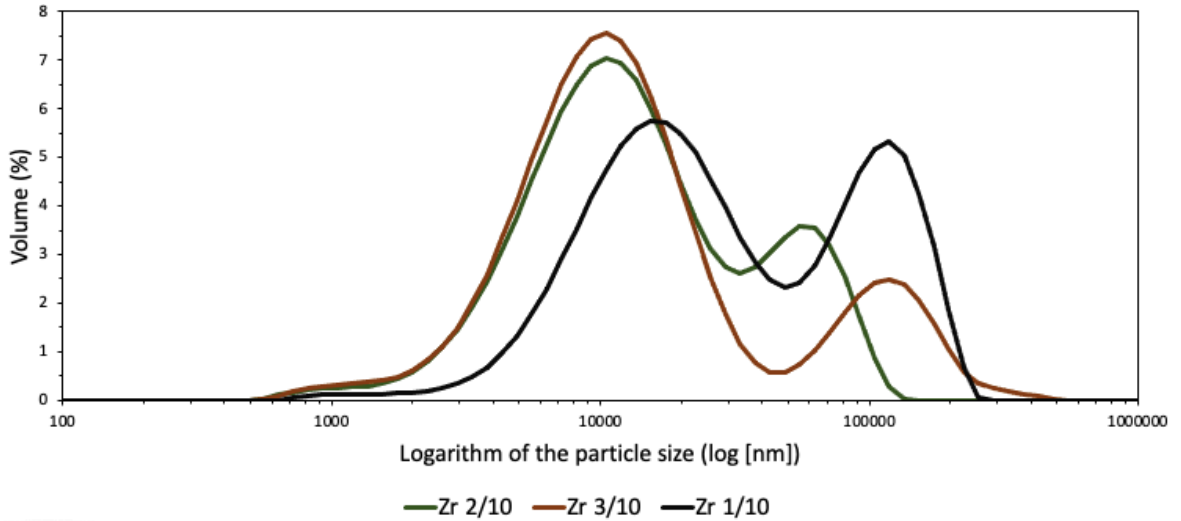


Figure 48 – Particle size distribution of Zr 1/10, Zr 2/10 and Zr 3/10 measured by LD.

Table 9 – Crystallite size calculated from the XRD diffraction pattern for CaO and ZrO₂ peaks

Feedstock	Zr 1/10	Zr 2/10	Zr 3/10
CaO peak			
Crystallite size (nm)	124.2	53.8	76.9
ZrO₂ peak			
Crystallite size (nm)	71.5	49.9	56.8

When analysing the weight loss for the three feedstocks during sintering, Zr 3/10 showed the least weight loss, as expected, due to higher stable phases. Nevertheless, this could also be attributed to lower percentage calcined due to inert phases limiting phase transformation and therefore limiting the transformation of Calcite to CaO (see **Figure 49**), as expressed previously. Due to lack of time, only one measurement per feedstock was done, and hence no error could be associated to these measurements.

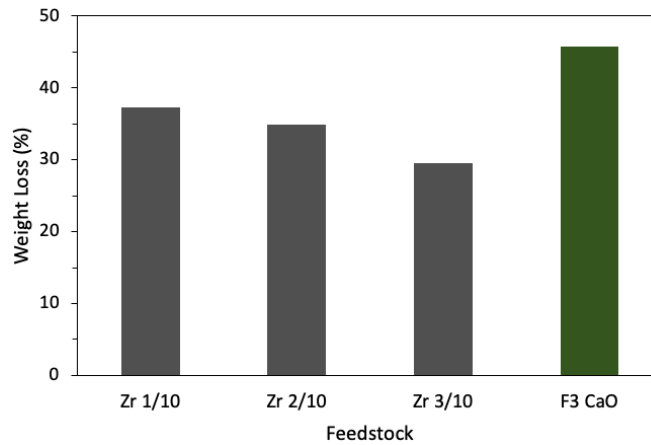


Figure 49 – Weight loss during sintering for Zr – CaO feedstocks in comparison with F3 CaO.

Further analysis through SEM micrographs showed that the three feedstocks shared a similar particle morphology, where the absence of big particles prevails, which explains the crystallite sizes found (see **Figure 50**). Furthermore, it seems that *Zr 3/10* had larger conglomerates. EDX analysis in **Table 10** confirmed the predicted tendencies of compositions of CaO and ZrO₂, even if the uncertainties obstruct any clear conclusion.

Table 10 – EDX Composition analysis for Zr 1/10, Zr 2/10 and Zr 3/10.

Oxide	Composition (%)		
	Zr 1/10	Zr 2/10	Zr 3/10
CaO	76 ± 16	53 ± 17	45 ± 22
ZrO ₂	19 ± 16	40 ± 15	44 ± 21
MgO	1 ± 1	0.2 ± 0.2	0.6 ± 0.3
Y ₂ O ₃	3 ± 2	5 ± 2	7 ± 3
Hf	-	1.1 ± 0.3	2 ± 1

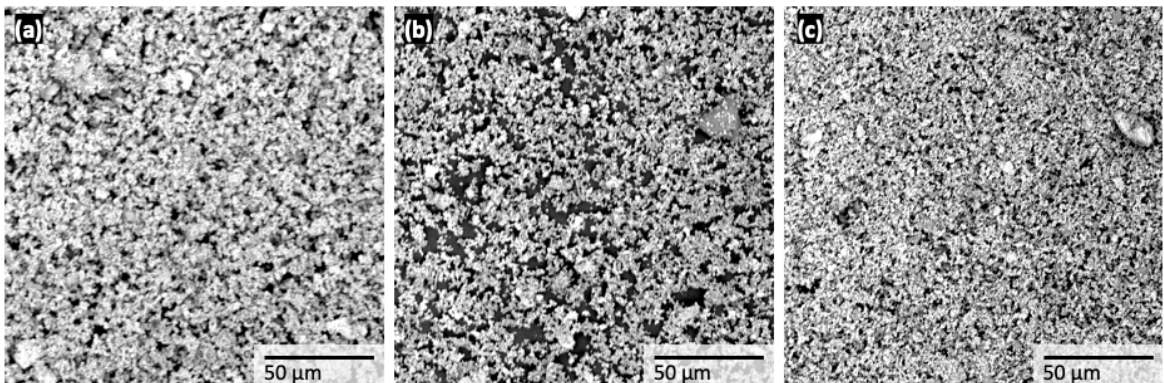


Figure 50 – SEM micrographs of (a) Zr 1/10, (b) Zr 2/10 and (c) Zr 3/10.

7.1.7. Ca(OH)_2 synthesis

Synthesis of Ca(OH)_2 following the procedure by Yoosuk *et al.* [26] with F3 CaO raw material gave a highly pure feedstock as it can be seen in the XRD diffraction pattern of **Figure 51**. Here, high sharp peaks can be observed that coincide with those found in the bibliography for Ca(OH)_2 (see **Annex C1**). Nonetheless, peaks above 53° could not be identified as no values were found in bibliography. Two of these were close to CaO peaks yet it is highly unlikely that they consisted of such compound as its other peaks are not visible. The crystallite size deduced from this XRD analysis was of 125.5 nm, much smaller than the results obtained from LD which ranged from 1 to 200 μm both without US and from 1 to 100 μm with US (see **Figure 52**). This difference indicates a slight tendency of this feedstock to form conglomerates, which would be detrimental for printing properties as it could obstruct the nozzle.

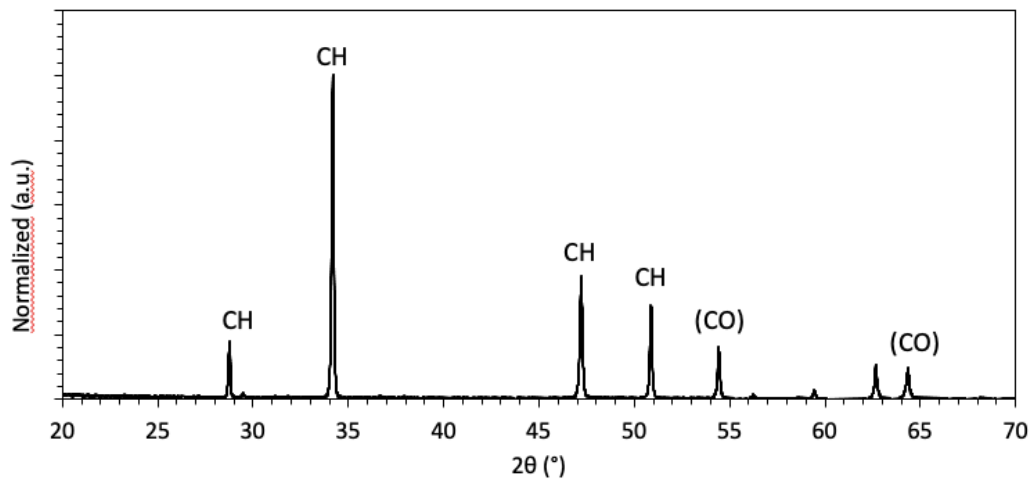


Figure 51 – Ca(OH)_2 XRD diffraction pattern showing CH (Ca(OH)_2) and possible CaO (CO).

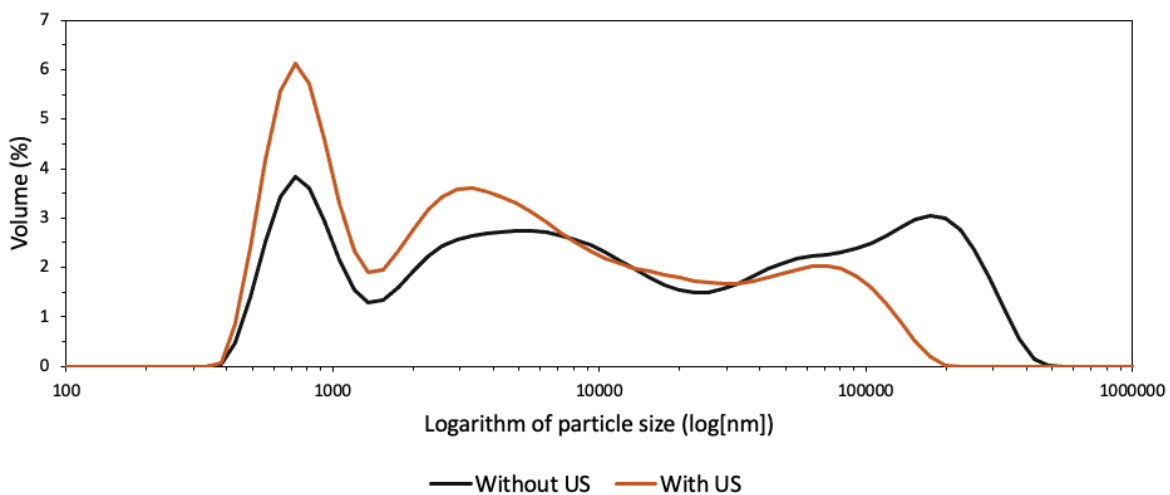


Figure 52 – Particle size distribution of Ca(OH)_2 both with and without US measured by LD.

The particle morphology of Ca(OH)_2 can be observed in the SEM micrograph of **Figure 53**, where no particle structure can be observed. Even though this probably results in a higher surface area and smaller particle size, the highly porous morphology could eventually be detrimental for mechanical and chemical stability.

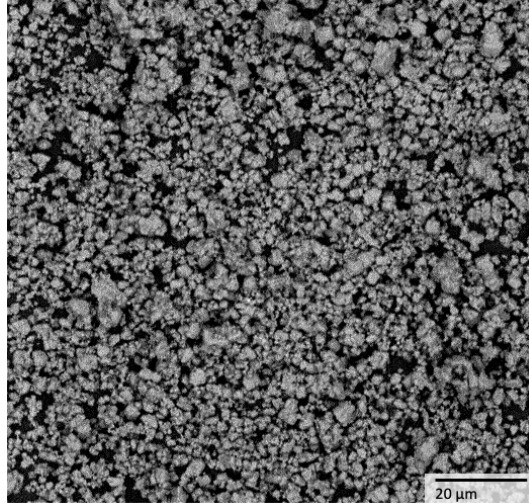


Figure 53 – Ca(OH)₂ SEM micrograph.

7.2. CaO sintering temperature

Using the calcite feedstock analyzed in **section 7.1.1**, the temperature at which complete calcination occurred was found. To do so, feedstock was warmed up to temperatures ranging from 500 to 800 °C. As commented before, weight loss can precisely allow us to know the percentage calcined due to the conversion from CaCO₃ to CaO. The results of such analysis can be seen in **Figure 54**, where weight loss is greater than that the theoretical weight loss during calcination of pure Calcite at temperatures above 700 °C. None the less, weight loss is expected to be slightly higher as it is possible that there are organic residues that withstood the treatment at 300 °C, as was the case for those calcined at 750 and 800 °C.

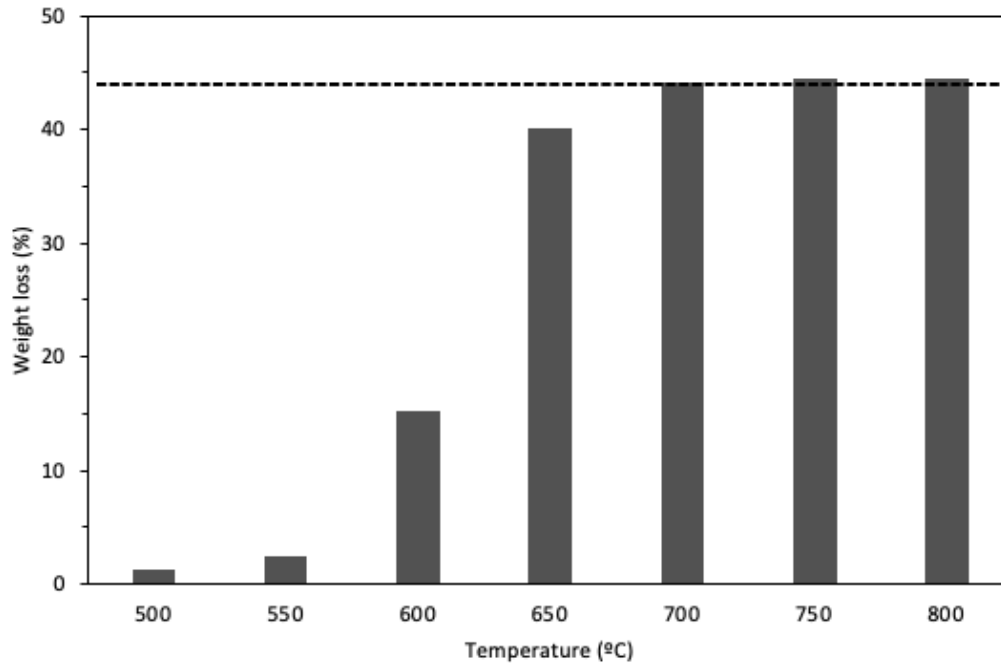


Figure 54 – Weight loss during sintering for temperatures ranging from 500 to 800 °C, showing theoretical weight loss as a dotted line at 44.0%.

When taking into consideration diffraction patterns obtained from XRD in **Figure 55**, it can be observed that calcination starts to occur at 600 °C and is complete at above 750 °C, where the Calcite peak disappears completely. At the same time, it can be observed that a 3rd phase is sintered between 650 and 750 °C, and disappears at 800 °C, which did not match any logical values found in bibliography. Finally, at 800 °C, the calcined CaO has sharp

3D Printing of CaO for Carbon Capture

peaks with little to no background noise. Hence, calcination at 800 °C seems to be the most ideal from XRD diffraction spectra.

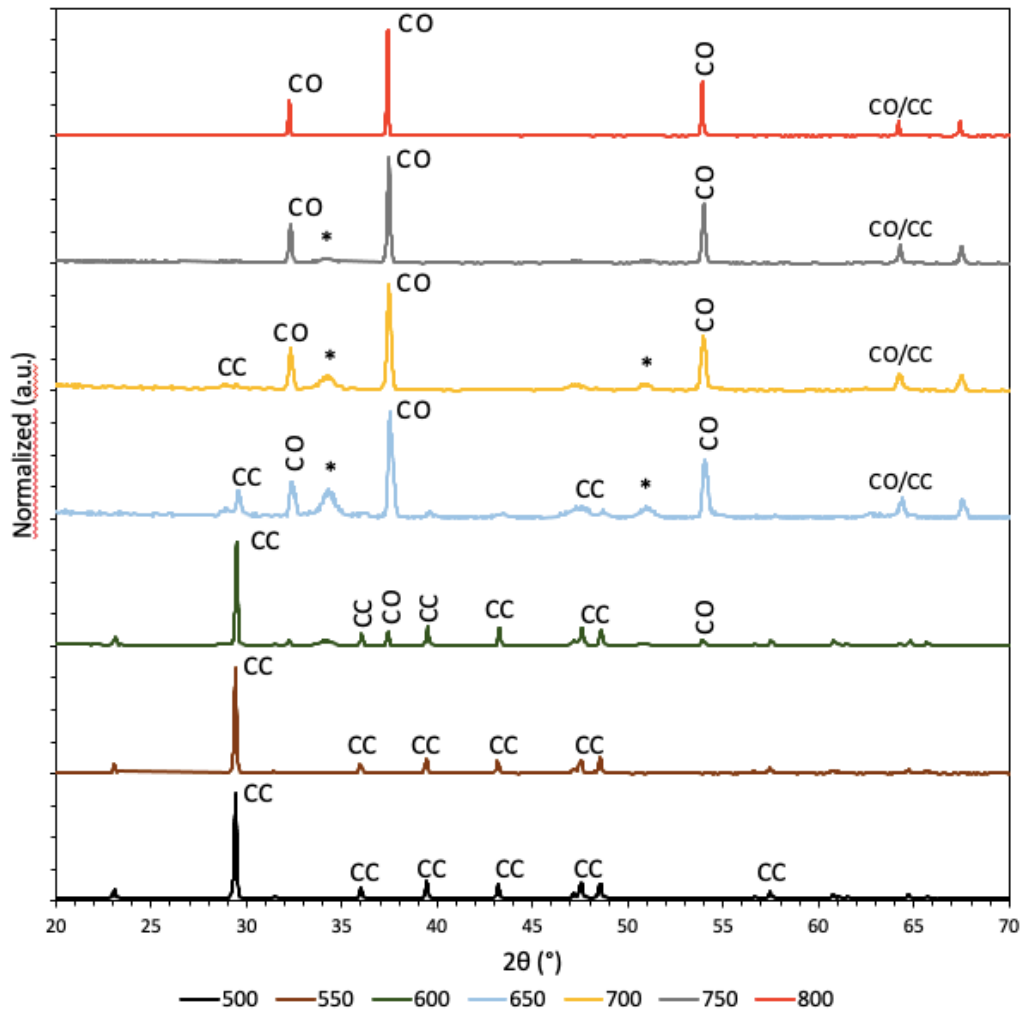


Figure 55– XRD spectra for CaCO₃ calcination at temperatures ranging from 500 to 800 °C, showing CC (Calcite CaCO₃), CO (CaO) and a third unknown compound (*).

The calculated crystallite sizes derived from the XRD diffraction spectra (see **Table 11**) showed a reduction of size at 600 °C that slowly increased as sintering temperature was higher. These results would confirm the calcination and following synthesis of particles that increases the crystallite size.

Table 11 – Crystallite sizes calculated from the XRD patterns of the various sintering temperatures.

Temperature (°C)	500	550	600	650	700	750	800
Crystallite Size (nm)	51.3	55.0	25.7	25.1	29.0	41.9	68.5

Finally, particle morphology was analyzed through SEM, seen in **Figure 56**, shows that from 700 °C onwards a porous structure like the morphology of *F3 CaO* is formed. Finally, large conglomerates of up to 80 μm for sintering at temperatures till 700 °C and of up to 40 μm for sintering at 750 and 800 °C can be observed.

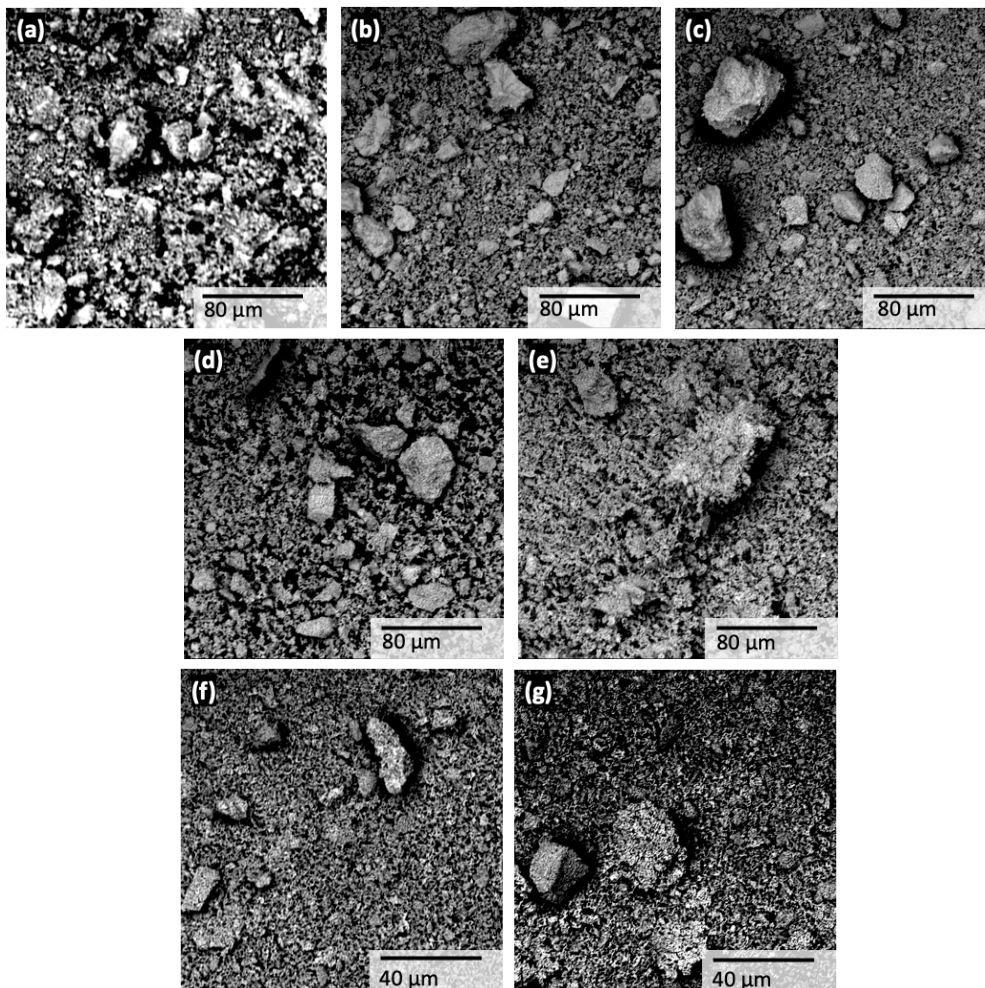


Figure 56 – Particle morphology of calcined CaCO_3 at (a) 500 °C, (b) 550 °C, (c) 600 °C, (d) 650 °C, (e) 700 °C, (f) 750 °C and (g) 800 °C.

Thus, taking all of this into account, it was determined that temperature at which complete calcination occurred was at 750 °C, yet to prevent effects from the unknown phase found

3D Printing of CaO for Carbon Capture

at such sintering temperature and as crystallite sizes showed a higher sintering at 800 °C, this second temperature was chosen to sinter samples henceforth.

7.3. Post-sintering treatments

As explained in *section 6.8*, several treatments were taken on calcined and sintered samples. In the following subsections, the results can be observed except for the incomplete carbonation process which is discussed in *section 7.4*.

7.3.1. Ethanol Bath

After 2 days in ethanol, samples dissolved as seen in *Figure 57*. Hence, this method was deemed unsuccessful and was disregarded.

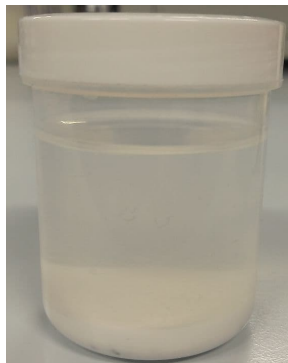


Figure 57 – Samples after being kept 2 days in ethanol.

7.3.2. Oil Bath

Samples were dipped in oil for 5 minutes after which they were stored in air. As can be seen in *Figure 58 (a)*, samples that had undergone this treatment were able to withstand up to 4 days, yet after 7 (see *Sample 58 (b)*), they became structurally unstable. Oil bath was therefore dismissed as well.

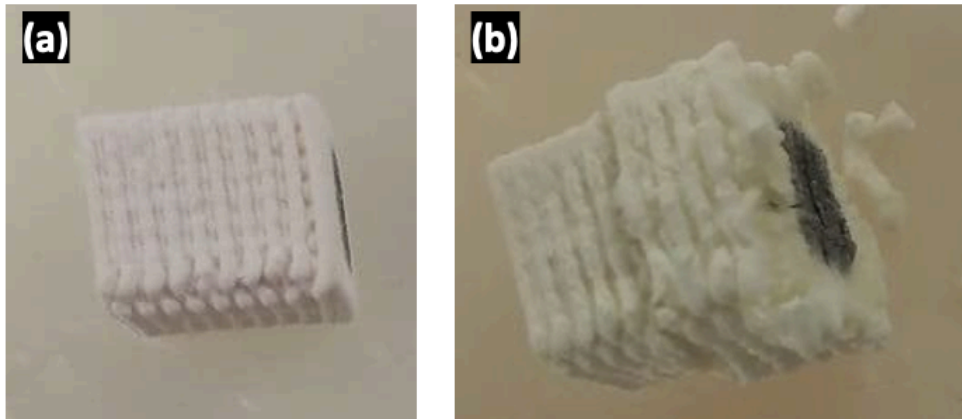


Figure 58 – Sinter samples that had been dipped in oil after (a) 4 days and (b) 7 days.

7.3.3. Lacquer treatment

After being applied lacquer, samples suffered anyway from the hydration reaction in air (see *Figure 59*), and therefore this treatment was also rejected.



Figure 59 – Samples that had been applied Lacquer after 2 days.

7.4. Pellet synthesis and reaction in air

From the feedstocks obtained previously, pellets were manufactured using a Uniaxial and a CIP machine, as explained in *section 6.6*. After this, they were left to rest in an unprotected environment, from which mechanical and chemical stability were analyzed. Chemical stability was done by measuring the mass of the pellets past 3 and 7 days, which can be visualized in *Figure 60*. Incomplete carburation of the pellet (CaCO_3 in the figure) led to the least weight gain (0.23% after 7 days), which supported by optical analysis in

3D Printing of CaO for Carbon Capture

Figure 61 and qualitative analysis led to the conclusion that it had not reacted with water in the air and thus had maintained mechanical stability the most. Furthermore, when compared to the weight gain of CaO of up to 77.4% after 7 days, the addition of inert phases successfully increased chemical stability, Mayenite phases doing so slightly better than Zirconia addition.

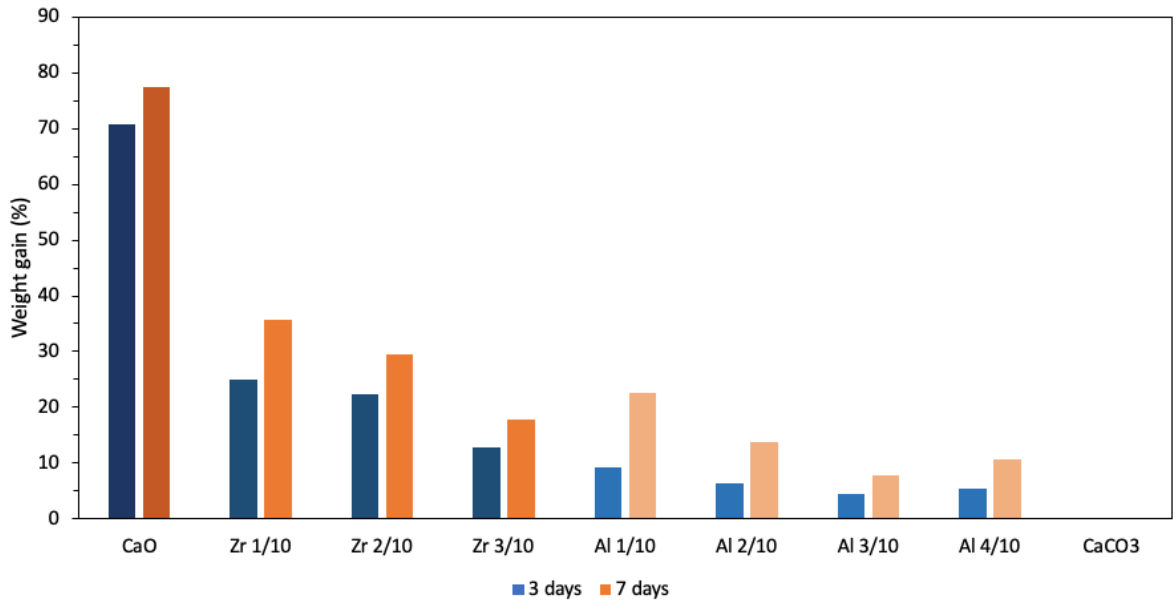


Figure 60 – Mass gain for the different feedstocks sintered after 3 and 7 days.



Figure 61 – Images of (a) Zr 1/10, (b) Zr 2/10, (c) Zr 3/10, (d) Al 1/10, (e) Al 2/10, (f) Al 3/10, (g) Al 4/10 and (h) CaO pellets sintered after (.1) 3 days and (.2) 7 days left in contact with air.

From visual observations, Al 3/10 stands out as it maintained quite successfully its initial shape and size without major cracks, opposed to the rest of feedstocks (see **Figure 61 (f)**). Al 2/10 and Al 4/10 also maintained shape yet showing a higher number of cracks of larger size (see **Figure 61 (e)** and **(g)**). Zirconia inert phases did not prevent the structural disintegration of the pellets completely, yet they did reduce reaction, with Zr 3/10 showing

3D Printing of CaO for Carbon Capture

the highest structural integrity (see **Figure 61 (a-c)**). Moreover, incompletely carbonated pellets (**Figure 62**) did not show any visible differences after 7 days left in contact with air. Finally, Ca(OH)_2 sintered feedstocks were not analyzed together with the other pellets as they disintegrated before being able to put on parafilm (see **Figure 63**). Thus, Ca(OH)_2 can be deemed unfit for CC the way it was processed in this Bachelor's degree.

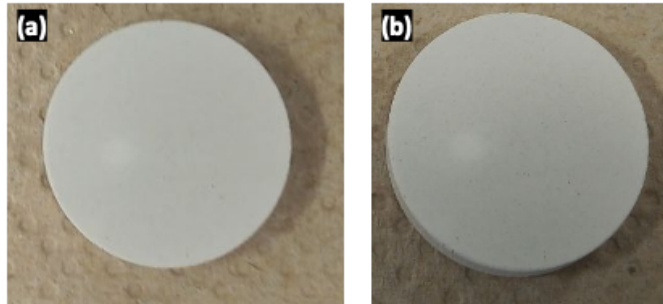


Figure 62 – Incomplete carbonation pellets after (a) 3 days and (b) 7 days.



Figure 63 – Ca(OH)_2 sintered pellets once taken out of the oven.

To further understand the properties of the incompletely carbonated pellets, they were cut in half and analyzed through SEM and EDX. From seeing **Figure 64**, we can first see a resemblance to calcined CaO F3 in **Figure 37**, yet slightly more compact. This can be attributed both to CIP applied as well as the sintering process. Analysis through EDX was not able to confirm the presence of CaCO_3 due to the carbon coating that had to be applied previously to analyze through SEM.

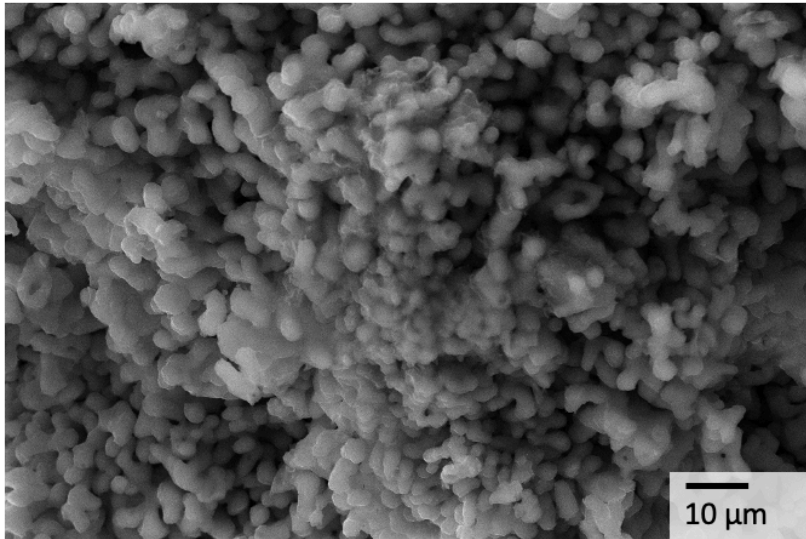


Figure 64 – SEM micrograph of pellet that underwent incomplete carbonation and sintering.

7.5. DIW printing

Using CaCO_3 feedstock, and the process explained in **section 6.11**, a honeycomb monolith with 50% infill designed previously by Álvarez *et al.* [4] was used. The result, as seen in **Figure 65** after synthesis and carburation, was quite successful, being able to maintain chemical stability. In spite of this, mechanical properties of the scaffold were quite fragile (broke easily), and the paste for printing showed difficulties after 1 hour printing. Hence, further investigation to improve both the paste by conducting in depth rheological analysis and printing parameters, as well as sintering procedure should be carried out.

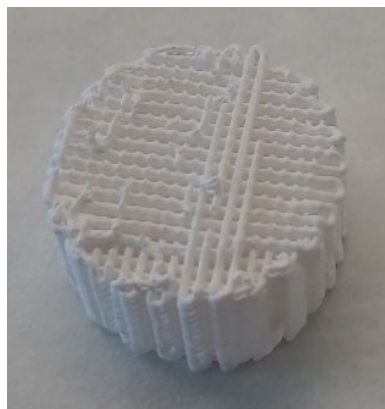


Figure 65 – Honeycomb monolith with 50% infill after synthesis and incomplete carburation treatment.

8. Sustainability report

The present Bachelor's project has strived at all moments to minimize its ecological footprint while aiming to create a viable product to diminish CO₂ concentrations in the environment. Nevertheless, the question remains whether this project has had a positive or negative impact on sustainability. The present chapter will try to answer this objectively and in the most transversal way possible by following the sustainability report stated by Climent *et al.* [49]. This report, centred around questioning the ecological scope, also analyses the social and economic impact of the project. To do so, **Table 12** is followed, dividing the analysis of the impact of the product in the three mentioned, and dividing these among three stages; research (referring to the impact in the lab), at use (referring to the impact if the product was to be used), and risks.

Table 12 – Sustainability Matrix elaborated by Climent *et al.* [49]

Scope	Stage		
	Research	At use	Risks
Ecologic	Direct impact caused during research	Ecological footprint of the product if used in industry	Risks that can cause a larger ecological footprint than expected
Economic	Budget that was needed to fulfil the project	Economic analysis for commercial viability of the product	Unexpected events that can elevate costs
Social	Impact on those people working on the project	Social impact if product was at widescale use	Set of social risks that may be caused by the product

From **Table 12**, a set of questions are laid out by Climent *et al* [49] to give as much objectivity to the sustainability report. These questions, seen in **Table 13**, will be answered in the following sections.

Table 13 – Questions parting from the sustainability matrix elaborated by Climent et al. [49]

Stage	Scope
Ecologic	
Research	Has the ecological footprint been quantified? What measures have been taken to reduce this impact and how have they affected?
At use	What will be the ecological footprint if such product is produced at a larger scale?
Risks	Are there scenarios that could end up increasing the ecological footprint?
Economic	
Research	What is the human and material cost of the project?
At use	If the project were to be produced at larger scale, what would be its cost? Have repairing costs been considered?
Risks	What risks are there that could reduce the project's viability?
Social	
Research	Has the project incurred in reconsiderations about personal, professional, or ethical values of those people implied in the project?
At use	Who will benefit from the use of the product? Is there a social group that may be negatively affected by it? To what extent?
Risks	Are there scenarios that could make the product negatively affect part of the society?

8.1. Ecological scope

Has the ecological footprint been quantified?

The ecological footprint was quantified using the *Granta Edupack* program, as seen in **Annex D**. This program however had the limitations that ES, Pluronic F127®, ethanol and deionized water could not be quantified due to lack of data. Hence, the impact from such elements were searched and added. The result can be observed in **Table 14**, with a grand total of **119.40 Kg of CO₂ eq.** for the whole project. On balance, the use of the oven, followed by the ethanol, had the greatest ecological impact in this project, and therefore, in future investigation should be a key aspect to reduce. Values for CO₂ emissions per kWh consumed correspond to the month of May 2021 for the Spanish electrical grid, which

3D Printing of CaO for Carbon Capture

amounted to 0.10 Kg CO₂·kWh⁻¹ [50]. Values of CO₂ emissions for ethanol were taken from the calculations of Dias de Oliveira *et al.* assuming corn-based ethanol was used [51]. Unfortunately, the ecological footprints of *Pluronic F-127*[®] and *deionized* water were not found.

Table 14 – Ecological Footprint calculations for this Bachelor’s project.

Scope	Kg CO ₂ eq. per unit	Amount used	Total (kg CO ₂ eq.)
Zirconia (if bought)	3.95 / Kg ZrO ₂	0.2 kg	0.79
Alumina (99.9% purity)	2.8 / Kg Al ₂ O ₃	0.3 kg	0.84
CaCO ₃ (if bought)	0.016 / kg CaO	1.5 kg	0.024
Oven	0.1 / kWh	324 kWh	110
Ball mill	0.1 / kWh	6.48 kWh	0.65
Printer	0.1 / kWh	0.2 kWh	0.02
Ethanol	0.524 / L ethanol	15 L	7.86
Zirconia disposal	0,014	0,2 kg	0.0028
Alumina disposal	0,014	0,3 kg	0.0042
CaO disposal	0,014	1,5 kg	0.021
Pluronic F-127 [®]	-	-	-
Deionized water	-	-	-
TOTAL	All products Bought		120.21
	Using waste materials		119.38

What measures have been taken to reduce this impact and how have they affected?

The main measures taken to reduce the impact of this project refer to the use and upcycling of waste raw materials. These achieved, as seen in **Table 14** a reduction in equivalent CO₂ emissions of around **0.81 kg CO₂ eq.** Furthermore, other actions that were taken to reduce the ecological impact were using the oven together with other companions of research when possible, that could eventually account for a reduction of 24 hours of oven, or 2.16 Kg of CO₂ eq. These actions were small in comparison to the grand total, hence further initiatives should have been taken to reduce the impact, focusing on the need of doing certain procedures and on understanding the problem associated to the products before

continuing the processes. If this was done, it is estimated that oven times could have been reduced by more than 50%.

What will be the ecological footprint if such product is produced at a larger scale?

In **Table 15**, the ecological footprint of a single, incompletely calcined, CaCO₃ scaffold is calculated, assuming mass production can reduce oven energy usage of the oven by a factor of 10. It is important to notice that in this case Pluronic F-127® effect might be more noticeable, yet that the electricity usage is still has the highest impact on the footprint.

Table 15 – Ecological footprint of 1 scaffold if it were to be mass produced.

Scope	Kg CO ₂ eq. per unit	Amount used	Total (Kg CO ₂ eq.)
Zirconia (if bought)	-	-	-
Alumina (99.9% purity)	-	-	-
CaCO ₃ (if bought)	0.016 / kg CaO	0.014 kg	2.24·10 ⁻⁴
Oven	0.1 / kWh	0.81 kWh	0.081
Ball mill	0.1 / kWh	-	-
Printer	0.1 / kWh	0.2 kWh	0.02
Ethanol	0.524 / L ethanol	-	-
Zirconia disposal	0.014	-	-
Alumina disposal	0.014	-	-
CaO disposal	0.014	0.014	1.96·10 ⁻⁴
Pluronic F-127®	-	-	-
Deionized water	-	-	-
TOTAL	All products Bought		0.01014
	Using waste materials		0.832

Are there scenarios that could end up increasing the ecological footprint?

Even though there are no risks such as accidents, leaks or malfunctioning that can lead to an increasing ecological footprint, there are several misuses that do have the potential to do so. Among these, the most important refer to the use of CC in those industries that will

3D Printing of CaO for Carbon Capture

inevitably lead to CO₂ emissions such as fossil fuel refinement. This is so as the reduction in emissions from these contaminating energy sources may indirectly lead to an increase in its use, following the *Jevon's paradox* also known as the *Khazzoom-Brookes postulate* [52]. These theories state that when new technologies increase the efficiency of a system, it can be expected that the rise in use of the technology will compensate the social or ecological benefits achieved by it. Cansino *et al.* tested this theory for energy efficiency actions in Spain, concluding that certain sectors such as the transport, industry or service sector did trigger rebound effects that ended increasing their use. Applied to CC, Ajay *et al.* [53] acknowledged the ecological risks that could come associated with delaying CO₂ reductions expecting that future generations could have the technology to achieve negative emissions at low costs.

8.2. Economic scope

What is the human and material cost of the project?

The human and material cost of the project as a whole was of around **18,582.15 €** with taxes. The economic analysis was done using the values provided by the *Work, Immigration and Social Security Ministry* [54] and the *Multiscale Research Center* [55], as seen in **Tables 16, 17 and 18**. From these, even if costs are high, most can be associated with the process followed throughout this thesis. Therefore, if the project was to be done again only to produce the piece concluded to have best chemical stability, the costs would reduce drastically. This is further discussed in the next question of the economic scope.

Table 16 – Cost of the equipment used during this Bachelor’s project

Equipment	Price (€/hr)	Time used (hr)	Total (€)
SEM	45.00	20	900.00
DRX	56.25	25	1,406.25
LD	60.00	12	720.00
Balance	10.30	1	10.30
3D printer	12.40	4	49.60
Nabethern and Energon Furnace	12.40	360	4,464.00
SpeedMixer	5.00	0.5	2.5
Ball mill	20	36	720
Distillation Equipment	25	24	600
Total	-	486,5	8,872.65

Table 17 – Cost of the materials used for this Bachelor’s project.

Material	Price (€/kg)	Amount used (kg)	Total (€)
Alumina	9.00	0.300	2.70
Pluronic F-127	262.00	0.05	13.10
Ethanol	8 .00(€/L)	15 L	120.00
ES	0.00	1.5	0.00
CaO (commercial)	5.00	0.2	1.00
ZrO ₂	0.00	0.2	0.00
CO ₂	35.00	0.1	3.50
TOTAL	-	-	140.30

Table 18 – Cost and time spent by the engineers and technicians in this Bachelor’s project.

Personnel	Salary (€/hr)	Time invested (hr)	Total (€)
Technical Assistance	80.00	10	800.00
Tutor	60.00	30	1,800.00
Time invested by author of study			
Search for information	9.62	80	769.60
Samples synthesis	9.62	150	1,443.00
Samples Characterization	9.62	100	962
Report elaboration	9.62	80	769.60
TOTAL	-	441	6,544.20

3D Printing of CaO for Carbon Capture

In **Table 19**, the total cost of the project is calculated.

Table 19 – Total cost of this Bachelor’s project as a sum of the three scopes explained in **Tables 16 - 18**.

Scope	Cost (€)
Equipment	8,872.65
Materials	140.30
Engineers and Technicians	5,744.20
TOTAL (without taxes)	15,557.15
Total (with taxes)	18,824.15

If the project were to be produced at larger scale, what would be its cost?

From the previous analysis, **Table 20** was made consisting only of those elements seen as necessary to produce one incompletely calcined scaffolding deemed as optimal in the results. As a result, each piece would be obtained at around 227.96 €. Through mass production would lower 90% of costs associated to the engineer, the oven, the speedmixer, the balance and the material by automatization of the process and industrial ovens with larger number of pieces, it can be deduced that prices may be as low as **22.80 €** per scaffold. If regeneration through hydration treatments were to be considered, price would be negligible as only steam at the same temperature as carbonation could be used [56].

Table 20 – Costs associated to the manufacture of one incompletely calcined scaffolding.

Element	Price	Amount to use	Total Price (€)
Pluronic F-127®	262.00 €/kg	0.0015 kg	0,39
ES	-	0.014 kg	0.00
CO ₂	35.00 €/Kg	0.05 kg	1.75
3D printer	12.40 €/hr	1 hr	12.40
SpeedMixer	5.00 €/hr	0.25 hr	1.25
Balance	10.30 €/hr	0.1 hr	1.03
Nabethern and Energon Furnace	12.40 €/hr	10 hr	124.00
Engineer	9.62 €/hr	5 hr	48.10
TOTAL	-	-	188.40
Total (with taxes)			227.96

If this last price of 22,80 € per scaffolding is assumed, and using the efficiency expressed by Wang *et al.* [3] of 14 mmol·g⁻¹ that some CaO sorbents have shown, the price per CO₂ capture may be calculated. To do so though, acceptable efficiencies of 40 cycles has been assumed, and over 1000 if inert phases and hydration regeneration techniques were to be applied at negligible costs [23]. Following calculations of **Annex E**, the final cost per ton of CO₂ absorbed in dollars could be of up to 79,017.40 \$·tCO₂⁻¹ in a conservative estimate (14g of scaffolding, 14.01 mmol·g⁻¹ efficiency, 40 cycles) and of 17.91 \$·tCO₂⁻¹ if an optimistic estimate is used (100g of scaffolding at same cost, 500% higher efficiency and 5000 cycles due to hydration regeneration techniques). Even though the difference among these two is of over 99%, both scenarios are possible, and only further research in the process could determine the final cost. Furthermore, it is important to note that this price would be account for the part of the budget of CC only regarding the preparation of the scaffold, as the energy of carbonation-calcination process and loss of efficiency of the industrial complex is not considered. Under these circumstances, it can be stated that the 3D printing of CaO requires further investigation to know if it is reliable or not for industrial applications.

Have repairing costs been considered?

As engineers, it is essential to come up with products that can easily be repaired, reused and disposed of once its life cycle ends. This project has not been able to consider these costs however since a final product was not tested. However, reparation techniques have been proposed such as hydration techniques or acid treatments. Further research in this topic applied to scaffoldings is therefore required.

What risks are there that could reduce the project's viability?

Risks that could reduce the project's viability are mainly subjected to the further investigation of alternative technologies whose efficiencies and cost make CaO based scaffoldings outdated, or, in an optimistic scenario, that the reductions in CO₂ achieved by alternative methods to CC make CC unnecessary.

8.3. Social scope

Has the project incurred in reconsiderations about personal, professional, or ethical values of those people implied in the project?

Yes, throughout the duration of the project, the necessity of CC and its viability has been questioned. As explained before, quite a large amount of means were used to be able to achieve the end product. The question arose whether if these would have had a greater and more positive effect if allocated in other research projects. Not only did the question arise because of the difficulties found throughout the project, yet also because of the various potentially negative effects that the product could have if it reached commercial viability. Nevertheless, as part of an in-education project, these resources also served to improve the knowledge in lab work of the projectist.

At the same time, another question that arose in the process of elaborating this project was the following:

How did the materials used affect the social surrounding of the researchers?

To answer this question, in the first stage of the project, ES were provided by the author of the experiment together with various members of the UPC community which volunteered to collect and give to the team their ES waste. This had at a small scale an educational effect to show the number of eggs we consume at our homes and the possible upcycling of this waste.

Who will benefit from the use of the product?

The use of CC, as explained previously, is believed to be the most useful both economically and ecologically in the industry to avoid direct emissions of CO₂. Thus, direct benefits from the use of the product will come from avoiding CO₂ emission taxes for those companies that nowadays have a greater ecological impact, such as the cement industry or energy industry. However, at a larger scale, countries have adopted in many cases binding CO₂

reduction goals that, if not achieved, may have legal and economic consequences. Thus, CC may benefit these countries. Finally, if used correctly, this technology would aid to reduce the CO₂ emissions in the atmosphere, and, at some point in the future, achieve negative emissions. This reductions in emissions could help to avoid an additional increase in global temperatures. Mitigating climate change is a goal from which the whole of the population, and especially those living in vulnerable areas in coastlines, natural disaster areas, or large cities, could benefit from.

Is there a social group that may be negatively affected by it? To what extent?

Again, the answer is affirmative. This however depends on the use that is given to the technology. One of the risks of this technology, as explained previously, is that present action is delayed trusting future generalization of CC. As Gambhir *et al.* [53] explain, this would raise an intergenerational equity issue, putting the burden of mobilizing a great number of means to future generations. These in most cases would be provided by governments, as benefits are not short term nor area specific, which in term would see themselves obligated to reduce public services, affecting those most vulnerable. In essence, to avoid such effects, CC must never be used as an excuse to delay or substitute further emission reduction actions, but to be applied where actions are not plausible, or to reach negative emissions.

9. Conclusions

From the present work, the following conclusions may be drawn:

- **ES** was able to be converted **to up to 98% pure CaO** through simple, low-cost treatments.
- The **use of ES for CC was deemed beneficial** as it showed higher purity than commercial CaO, a morphology with greater surface area ideal for CC, and a reduced particle size ideal for 3D printing.
- **Use of inert phases increased chemical stability** yet still lacked the ability to be inert against the hydration reaction. Among inert phases, **molar ratios of Al to Ca of 3:10 and 4:10** proved to be the best candidates.
- The process of **sintering followed by an incomplete carburation process gave mechanically and chemically stable products**. Furthermore, this allowed for the correct 3D printing of ceramic pieces through DIW.
- Post-sintering treatments such as storage in ethanol, bathing in oil or covering in lacquer deemed unsuccessful as hydration reaction still occurred.
- Using Ca(OH)_2 as an initial feedstock did not help to improve mechanical stability during hydration reaction at room temperature.
- Further research is needed to investigate the mechanical and chemical properties of 3D printed scaffolds.
- The **ecological footprint** of the project was relatively low, being composed of mainly by the **energy usage of the ovens**.

- The sustainability report proved that **further investigation is needed to conclude if the project is economically viable**. Still, risks such as incorrect use of the technology or progress in other CC processes may reduce the utility of the product.
- The product may be described as having a neutral or slightly positive impact in society today, with risks that could end up affecting negatively future generations if the technology was generalized.

Bibliography

1. Carbon Dioxide. A: NASA [online]. [Consulted: 27 Decembre 2020]. Available at <https://climate.nasa.gov/vital-signs/carbon-dioxide/>.
2. Lindsey, R. Climate Change: Atmospheric Carbon Dioxide. A: *Nature*. 2020, Vol. 453, núm. 7193. ISSN 14764687.
3. Wang, J. et al. Recent advances in solid sorbents for CO₂ capture and new development trends. A: *Energy and Environmental Science*. Royal Society of Chemistry, 2014, Vol. 7, núm. 11, p. 3478-3518. ISSN 17545706. DOI 10.1039/c4ee01647e.
4. Àlvarez Maté, F. et al. *3D Printing of α -Al₂O₃ for Catalytic Applications*. Universitat Politècnica de Catalunya (UPC), 2020.
5. Intergovernmental Panel on Climate Change. *Climate Change 2014 Mitigation of Climate Change*. 2014. ISBN 9781107654815. DOI 10.1017/cbo9781107415416.
6. Ritchie, H. i Roser, M. Emissions by Sector. A: .
7. Huang, Z., Karami, D. i Mahinpey, N. Study on the efficiency of multiple amino groups in ionic liquids on their sorbents performance for low-temperature CO₂ capture. A: *Chemical Engineering Research and Design* [online]. Institution of Chemical Engineers, 2021, Vol. 167, p. 198-206. ISSN 02638762. DOI 10.1016/j.cherd.2021.01.016.
8. Ministerio de Ciencia e Innovación. Web of Science. At: [online]. [Consulted: 23 January 2021]. Available at <https://apps.webofknowledge.com>.
9. Durán-Guevara, M.B. et al. Potassium-based sorbents using mesostructured γ -alumina supports for low temperature CO₂ capture. At: *Ceramics International* [online]. Elsevier, 2015, Vol. 41, núm. 2, p. 3036-3044. ISSN 02728842. DOI 10.1016/j.ceramint.2014.10.140.
10. Tahir, M. i Tahir, B. Dynamic photocatalytic reduction of CO₂ to CO in a honeycomb

monolith reactor loaded with Cu and N doped TiO₂ nanocatalysts. At: *Applied Surface Science* [online]. Elsevier B.V., 2016, Vol. 377, p. 244-252. ISSN 01694332. DOI 10.1016/j.apsusc.2016.03.141.

11. National Center for Biotechnology Information. Magnesium oxide. At: [online]. 2021. [Consulted: 26 January 2021]. Available at <https://pubchem.ncbi.nlm.nih.gov/compound/Magnesium-oxide>.

12. Carter, C.B. i Norton, M.G. *Ceramic materials: Science and engineering*. 2013. DOI 10.1007/978-1-4614-3523-5.

13. Yu, C.H., Huang, C.H. i Tan, C.S. A review of CO₂ capture by absorption and adsorption. At: *Aerosol and Air Quality Research*. 2012, Vol. 12, núm. 5, p. 745-769. ISSN 16808584. DOI 10.4209/aaqr.2012.05.0132.

14. Antzara, A., Heracleous, E. i Lemonidou, A.A. Improving the stability of synthetic CaO-based CO₂ sorbents by structural promoters. At: *Applied Energy* [online]. Elsevier Ltd, 2015, Vol. 156, p. 331-343. ISSN 03062619. DOI 10.1016/j.apenergy.2015.07.026.

15. Sun, Z. et al. Ionic diffusion through Calcite (CaCO₃) layer during the reaction of CaO and CO₂. At: *Chemical Engineering Science* [online]. Elsevier, 2012, Vol. 81, p. 164-168. ISSN 00092509. DOI 10.1016/j.ces.2012.05.042.

16. Biasin, A. et al. Investigation of CaO-CO₂ reaction kinetics by in-situ XRD using synchrotron radiation. At: *Chemical Engineering Science* [online]. Elsevier, 2015, Vol. 127, p. 13-24. ISSN 00092509. DOI 10.1016/j.ces.2014.12.058.

17. Sun, H. et al. Progress in the development and application of CaO-based adsorbents for CO₂ capture—a review. At: *Materials Today Sustainability*. 2018, Vol. 1-2, p. 1-27. ISSN 25892347. DOI 10.1016/j.mtsust.2018.08.001.

18. G. Heinrich, J. i M. Gomes, C. Introduction to Ceramics Processing. At: *Journal of The Electrochemical Society*. 1977, Vol. 124, núm. 3. ISSN 00134651.

3D Printing of CaO for Carbon Capture

19. Ströhle, J. et al. Carbonate looping experiments in a 1 MWth pilot plant and model validation. At: *Fuel*. 2014, Vol. 127, p. 13-22. ISSN 00162361. DOI 10.1016/j.fuel.2013.12.043.
20. Witoon, T. Characterization of calcium oxide derived from waste eggshell and its application as CO₂ sorbent. At: *Ceramics International*. 2011, Vol. 37, núm. 8, p. 3291-3298. ISSN 02728842. DOI 10.1016/j.ceramint.2011.05.125.
21. Salaudeen, S.A. et al. Hydrogen-rich gas stream from steam gasification of biomass: Eggshell as a CO₂ sorbent. At: *Energy and Fuels*. 2020, Vol. 34, núm. 4, p. 4828-4836. ISSN 15205029. DOI 10.1021/acs.energyfuels.9b03719.
22. Blamey, J. et al. The calcium looping cycle for large-scale CO₂ capture. At: *Progress in Energy and Combustion Science* [online]. Elsevier Ltd, 2010, Vol. 36, núm. 2, p. 260-279. ISSN 03601285. DOI 10.1016/j.pecs.2009.10.001.
23. Hu, Y. et al. Incorporation of CaO into inert supports for enhanced CO₂ capture: A review. At: *Chemical Engineering Journal* [online]. Elsevier, 2020, Vol. 396, núm. April, p. 125253. ISSN 13858947. DOI 10.1016/j.cej.2020.125253.
24. Hu, Y., Lu, H. i Li, H. Single step fabrication of spherical CaO pellets via novel agar-assisted moulding technique for high-temperature CO₂ capture. At: *Chemical Engineering Journal* [online]. Elsevier B.V., 2021, Vol. 404, núm. September 2020, p. 127137. ISSN 13858947. DOI 10.1016/j.cej.2020.127137.
25. Koirala, R., Reddy, G.K. i Smirniotis, P.G. Single nozzle flame-made highly durable metal doped ca-based sorbents for CO₂ capture at high temperature. At: *Energy and Fuels*. 2012, Vol. 26, núm. 5, p. 3103-3109. ISSN 08870624. DOI 10.1021/ef3004015.
26. Yoosuk, B. et al. Improving transesterification acitvity of CaO with hydration technique. At: *Bioresource Technology* [online]. Elsevier Ltd, 2010, Vol. 101, núm. 10, p. 3784-3786. ISSN 09608524. DOI 10.1016/j.biortech.2009.12.114.

27. Criado, Y.A., Alonso, M. i Abanades, J.C. Kinetics of the $\text{CaO}/\text{Ca}(\text{OH})_2$ hydration/dehydration reaction for thermochemical energy storage applications. At: *Industrial and Engineering Chemistry Research*. 2014, Vol. 53, núm. 32, p. 12594-12601. ISSN 15205045. DOI 10.1021/ie404246p.
28. Diego, M.E., Arias, B. i Abanades, J.C. Investigation of the dynamic evolution of the CO_2 carrying capacity of solids with time in La Pereda 1.7 MWth calcium looping pilot plant. At: *International Journal of Greenhouse Gas Control* [online]. Elsevier, 2020, Vol. 92, núm. May 2019, p. 102856. ISSN 17505836. DOI 10.1016/j.ijggc.2019.102856.
29. Kim, K. et al. Performance comparison of moving and fluidized bed sorption systems for an energy-efficient solid sorbent-based carbon capture process. At: *Energy Procedia*. Elsevier B.V., 2014, Vol. 63, p. 1151-1161. ISSN 18766102. DOI 10.1016/j.egypro.2014.11.125.
30. Cree, D. i Rutter, A. Sustainable Bio-Inspired Limestone Eggshell Powder for Potential Industrialized Applications. At: *ACS Sustainable Chemistry and Engineering*. 2015, Vol. 3, núm. 5, p. 941-949. ISSN 21680485. DOI 10.1021/acssuschemeng.5b00035.
31. Nawar, A. et al. Enhanced CO_2 capture using organic acid structure modified waste eggshell derived CaO sorbent. At: *Journal of Environmental Chemical Engineering* [online]. Elsevier Ltd, 2021, Vol. 9, núm. 1, p. 104871. ISSN 22133437. DOI 10.1016/j.jece.2020.104871.
32. Dwivedi, S.P., Sharma, S. i Mishra, R.K. Characterization of waste eggshells and CaCO_3 reinforced AA2014 green metal matrix composites: A green approach in the synthesis of composites. At: *International Journal of Precision Engineering and Manufacturing*. 2016, Vol. 17, núm. 10, p. 1383-1393. ISSN 20054602. DOI 10.1007/s12541-016-0164-z.
33. Chen, Z. et al. 3D printing of ceramics: A review. At: *Journal of the European Ceramic Society*. 2019, Vol. 39, núm. 4, p. 661-687. ISSN 1873619X. DOI 10.1016/j.jeurceramsoc.2018.11.013.

3D Printing of CaO for Carbon Capture

34. Lind, A. et al. Multi-purpose structured catalysts designed and manufactured by 3D printing. At: *Materials and Design*. 2020, Vol. 187, p. 1-8. ISSN 18734197. DOI 10.1016/j.matdes.2019.108377.
35. Stuecker, J.N. et al. Advanced Support Structures for Enhanced Catalytic Activity. At: *Industrial and Engineering Chemistry Research*. 2004, Vol. 43, núm. 1, p. 51-55. ISSN 08885885. DOI 10.1021/ie030291v.
36. Rahaman, M.N. *Ceramic Processing*. CRC Press, 2017. DOI 10.1201/9781315276045.
37. Pandit, N.K. i McIntyre, H.J. Nivedita K. Pandit and Holly J. McIntyre. At: *Pharmaceutical development and technology*. 1997, Vol. 2, núm. 2, p. 181-184.
38. Zhang, X., Wu, X. i Shi, J. Additive manufacturing of zirconia ceramics: a state-of-the-art review. At: *Journal of Materials Research and Technology* [online]. Korea Institute of Oriental Medicine, 2020, Vol. 9, núm. 4, p. 9029-9048. ISSN 22387854. DOI 10.1016/j.jmrt.2020.05.131.
39. Tiwari, S., Singh, P.K. i Kumar, S. Variation of density in additive manufacturing of ceramic parts: A review. At: *Materials Today: Proceedings* [online]. Elsevier Ltd, 2021, núm. xxxx. ISSN 22147853. DOI 10.1016/j.matpr.2021.03.070.
40. Awogbemi, O., Inambao, F. i Onuh, E.I. Modification and characterization of chicken eggshell for possible catalytic applications. At: *Heliyon* [online]. Elsevier Ltd, 2020, Vol. 6, núm. 10, p. e05283. ISSN 24058440. DOI 10.1016/j.heliyon.2020.e05283.
41. Huang, X. et al. Physicochemical and structural characteristics of nano eggshell calcium prepared by wet ball milling. At: *Lwt* [online]. Elsevier, 2020, Vol. 131, núm. June, p. 109721. ISSN 00236438. DOI 10.1016/j.lwt.2020.109721.
42. Baláž, M. Ball milling of eggshell waste as a green and sustainable approach: A review. At: *Advances in Colloid and Interface Science*. 2018, Vol. 256, p. 256-275. ISSN 00018686. DOI 10.1016/j.cis.2018.04.001.

43. Zhao, M. et al. Durability of CaO-CaZrO₃ sorbents for high-temperature CO₂ capture prepared by a wet chemical method. At: *Energy and Fuels*. 2014, Vol. 28, núm. 2, p. 1275-1283. ISSN 08870624. DOI 10.1021/ef4020845.
44. Callister, W.D. Materials science and engineering: An introduction (2nd edition). At: *Materials & Design*. 1991, Vol. 12, núm. 1. ISSN 02613069. DOI 10.1016/0261-3069(91)90101-9.
45. Leng, Y. *Materials characterization: Introduction to microscopic and spectroscopic methods: Second edition*. 2013. DOI 10.1002/9783527670772.
46. D'Silva, G.J., Goanta, V. i Ciocanel, C. Fracture toughness evaluation of Ni₂MnGa magnetic shape memory alloys by Vickers micro indentation. At: *Engineering Fracture Mechanics* [online]. Elsevier Ltd, 2021, Vol. 247, núm. August 2020, p. 107655. ISSN 00137944. DOI 10.1016/j.engfracmech.2021.107655.
47. Chaibundit, C. et al. Effect of ethanol on the gelation of aqueous solutions of Pluronic F127. At: *Journal of Colloid and Interface Science* [online]. Elsevier Inc., 2010, Vol. 351, núm. 1, p. 190-196. ISSN 00219797. DOI 10.1016/j.jcis.2010.07.023.
48. Zaki, A. et al. Investigation of Ca₁₂Al₁₄O₃₃ Mayenite for hydration/dehydration thermochemical energy storage. At: *Journal of Energy Storage* [online]. Elsevier, 2020, Vol. 31, núm. June, p. 101647. ISSN 2352152X. DOI 10.1016/j.est.2020.101647. Available at: <https://doi.org/10.1016/j.est.2020.101647>.
49. Climent, J. et al. El informe de sostenibilidad del Trabajo de Fin de Grado del área de las ingenierías. At: *REDU. Revista de Docencia Universitaria*. 2018, Vol. 16, núm. 2, p. 75. ISSN 1887-4592. DOI 10.4995/redu.2018.10092.
50. Red Eléctrica de España. EMISIONES Y FACTOR DE EMISIÓN DE CO₂ EQ. DE LA GENERACIÓN (tCO₂ eq. | tCO₂ eq./MWh) | Sistema eléctrico:peninsular. At: [online]. 2021. [Consulted: 7 June 2021]. Available at: <https://www.ree.es/es/datos/generacion/no->

3D Printing of CaO for Carbon Capture

renovables-detalle-emisiones-CO2.

51. DIAS DE OLIVEIRA, M.E., VAUGHAN, B.E. i RYKIEL JR., E.J. Ethanol as Fuel: Energy, Carbon Dioxide Balances, and Ecological Footprint. At: *Bioscience Oxford Journal*. 2014, núm. March, p. 1-504. DOI 10.1641/0006-3568(2005)055[0593:EAFECD]2.0.CO;2.

52. Cansino, J.M., Román-Collado, R. i Merchán, J. Do Spanish energy efficiency actions trigger JEVON'S paradox? At: *Energy*. 2019, Vol. 181, núm. 2019, p. 760-770. ISSN 03605442. DOI 10.1016/j.energy.2019.05.210.

53. Gambhir, A. i Tavoni, M. Direct Air Carbon Capture and Sequestration: How It Works and How It Could Contribute to Climate-Change Mitigation. At: *One Earth* [online]. The Authors, 2019, Vol. 1, núm. 4, p. 405-409. ISSN 25903322. DOI 10.1016/j.oneear.2019.11.006.

54. Ministerio de Trabajo, M. y S.S. *Boletín Oficial del Estado: Ministerio De Trabajo , Migraciones*. 2019. 2019. ISBN 9900434501.

55. UPC. Barcelona Center in Multiscale Science and Engineering. At: [online]. 2021. Available at: <https://multiscale.upc.edu/en/infrastructure/services-and-prices>.

56. Li, Z.H. et al. Effect of steam on CaO regeneration, carbonation and hydration reactions for CO₂ capture. At: *Fuel Processing Technology* [online]. Elsevier B.V., 2016, Vol. 151, p. 101-106. ISSN 03783820. DOI 10.1016/j.fuproc.2016.05.019.

57. Baláž, M. et al. Eggshell biomaterial: Characterization of nanophase and polymorphs after mechanical activation. At: *Advanced Powder Technology*. 2015, Vol. 26, núm. 6, p. 1597-1608. ISSN 15685527. DOI 10.1016/j.appt.2015.09.003.

58. Akbarzadeh, A., Ahmadelouydarab, M. i Niaei, A. Capabilities of α -Al₂O₃, γ -Al₂O₃, and bentonite dry powders used in flat plate solar collector for thermal energy storage. At: *Renewable Energy* [online]. Elsevier Ltd, 2021, Vol. 173, p. 704-720. ISSN 18790682. DOI 10.1016/j.renene.2021.04.026.

59. Dias, A.P.S. i Ramos, M. On the storage stability of CaO biodiesel catalyst. Hydration and carbonation poisoning. At: *Journal of Environmental Chemical Engineering* [online]. Elsevier Ltd, 2021, Vol. 9, núm. 1, p. 104917. ISSN 22133437. DOI 10.1016/j.jece.2020.104917.


60. Musyarofah et al. XRD , WAXS , FTIR , and XANES studies of silica-zirconia systems. At: *Ceramics International* [online]. Elsevier Ltd and Techna Group S.r.l., 2019, Vol. 45, núm. 12, p. 15660-15670. ISSN 0272-8842. DOI 10.1016/j.ceramint.2019.05.078.

61. Chandra, N. et al. Synthesis and characterization of nano-sized zirconia powder synthesized by single emulsion-assisted direct precipitation. At: *Journal of Colloid and Interface Science* [online]. Elsevier Inc., 2010, Vol. 342, núm. 2, p. 327-332. ISSN 00219797. DOI 10.1016/j.jcis.2009.10.065.

62. Kumar, A. et al. Microstructure and mechanical properties of nano Y_2O_3 and ZrO_2 dispersed austenite steel. At: *Materials Today: Proceedings* [online]. Elsevier Ltd., 2020, Vol. 21, p. 1793-1799. ISSN 22147853. DOI 10.1016/j.matpr.2020.01.233.

Annex A

A1. CaO feedstock data sheet

 www.sigmaaldrich.com

SAFETY DATA SHEET Version 6.3
according to Regulation (EC) No. 1907/2006 Revision Date 18.05.2020
Print Date 10.06.2021
GENERIC EU MSDS - NO COUNTRY SPECIFIC DATA - NO OEL DATA

SECTION 1: Identification of the substance/mixture and of the company/undertaking

1.1 Product identifiers

Product name : Calcium oxide

Product Number : 208159

Brand : Aldrich

REACH No. : A registration number is not available for this substance as the substance or its uses are exempted from registration, the annual tonnage does not require a registration or the registration is envisaged for a later registration deadline.

CAS-No. : 1305-78-8

1.2 Relevant identified uses of the substance or mixture and uses advised against

Identified uses : Laboratory chemicals, Manufacture of substances

1.3 Details of the supplier of the safety data sheet

Company : Merck Life Science S.L.
Calle Maria de Molina 40
E-28006 MADRID

Telephone : +34 916 619 977

Fax : +34 916 619 642

E-mail address : serviciotecnico@merckgroup.com

1.4 Emergency telephone number

Emergency Phone # : 900-868538 (CHEMTREC España)
+(34)-931768545 (CHEMTREC internacional)

SECTION 2: Hazards identification

2.1 Classification of the substance or mixture

Classification according to Regulation (EC) No 1272/2008

Skin irritation (Category 2), H315

Serious eye damage (Category 1), H318

Specific target organ toxicity - single exposure (Category 3), Respiratory system, H335

For the full text of the H-Statements mentioned in this Section, see Section 16.

2.2 Label elements

Labelling according Regulation (EC) No 1272/2008


Aldrich- 208159

The life science business of Merck operates as MilliporeSigma in the US and Canada

Page 1 of 9



3D Printing of CaO for Carbon Capture

Pictogram	
Signal word	Danger
Hazard statement(s)	
H315	Causes skin irritation.
H318	Causes serious eye damage.
H335	May cause respiratory irritation.
Precautionary statement(s)	
P280	Wear eye protection/ face protection.
P302 + P352	IF ON SKIN: Wash with plenty of water.
P305 + P351 + P338 +	IF IN EYES: Rinse cautiously with water for several minutes.
P310	Remove contact lenses, if present and easy to do. Continue rinsing. Immediately call a POISON CENTER/ doctor.
Supplemental Hazard Statements	none

2.3 Other hazards

This substance/mixture contains no components considered to be either persistent, bioaccumulative and toxic (PBT), or very persistent and very bioaccumulative (vPvB) at levels of 0.1% or higher.

SECTION 3: Composition/information on ingredients

3.1 Substances

Synonyms	: Quicklime Lime
Formula	: CaO
Molecular weight	: 56,08 g/mol
CAS-No.	: 1305-78-8
EC-No.	: 215-138-9

Component	Classification	Concentration
Calcium oxide	Skin Irrit. 2; Eye Dam. 1; STOT SE 3; H315, H318, H335 Concentration limits: 20 %: STOT SE 3, H335;	<= 100 %

For the full text of the H-Statements mentioned in this Section, see Section 16.

SECTION 4: First aid measures

4.1 Description of first aid measures

General advice

Consult a physician. Show this safety data sheet to the doctor in attendance.

If inhaled

If breathed in, move person into fresh air. If not breathing, give artificial respiration. Consult a physician.

Aldrich- 208159

Page 2 of 9

The life science business of Merck operates as MilliporeSigma in the US and Canada



3D Printing of CaO for Carbon Capture

Body Protection

Complete suit protecting against chemicals, The type of protective equipment must be selected according to the concentration and amount of the dangerous substance at the specific workplace.

Respiratory protection

Where risk assessment shows air-purifying respirators are appropriate use a full-face particle respirator type N100 (US) or type P3 (EN 143) respirator cartridges as a backup to engineering controls. If the respirator is the sole means of protection, use a full-face supplied air respirator. Use respirators and components tested and approved under appropriate government standards such as NIOSH (US) or CEN (EU).

Control of environmental exposure

Prevent further leakage or spillage if safe to do so. Do not let product enter drains. Discharge into the environment must be avoided.

SECTION 9: Physical and chemical properties

9.1 Information on basic physical and chemical properties

a) Appearance	Form: powder
b) Odour	odourless
c) Odour Threshold	No data available
d) pH	12,6 at 20 °C (saturated solution)
e) Melting point/freezing point	Melting point: 2.580 °C
f) Initial boiling point and boiling range	2.850 °C - lit.
g) Flash point	does not flash
h) Evaporation rate	No data available
i) Flammability (solid, gas)	No data available
j) Upper/lower flammability or explosive limits	No data available
k) Vapour pressure	Not applicable
l) Vapour density	No data available
m) Relative density	3,3 g/mL at 25 °C
n) Water solubility	1,65 g/l at 20 °C - OECD Test Guideline 105 - Risk of violent reaction.
o) Partition coefficient: n-octanol/water	Not applicable
p) Auto-ignition temperature	No data available
q) Decomposition temperature	No data available

Aldrich- 208159

Page 5 of 9

The life science business of Merck operates as MilliporeSigma in the US and Canada



A2. α -Al₂O₃ feedstock data sheet



Global Product Data

CT 3000 LS SG

Product Description

Almatis Alumina CT3000 LS SG is a special purpose low soda high reactive alumina. It combines high fired density with very low impurities.

Product Features

High fired density > 3,90 g/cm³ at 1540 °C 1 hour soak time and > 3,94 g/cm³ at 1600 °C 1 hour soak time. Very low impurities.

Applications

High end ceramic pieces where high sintered density and low impurities are required.

Chemical Analysis		typical
Al ₂ O ₃	[%]	99.8
Na ₂ O	[%]	0.03
Fe ₂ O ₃	[%]	0.015
SiO ₂	[%]	0.015
MgO	[%]	0.040
CaO	[%]	0.015

Properties		typical
Specific Surface area / BET		7.80 m ² /g
Particle Size / D50 Cilas		0.5 µm
Particle Size / D90 Cilas		2.0 µm
Green density (90 MPa)		2.24 g/cm ³
Fired density (1540 °C / 1600 °C)		3.91 g/cm ³ / 3.95 g/cm ³
Shrinkage (1540 °C / 1600 °C)		16.8 % / 17.3 %

All data are based upon Almatis standard test methods.

The typical properties are based upon the actual averages from production data.

Think alumina, think Almatis.

GP-RCP/024/R02/0812/MSDS 387





CT 3000 LS SG

Standard Packaging

- 25 kg paper bags on 1 mt pallet
- 1000 kg big bag, discharge sleeve and shrink wrapped



Contacts for sales, technical information and application assistance

Almatis GmbH

Giulinistrasse 2
67065 Ludwigshafen
Germany

☎ 49 621 5707 0
☎ 49 621 5707 130

Almatis B.V.

Theemsweg 30
3197KM Botlek RT
The Netherlands

☎ 31 181 2701 00
☎ 31 181 2178 53

Almatis, Inc.

501 West Park Road
Leetsdale, PA 15056, USA

☎ 800 643 8771 General
☎ 1 412 630 2800
☎ 1 412 630 2900

Qingdao Almatis Co., Ltd.

F15, Sunshine Tower
61 Hongkong Middle Road
Qingdao, 266071
P.R. China

☎ 86 532 8572 8035
☎ 86 532 8572 8551

Qingdao Almatis Trading Co., Ltd.

Room 1807, Eton Place
69 Dong Fang Road
Shanghai, 200120
P.R. China

☎ 86 21 5879 4987
☎ 86 21 5879 6502

Almatis do Brasil Ltda.

Avenida Jose de Souza
Campos, 243
2º Andar – Cambui
13025-320 – Campinas,
SP – Brasil

☎ 55 19 3515-1400
☎ 55 19 3515-1410



ALMATIS
PREMIUM ALUMINA

Almatis GmbH
Lyoner Straße 9
60528 Frankfurt/Germany

Phone 49 69 957 341 0
Fax 49 69 957 341 13

info@almatis.com
www.almatis.com

Almatis Alumina Private Limited

Kankaria Estate
2nd Floor
6, Little Russell Street
Kolkata 700-071, India

☎ 91 33 2289 4694
☎ 91 33 2289 4693

Almatis Limited


Morimura Bldg.
1-3-1 Toranomom
Minato-ku, Tokyo 105-8451
Japan

☎ 81 3 3502 2371
☎ 81 3 3502 2375

MSDS 387



A3. Datasheet for powders from which R60 and R60C originate.



GY3Z-R60 3mol% Y₂O₃ stabilized ZrO₂
Ready-To-Press granules

Technical data sheet

04/2019

Zr Chemical composition (wt%)

Y ₂ O ₃ ^a	Al ₂ O ₃ ^a	SiO ₂ ^b	Na ₂ O ^b	TiO ₂ ^b	Fe ₂ O ₃ ^b	L.O.I. ^c
5.4±0.20	0.25±0.05	<0.02	<0.02	<0.005	<0.005	2.5 - 3.5

^a: XRF method ; ^b: ICP method ; ^c: Loss On Ignition 20 → 1000°C

Physical properties

Granule size			
d50		60	µm
d90		<120	µm
Specific surface area BET		6.0 – 8.0	m ² /g
Loos bulk density ^a		1.3	g/cm ³
Flowability ^a		>0.85	g/s


^a: Hall cup

Benefits

- Excellent densification thanks to fine and homogeneous zirconia particles
- Advanced engineered binder system for easy pressing (uniaxial & isostatic)
- GY3Z-R60 allows the manufacturing of ceramic parts with outstanding mechanical performance

Contact us

SEPR - Saint-Gobain ZirPro
B.P. 60025 - Bâtiment L
2539, Route de Sorgues
84131 Le Pontet Cedex
France
Email: zirpro@saint-gobain.com



www.zirpro.com



Ceramic properties^a

Green density	3.0	-
Sintered density	≥ 6.05	-
Bending strength ^b	1000	MPa
Hardness ^c : HV _{0,3/15}	1250	HV
Fracture toughness ^d : K _{Ic}	5.5	MPa.m ^{1/2}

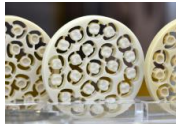

^a: uniaxial pressing at 100MPa / Sintering 1450°C – 2hrs
^b: 4-points MOR (ISO 6872)
^c: Vickers indentation (ISO 6507)
^d: DCM (ISO 146 27)

Main applications

→ Advanced technical ceramics

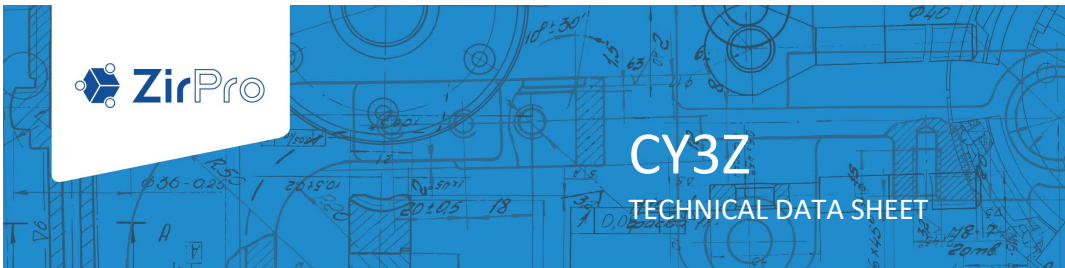
→ Dental standard grades



These values have been obtained with Saint-Gobain ZirPro's specific control means. They are offered for information and verification and are not, in part or totally, to be considered as a warranty for which we assume legal responsibility. Saint-Gobain is neither responsible nor liable for results obtained from the use of the products.

A4. Datasheet of the powders from which residue RA originates.



01/2021

✦ CY3Z GRADES ARE HIGH PERFORMANCE YTTRIA-DOPED ZIRCONIA POWDERS

CY3Z grades are 3 mol% yttria-stabilized zirconia powders made by chemical process. Their high purities (>99.9%) and the tight control of the physical characteristics enable the manufacturing high performance zirconia ceramic parts.

Two grades of CY3Z with different specific surface area are available:

- CY3Z-RS grade (SSA of 7m²/g) for ceramic parts made by injection molding, additive manufacturing or casting.
- CY3Z-MS grade with (SSA of 15m²/g) for the manufacturing of small size ceramic parts with fine microstructure by injection molding or additive manufacturing.

CY3Z grades are also available with 0.25wt% alumina (CY3Z-RA, CY3Z-MA) for improved reactivity.

📏 TYPICAL PARTICLE SIZE & SPECIFIC SURFACE AREA

	Particle size ^a (µm)		Specific Surface Area ^b (m ² /g)	Ceramic part features
	D50	D90		
CY3Z-MA	0.2	<1.0	15	Fine ceramic microstructure High hydrothermal resistance
CY3Z-MS				
CY3Z-RA	0.4	<1.0	7	Easy-to-process High mechanical performance
CY3Z-RS				

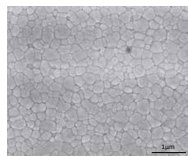
^a: Laser diffraction - ^b: B.E.T. measurement

🧪 CHEMICAL ANALYSIS

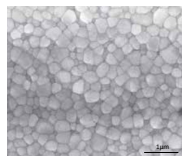
	Chemistry (wt%) ^a						L.O.I. ^b (wt%)
	Al ₂ O ₃	Y ₂ O ₃	SiO ₂	Na ₂ O	TiO ₂	Fe ₂ O ₃	
CY3Z-MA	0.25±0.05						<1.0
CY3Z-MS	<0.02						
CY3Z-RA	0.25±0.05	5.40±0.20	<0.02	<0.02	<0.005	<0.005	
CY3Z-RS	<0.02						

^a: I.C.P. - ^b: Loss weight from 20°C to 1000°C

🔍 CY3Z-M AND CY3Z-R GRADES ALLOW TO OBTAIN FINE MICROSTRUCTURE



Ceramic part based on CY3Z-MA



Ceramic part based on CY3Z-RA

📦 PACKAGING

- 25kg plastic pail

⚙️ MAIN APPLICATIONS

- Technical ceramics : optical fiber connectors, plungers, valves, bearings, grinding media, biomedical



Structural ceramic parts



Optical fiber connectors

The contents of this data sheet are given in good faith but without warranty.

SEPR – SAINT-GOBAIN ZIRPRO
B.P. 60025 - Batiment L
539, route de Sorgues
84131 Le Pontet Cedex - France
zirpro@saint-gobain.com
Tél : +33 4 90 32 70 02
www.zirpro.com

Annex B

B.1 EDX Results for F1, F2, F3, and F4.

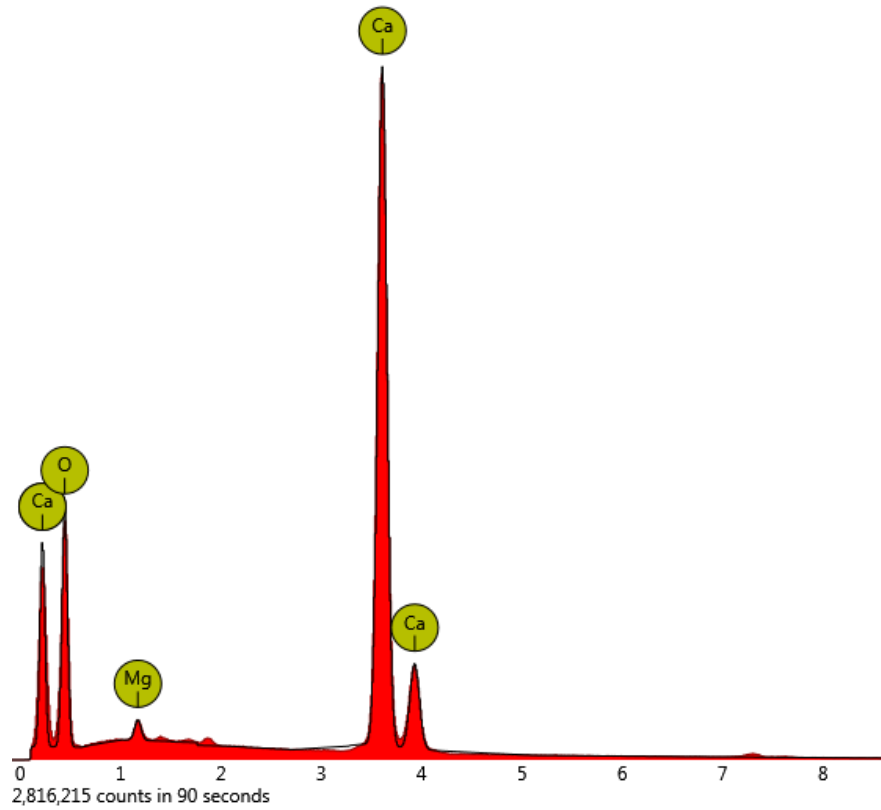


Figure 66 – EDX intensity patterns for F1.

3D Printing of CaO for Carbon Capture

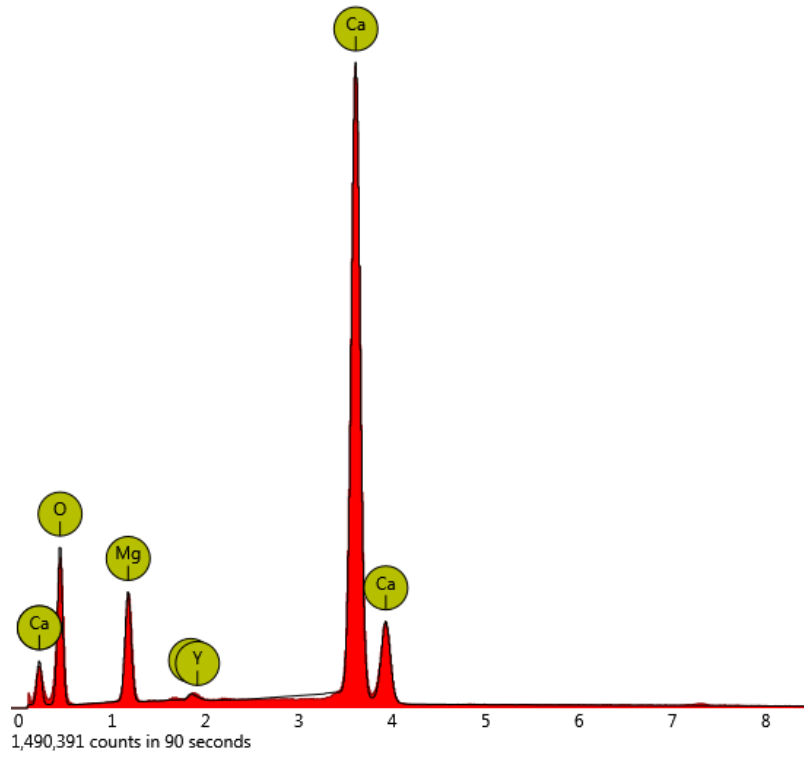


Figure 67 – EDX intensity patterns for F2.

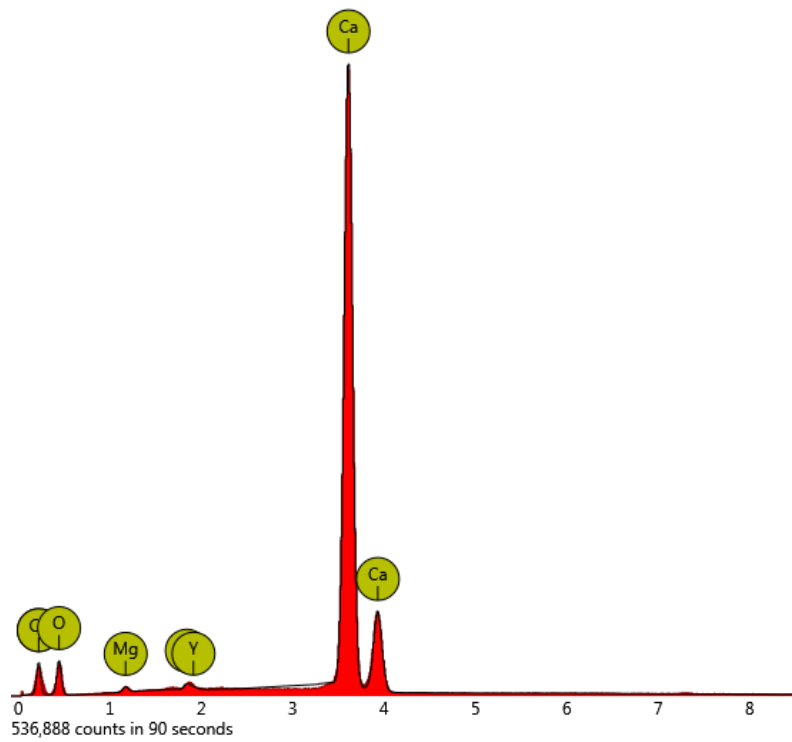


Figure 68 – EDX intensity patterns for F3.

3D Printing of CaO for Carbon Capture

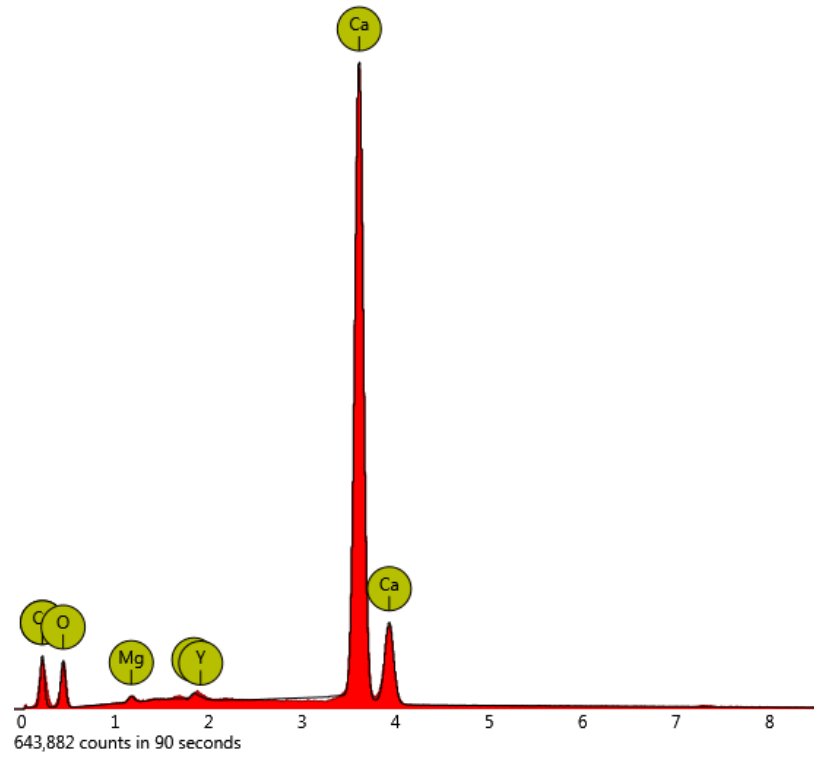


Figure 69 – EDX intensity patterns for F4.

B.2 EDX results for R60, R60C and RA

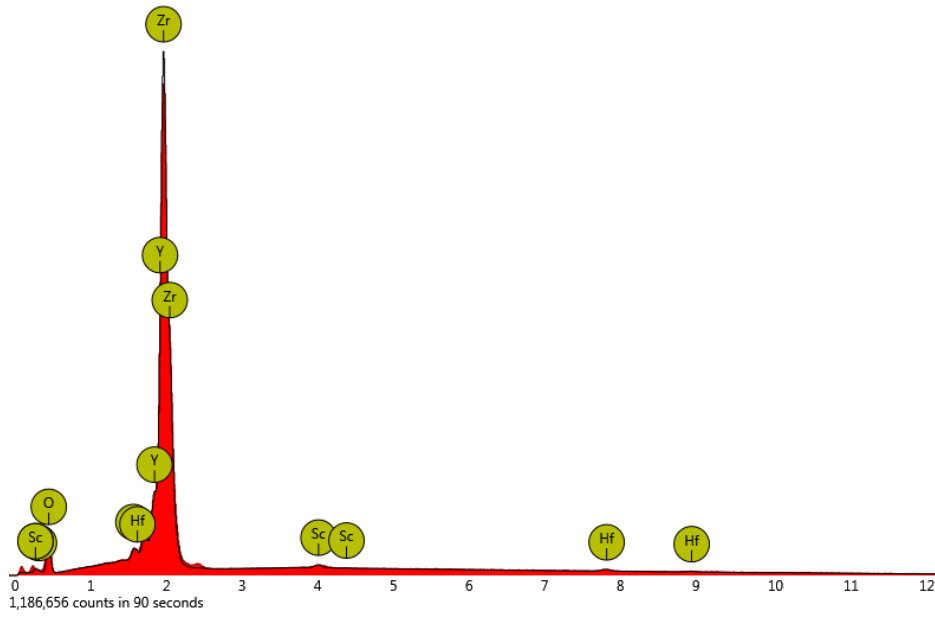


Figure 70 - EDX intensity patterns for R60.

3D Printing of CaO for Carbon Capture

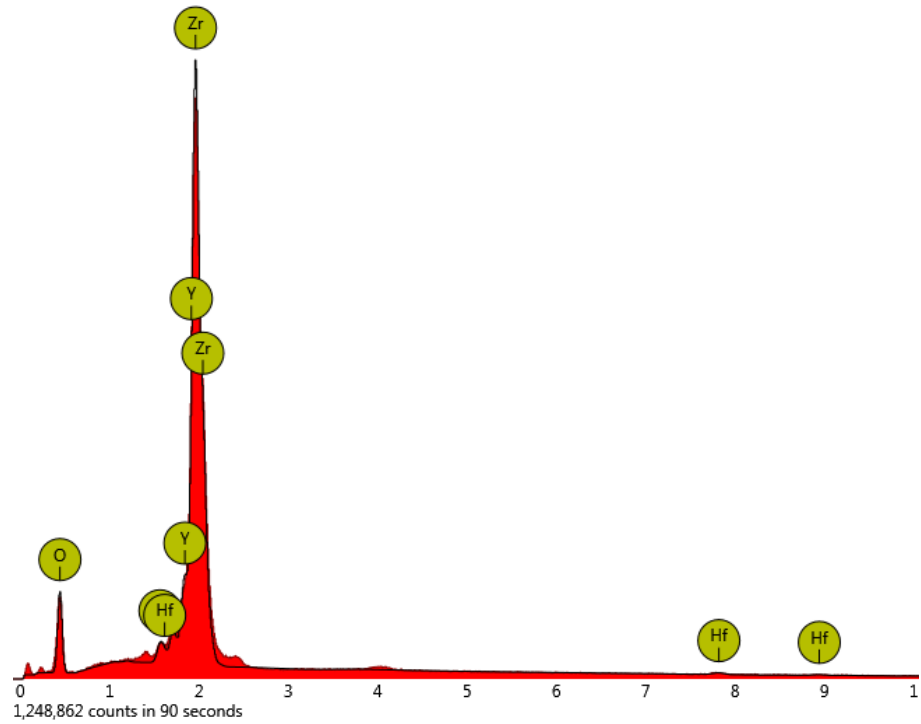


Figure 71 - EDX intensity patterns for R60C.

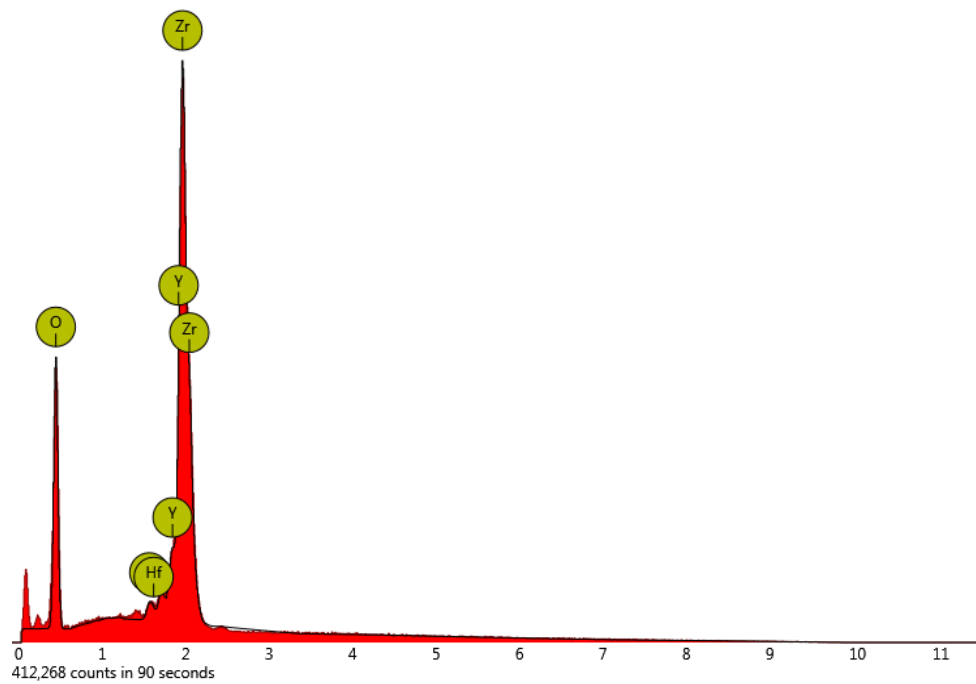


Figure 72 - EDX intensity patterns for RA.

Annex C

C1 XRD bibliography values for the various elements found in the diffraction patterns

Table 21 – Table showing XRD 2θ values for CaO, CaCO₃, α -Al₂O₃, Ca₃Al₂O₆, MgO, CaZrO₃, Ca(OH)₂, Ca₁₂Al₁₄O₃₃, ZrO₂ and Y₂O₃.

Literature Source and Material	Peaks, 2θ (°)
Sun et al. [15] CaCO ₃ (Calcite, values up to 70°)	23.1, 29.8 (highest intensity), 36.2, 39.7, 43.2, 47.2, 47.5, 48.6, 56.7, 57.7, 60.8, 61.1, 61.5, 63.1, 65.0, 65.2
Sun et al. [15] CaO (values up to 70°)	32.2, 37.6 (highest intensity), 54.0, 64.4, 67.6
Dwivedi et al. [32] CaCO ₃ (ES, values up to 75°)	23.1, 26.7, 29.5 (highest intensity), 36.1, 39.6, 43.2, 47.7, 48.9, 52.9, 56.1, 60.0, 64.2, 65.2
Baláz et al. [57] CaCO ₃ (Calcite and Aragonite peaks, values up to 35°)	23.1 (Calcite), 26.2 (Aragonite), 29.5 (Calcite), 31.6 (Calcite), 33.1 (Aragonite)
Akbarzadeh et al. [58] α -Al ₂ O ₃	25.6, 35.1, 37.8, 43.5 (highest intensity), 53.8, 57.7, 61.3 (low intensity), 66.9, 68.3, 77.0 (low intensity)
Antzara et al. [14] Ca ₃ Al ₂ O ₆ (Aluminate)	33.0, 47.6, 59.2, 69.7
Antzara et al. [14] MgO	43.0, 62.2
Antzara et al. [14] CaZrO ₃	22.0, 31.7, 45.0, 50.8, 55.6, 56.5, 65.9, 74.9

3D Printing of CaO for Carbon Capture

Table 21 – Table showing XRD 2θ values for CaO, CaCO₃, α -Al₂O₃, Ca₃Al₂O₆, MgO, CaZrO₃, Ca(OH)₂, Ca₁₂Al₁₄O₃₃, ZrO₂ and Y₂O₃ (continuation).

Literature Source and Material	Peaks, 2θ (°)
Antzara <i>et al.</i> [14] Ca(OH)₂	17.8, 34.0, 50.8
Soares Dias <i>et al.</i> [59] (Ca(OH)₂	17.2, 28.8, 34.0, 47.3, 51.0
Zaki <i>et al.</i> [48] Ca₁₂Al₁₄O₃₃ (Mayenite)	18.0, 21.0, 23.3, 27.9, 29.9, 33.3, 35.1, 36.8, 38.2, 41.2, 42.7, 44.0, 46.9, 48.0, 49.2, 51.9, 53.0, 54.1, 55.2, 56.5, 57.0, 58.8, 60.9, 62.0, 63.0, 64.1, 65.1, 66.2, 67.2, 69.3, 70.2, 71.3, 72.2, 73.4, 74.3, 75.2, 77.2, 78.1, 79.1
Musyarofah <i>et al.</i> [60] ZrO₂ (tetragonal)	30.2, 34.9, 35.2, 50.2, 58.1, 60.3
Chandra <i>et al.</i> [61] ZrO₂ (monoclínica)	28.2, 31.5, 33.9, 34.7, 35.4
Kumar <i>et al.</i> [62] Y₂O₃ (Yttria)	27.9, 32.1, 43.1, 44.0 (low intensity), 46.5, 50.2, 55.0

Annex D

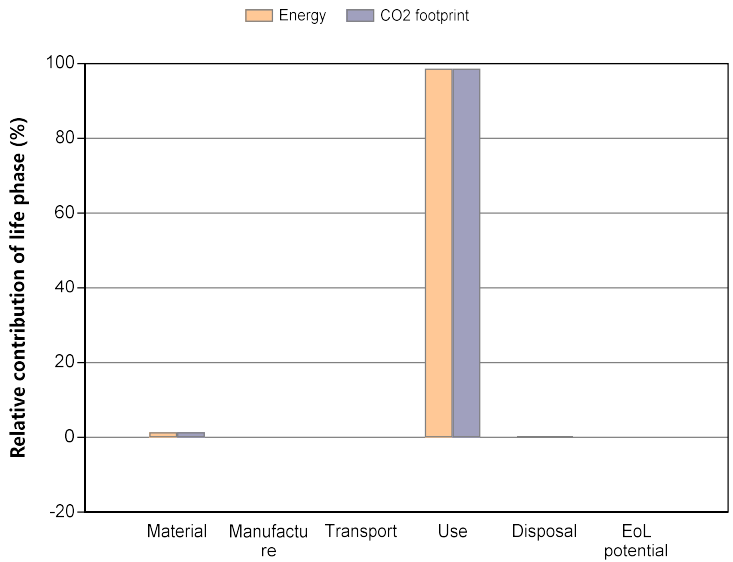
D.1 Ecological footprint EduPack calculations



Eco Audit Report

Product name: Product
 Country of use: Europe
 Product life (years): 1

Summary:



[Energy details](#)

[CO2 footprint details](#)

Phase	Energy (MJ)	Energy (%)	CO2 footprint (kg)	CO2 footprint (%)
Material	30,1	1,3	1,64	1,4
Manufacture	0	0,0	0	0,0
Transport	0	0,0	0	0,0
Use	2,3e+03	98,7	114	98,6
Disposal	0,12	0,0	0,0084	0,0
Total (for first life)	2,33e+03	100	116	100
End of life potential	0		0	

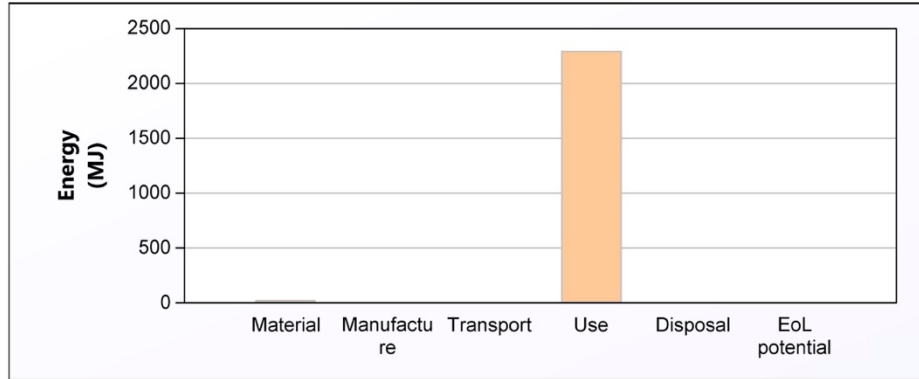
3D Printing of CaO for Carbon Capture



Eco Audit Report

Energy Analysis

[Summary](#)



	Energy (MJ/year)
Equivalent annual environmental burden (averaged over 1 year product life):	2,33e+03

Detailed breakdown of individual life phases

Material:

[Summary](#)

Component	Material	Recycled content* (%)	Part mass (kg)	Qty.	Total mass (kg)	Energy (MJ)	%
Zirconia	Zirconia (Y2O3 stabilized)	Virgin (0%)	0,2	1	0,2	14	47,9
Alumina	Alumina (99.9%)	Virgin (0%)	0,3	1	0,3	16	51,9
CaO	Calcium carbonate (p)	Virgin (0%)	0,1	1	0,1	0,057	0,2
Total				3	0,6	30	100

*Typical: Includes 'recycle fraction in current supply'

Manufacture:

[Summary](#)

Component	Process	Amount processed	Energy (MJ)	%
Total				100

3D Printing of CaO for Carbon Capture

Transport:

[Summary](#)

Breakdown by transport stage

Stage name	Transport type	Distance (km)	Energy (MJ)	%
Total				100

Breakdown by components

Component	Mass (kg)	Energy (MJ)	%
Zirconia	0,2	0	
Alumina	0,3	0	
CaO	0,1	0	
Total	0,6	0	100

Use:

[Summary](#)

Static mode

Energy input and output type	Electric to thermal
Country of use	Europe
Power rating (W)	1,8e+03
Usage (hours per day)	12
Usage (days per year)	15
Product life (years)	1

Relative contribution of static and mobile modes

Mode	Energy (MJ)	%
Static	2,3e+03	100,0
Mobile	0	
Total	2,3e+03	100

3D Printing of CaO for Carbon Capture

Disposal:

[Summary](#)

Component	End of life option	Energy (MJ)	%
Zirconia	Landfill	0,04	33,3
Alumina	Landfill	0,06	50,0
CaO	Landfill	0,02	16,7
Total		0,12	100

EoL potential:

Component	End of life option	Energy (MJ)	%
Zirconia	Landfill	0	
Alumina	Landfill	0	
CaO	Landfill	0	
Total		0	100

Notes:

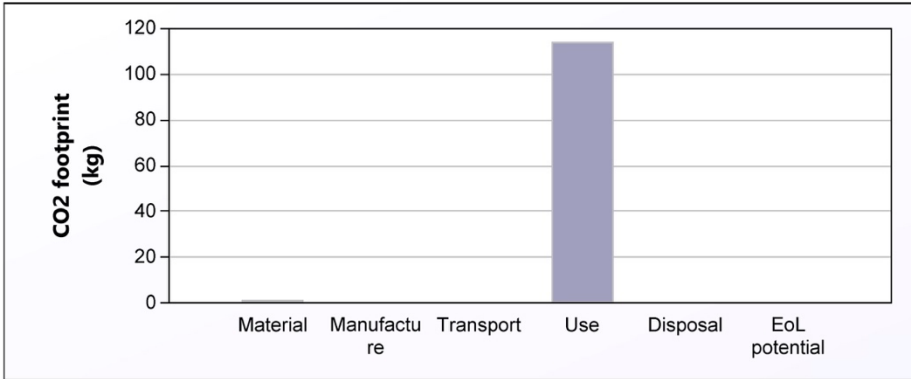
[Summary](#)



Eco Audit Report

CO2 Footprint Analysis

[Summary](#)



	CO2 (kg/year)
Equivalent annual environmental burden (averaged over 1 year product life):	116

Detailed breakdown of individual life phases

Material:

[Summary](#)

Component	Material	Recycled content* (%)	Part mass (kg)	Qty.	Total mass (kg)	CO2 footprint (kg)	%
Zirconia	Zirconia (Y2O3 stabilized)	Virgin (0%)	0,2	1	0,2	0,79	48,5
Alumina	Alumina (99.9%)	Virgin (0%)	0,3	1	0,3	0,84	51,4
CaO	Calcium carbonate (p)	Virgin (0%)	0,1	1	0,1	0,0016	0,1
Total				3	0,6	1,6	100

*Typical: Includes 'recycle fraction in current supply'

Manufacture:

[Summary](#)

Component	Process	Amount processed	CO2 footprint (kg)	%
Total				100

3D Printing of CaO for Carbon Capture

Transport:

[Summary](#)

Breakdown by transport stage

Stage name	Transport type	Distance (km)	CO2 footprint (kg)	%
Total				100

Breakdown by components

Component	Mass (kg)	CO2 footprint (kg)	%
Zirconia	0,2	0	
Alumina	0,3	0	
CaO	0,1	0	
Total	0,6	0	100

Use:

[Summary](#)

Static mode

Energy input and output type	Electric to thermal
Country of use	Europe
Power rating (W)	1,8e+03
Usage (hours per day)	12
Usage (days per year)	15
Product life (years)	1

Relative contribution of static and mobile modes

Mode	CO2 footprint (kg)	%
Static	1,1e+02	100,0
Mobile	0	
Total	1,1e+02	100

3D Printing of CaO for Carbon Capture

Disposal:

[Summary](#)

Component	End of life option	CO2 footprint (kg)	%
Zirconia	Landfill	0,0028	33,3
Alumina	Landfill	0,0042	50,0
CaO	Landfill	0,0014	16,7
Total		0,0084	100

EoL potential:

Component	End of life option	CO2 footprint (kg)	%
Zirconia	Landfill	0	
Alumina	Landfill	0	
CaO	Landfill	0	
Total		0	100

Notes:

[Summary](#)

Annex E

E.1 Cost of CC following the procedure defended in the present thesis

Conservative Calculations

$$C = \frac{C_s}{M_s * \mu * M_{CO_2} * N}$$

$$\frac{22.80 * 10^9 * 1,21 \$ \cdot \text{€}^{-1}}{14g * 14.01mmol \cdot g^{-1} * 44g \cdot mol^{-1} * 40} = 79,917.40 \$ \cdot tCO_2^{-1}$$

C = Cost in dollars per ton of CO₂ captured.

C_s = Cost of manufacturing one scaffold.

M_s = Mass of one scaffold.

μ = Efficiency of the scaffold.

M_{CO_2} = Molar mass of CO₂

N = Number of adsorption-desorption cycles for which the scaffold can be used.

Optimistic Calculations

$$\frac{22.80 * 10^9 * 1,21 \$ \cdot \text{€}^{-1}}{100g * 70.05mmol \cdot g^{-1} * 44g \cdot mol^{-1} * 5000} = 17.91 \$ \cdot tCO_2^{-1}$$